

Technische Universität München
Lehrstuhl für Medientechnik

Perceptual Haptic Data Communication for Telepresence and Teleaction

Dipl.-Inf. Univ. Julius Kammerl

Vollständiger Abdruck der von der Fakultät für Elektrotechnik und Informationstechnik der Technischen Universität München zur Erlangung des akademischen Grades eines

Doktor-Ingenieurs (Dr.-Ing.)

genehmigten Dissertation.

Vorsitzender: Univ.-Prof. Dr. sc. Samarjit Chakraborty

Prüfer der Dissertation: 1. Univ.-Prof. Dr.-Ing. Eckehard Steinbach

2. Univ.-Prof. Dr.-Ing. Sandra Hirche

Die Dissertation wurde am 25.01.2012 bei der Technischen Universität München eingereicht und durch die Fakultät für Elektrotechnik und Informationstechnik am 23.05.2012 angenommen.

Perceptual Haptic Data Communication for Telepresence and Teleaction

Dipl.-Inf. Univ. Julius Kammerl

July 16, 2012

Acknowledgments

This dissertation presents large parts of my work as a research scientist and teaching assistant at the Institute for Media Technology (LMT) at the Technische Universität München (TUM). My research was supported by the German Research Foundation (DFG), part of the Collaborative Research Center SFB 453 on “High-Fidelity Telepresence and Teleaction” and a PhD scholarship from the “Universität Bayern e.V.”.

First of all, I would like to express my gratitude to my supervisor Prof. Eckehard Steinbach for giving me the opportunity to investigate the very exciting research field of haptic communications. Despite his busy schedule, he always found time to discuss my ideas and challenges while leaving room for creativity and individual development. His helpful suggestions, advice and guidance significantly contributed to my research work. Furthermore, I would like to thank Prof. Sandra Hirche for accepting to be the second reviewer of this dissertation and Prof. Samarjit Chakraborty for heading the committee.

My sincere appreciation also goes to all my current and former colleagues of the LMT haptics group, especially to Dr. Peter Hinterseer, Rahul Gopal Chaudhari, Fernanda Brandi and Xiao Xu. They contributed considerably to this dissertation and many of the achievements presented would not have been possible without their support. Furthermore, I am very grateful to my colleague Florian Schweiger who, although not directly involved in my research topic, contributed significantly to my research work with his mathematical expertise. The pleasant conversations with my colleagues Georg Schroth, Robert Huitl and Sebastian Hilsenbeck also supported my work with inspiring perspectives to consider. Special thanks also go out to my close collaborators from the Collaborative Research Center 453. In particular, the joint work with Iason Vittorias, Prof. Sandra Hirche and Dr. Angelika Peer from the Institute for Control Engineering, TUM, was very enjoyable and resulted in several joint publications. Furthermore, I would like to thank Verena Nitsch and Prof. Berthold Färber from the University of the Armed Forces for the fruitful collaboration and for guiding me through the exciting research field of psychophysics. I would also like to thank Prof. Abdulmotaleb El Saddik for giving me the opportunity to broaden my research at the Multimedia Communications Research Laboratory of the University of Ottawa in September 2008. The joint collaboration with him, Dr. Mohamad Eid and Dr. Jongeun Cha resulted in several journal and conference publications. Special thanks also go also to Hawkeye King and Prof. Blake Hannaford from the University of Washington who visited the Institute for Media Technology in April 2009 and with whom I worked on Internet-based haptic communication. Very special thanks go to Prof. Subhasis Chaudhuri, who visited our research group at TUM several times and significantly contributed to my research.

I would also like to thank all my students who contributed considerably to this dissertation. Special thanks go hereby to Zike Chen for his contributions on *model-mediated prediction* and Bingqing Gu for her work on *perceptual haptic offline compression*. Furthermore, I would like to thank my working student Xiaojun Ma for his contributions on the development of the *SIP-based teleoperation* demonstrator system. My appreciation also goes to the professional administrative support provided by Ingrid Jamrath, Dr. Martin Maier and Gabriele Kohl. They always kindly and competently helped me in every administrative matter I had.

My final and most sincere thanks go to my beloved girlfriend Christiane and my parents who always supported me in every possible way.

Munich, December 2011

Julius Kammerl

Abstract

Telepresence and teleaction (TPTA) systems enable a human operator to execute complex tasks within an inaccessible, dangerous, and/or scaled environment. Their goal is to provide a local and realistic immersion of the remote environment. In this context, the communication of haptic signals (velocity and force) plays an important role. As the exchange of haptic information over the communication channel closes a global control loop between the human and the remote environment, the design and the development of methods for perceptual haptic communication must be carefully adapted to expected communication latency and network performance.

This dissertation presents a broad spectrum of methods for the perceptual communication of haptic signals. Challenging in this context is the design of an accurate psychophysical model of human haptic perception. It enables the mapping of neural excitements to a perception sensation in the human brain which can be used to reveal absolute and relative perception thresholds. This allows for controlling the intensity of compression artefacts in order to keep them below human haptic perception thresholds. Accordingly, the integration of additional findings from psychophysics into the perceptual model promises improved adaptation to the haptic discrimination thresholds which can be exploited in the context of perceptual haptic data compression. In addition, the application of environment models in haptic communication is proposed. Specifically, the bidirectional nature of haptic communication in TPTA systems enables the estimation of the geometry and impedance characteristics of the remote surface in contact. This enables the decoupling of the global haptic control loop which allows for improved transparency and compression performance. In addition to real-time communication of haptic signals, the development of offline compression methods is also of great interest. To this end, a perceptual haptic offline compression scheme is proposed which exploits knowledge about pending perception bounds resulting in an additional entropy minimization of the compressed data. Furthermore, to enable a theoretical analysis of the proposed methods for perceptual haptic communication, a mathematical framework based on stochastic models of haptic signals is discussed. Additionally, the impact of communication uncertainties such as communication latency and packet loss is addressed. Here, a modified control scheme for time-delayed haptic communication is presented which ensures stable operation and an efficient utilization of the haptic communication channel. Furthermore, a novel low-delay and perceptually-motivated haptic communication scheme is proposed, which is robust to data loss on the haptic channel. In order to manage and control TPTA sessions, as well as to facilitate the integration of the developed perceptual communication methods into the haptic communication system, a flexible communication framework is proposed which is based on standard Internet communication protocols. All developed methods and architectures are validated in experimental user studies.

Kurzfassung

Telepräsenz- und Teleaktionssysteme (TPTA) ermöglichen einem menschlichen Operator das Ausführen komplexer Manipulationsaufgaben in einer unerreichbaren, gefährlichen und/oder skalierten Umgebung. Zentrale Aufgabe dieser Technik ist es, eine möglichst wirklichkeitsnahe Immersion der entfernten Umgebung lokal zu erzeugen. Dabei spielt die Kommunikation haptischer Datenströme (Bewegung und Kraft) eine zentrale Rolle. Da der Austausch von haptischen Sensordaten über die Kommunikationsstrecke hinweg einen geschlossenen Regelkreis darstellt, ergeben sich strenge Anforderungen an die Kommunikationslatenz und die Übertragungszuverlässigkeit.

In dieser Arbeit wird ein breites Spektrum von Methoden zur wahrnehmungsbasierten haptischen Datenkommunikation vorgestellt. Eine wesentliche Herausforderung ist in diesem Zusammenhang der Entwurf eines psychophysischen Modells der menschlichen haptischen Wahrnehmung. Dieses erlaubt die Beziehung zwischen einem vorhandenem Stimulus und der daraus resultierenden Reaktion im Gehirn darzustellen und ermöglicht somit, in Form eines parametrisierten Instrumentes, den Grad der Wahrnehmbarkeit zu erkennen, zu detektieren und zu bewerten. Auf diese Weise kann kompressionsbedingte Signalstörung kontrolliert unter haptischen Wahrnehmungsschwellen gehalten werden. Die Integration zusätzlicher psychophysischer Erkenntnisse in das psychophysische Modell stellt somit zusätzliche Leistungssteigerungen in Aussicht. Darüber hinaus wird der Einsatz von Umgebungsmodellen in der haptischen Datenkommunikation untersucht. Diese erlauben eine Entkopplung des globalen haptischen Regelkreises, welche sich zur Effizienzsteigerung haptischer Datenkompressionsverfahren erfolgreich ausnutzen lässt. Zusätzlich zur wahrnehmungsbasierten Echtzeit-Kommunikation, werden auch Methoden zur Offline-Kompression haptischer Datensätze untersucht. Dazu wird ein Verfahren vorgestellt, welches Wissen über die angewendete Wahrnehmungsschwellen ausnutzt, um die Entropie der komprimierten haptischen Datensätze weiter zu reduzieren. Zur theoretischen Analyse der entwickelten Kommunikationsmethoden wird darüber hinaus ein Framework vorgestellt, welches das Verhalten entwickelter Algorithmen im theoretischen Experiment simulieren lässt. Zusätzlich werden die Auswirkungen von kommunikationsnetzinduzierten Unsicherheiten in Form von Totzeiten und Paketverlusten betrachtet. Hierzu wird eine modifizierte Regelungsarchitektur untersucht, welche wahrnehmungsbasierte haptische Datenkommunikation bei zeitverzögerter Kommunikation ermöglicht und auf diese Weise die Stabilität und effiziente Ausnutzung des Kommunikationskanals im TPTA-System sicherstellt. Weiterhin wird ein neuartiges Verfahren vorgestellt, das eine wahrnehmungsbasierte Kompensation von Paketverlust auf der haptischen Kommunikationsstrecke ermöglicht. Zur Steuerung und Verwaltung von TPTA Sitzungen, sowie zur Integration der entwickelten Methoden und Verfahren wird darüber hinaus ein flexibles Kommunikationsframework vorgestellt. Alle entwickelten Methoden und Architekturen werden mittels experimentellen Studien validiert.

Contents

Notation	ix
1 Introduction	1
1.1 Main Contributions and Outline of the Dissertation	3
2 Background & Related Work	7
2.1 Telepresence and Teleaction Systems	7
2.1.1 System Overview	7
2.1.2 Haptic Communication	9
2.1.3 Control & Stability	10
2.1.4 Evaluation Methods	14
2.2 Human Haptic Perception	16
2.2.1 Human Haptic Perception System	16
2.2.2 Limitations of Human Haptic Perception	17
2.3 Haptic Data Compression	19
2.3.1 Related Work	20
2.3.2 Perceptual Predictive Compression Scheme	21
2.3.3 Perceptual Deadband Approach	22
2.3.4 Haptic Signal Prediction	22
2.3.5 Perceptual Deadband Parameter k	25
2.4 Chapter Summary	26
3 Perceptual Compression of Haptic Signals	27
3.1 Extended Psychophysical Model for Perceptual Haptic Data Compression . .	28
3.1.1 Direction-dependent Multi-DoF Perceptual Deadzone	28
3.1.2 Velocity-adaptive Perceptual Deadbands	34
3.2 Model-mediated Haptic Communication	41
3.2.1 Model-mediated Haptic Data Compression	41
3.2.2 Model-mediated Prediction	49
3.2.3 Event-based Coding using Contact Models	55
3.3 Perceptual Haptic Coding of Recorded Telemanipulation Sessions	65
3.3.1 Recording and Replay of Multimodal TPTA Sessions	65
3.3.2 Perceptual Offline Compression	67
3.4 Theoretical Analysis of Perceptual Deadband Coding	75
3.4.1 Perceptual Deadband Sampler	75
3.4.2 Stochastic Input Model for Haptic Signals	76
3.4.3 Theoretical Analysis	76
3.4.4 Experimental Evaluation	82
3.5 Chapter Summary	85

4	Haptic Communication and Coding Architectures	87
4.1	Perceptual Haptic Compression with Time-delayed Communication	88
4.1.1	Wave Variable Control	88
4.1.2	Local Computation of Wave Variables	89
4.1.3	Passivity-preserving PD compression	91
4.1.4	Experimental Evaluation	92
4.2	Error-resilient Haptic Communication	95
4.2.1	Architecture for Perceptually Robust Haptic Communication	95
4.2.2	Receiver State Estimation using Markov Decision Trees	96
4.2.3	Receiver State Estimation using Multivariate Gaussian Models	97
4.3	Multimodal Telepresence Sessions using the Session Initiation Protocol (SIP) .	104
4.3.1	Internet-based Transport Streams and Session Control	104
4.3.2	System Parameter Negotiation	105
4.3.3	SIP-based Communication Framework	106
4.3.4	Demonstrator System	108
4.4	Chapter Summary	110
5	Conclusion and Outlook	113
5.1	Concluding Remarks	113
5.2	Outlook	115
	List of Figures	117
	List of Tables	121
	Bibliography	123

Notation

Abbreviations

ACK Acknowledgement (Data Packet)

ANOVA ANalysis Of VARiance

AR Autoregressive

COM Communication Channel

DoF Degree of Freedom

EBH Event-based Haptics

GUI Graphical User Interface

HIP Haptic Interface Point

HSI Human-System Interface

IP Internet Protocol

JND Just Noticeable Differences

LCWV Locally Computed Wave Variables

OP Operator

PD Perceptual Deadband/Deadzone

PDF Probability Density Function

RTCP Real-Time Transport Control Protocol

RTP Real-Time Transport Protocol

SDP Session Description Protocol

SIP Session Initiation Protocol

SVD Singular Vector Decomposition

TCP Transmission Control Protocol

TOP Teleoperator

TPTA Telepresence and Teleaction

UDP User Datagram Protocol

Scalars, Vectors, and Matrices

Scalars are denoted by upper and lower case letters in italic type. *Vectors* are denoted by lower case letters in boldface type. *Matrices* are denoted by upper case letters in boldface type.

x scalar

\mathbf{x} vector

X matrix

$f(\cdot)$ function

\dot{x}, \ddot{x} equivalent to $\frac{d}{dt}x, \frac{d^2}{dt^2}x$

$|\cdot|$ norm

Subscripts and Superscripts

x_h value x associated with the human

x_e value x associated with the environment

x_m value x associated with the human-system interface (master)

x_s value x associated with the teleoperator (slave)

x^d desired value x

\hat{x} estimated/reconstructed value x

\bar{x} mean of x

Symbols and Abbreviations

\mathbf{x} Position signal

\mathbf{f} Force feedback signal

\mathbf{h} General haptic signal

\mathbf{p} Predicted haptic signal

k Perceptual deadband parameter

1 Introduction

The development of techniques for overcoming distances and gaining access to inaccessible real or even virtual environments has been addressed by engineers and scientists for a long time. Various successful developments and products have been designed and many of them strongly dominate our daily life. Starting with the development of the *telescope* (1593, Galileo Galilei) providing the capability of observing from a distance, the *telegraphy* (1833, Samuel Morse) allowing writing from a distance, the *telephony* (1860, Antonio Meucci / 1876, Alexander Bell & Thomas Watson) enabling talking from a distance, the *television* providing the capability of seeing from a distance (1883, Paul Nipkow), techniques for receiving, transmitting and exchanging information between distant environments have always been a subject of intensive research. The prefix *tele* origins from the Greek word "τηλε" meaning "remote distance".

Over the past 50 years, research on overcoming distance has made significant efforts to further improve such *tele*-technologies. In addition to the transmission of visual, audio and text information, so called *telepresence* and *teleaction* (TPTA) systems provide the exchange of haptic information. Haptic perception refers to the sense of touch consisting of the kinesthetic and the tactile sense. The kinesthetic sense processes information about the position and orientation of the human body as well as changes thereof (perception of velocity, acceleration, forces and torques on joints, etc.). In addition, the tactile sense located on the skin acquires information about contacts with the environment. Hence, the integration of the haptic modality into TPTA systems enables physical access to environments that are distant, inaccessible, scaled to macro- or nano-dimensions or hazardous for human beings. In this context, mechanical energy needs to be exchanged between a human operator and a *teleoperator* that operates within a remote or virtual environment. R.C. Goertz was one of the first researchers who developed an electro-mechanical TPTA system in 1954 at Argonne National Lab (USA) to aid in the handling of nuclear material [112]. During the mid 1960's, teleoperation technology rapidly spread in the medical field. Wheelchairs for quadriplegics were developed which can be commanded by the tongue and breath. In addition the powerful capabilities of TPTA systems in surgery scenarios were discovered. In 1966, the US Navy designed a cable controlled underwater vehicle for bomb retrieval from the deep ocean. Interestingly, experiments with time-delayed communication first revealed the critical instability problems of force reflection in 1965 [73, 74]. A comprehensive historical survey on teleoperation systems can be found in [112].

TPTA systems enable a human operator to locally immerse into a remote and/or virtual environment. Overcoming barriers such as distance or matter and gaining access to remote environments open up many novel application scenarios where the possibility of remote operation and remote task execution is of great relevance. Consequently, TPTA systems are already established in many fields of application enabling a human operator to execute complex tasks in reduced time, with lower costs, improved precision/performance and minor risk of injury [112].

This applies to TPTA on-orbit scenarios, where TPTA systems are operating in space which is a hostile environment for human beings. Instead of performing costly manned space travels, remotely controlled robots represent an alternative solution for space exploration, on-orbit servicing (satellites, space stations), scientific experiments in space, etc. The first space explorations of Mars were remotely performed by NASA with the planetary rovers "Mars Pathfinder" (1997) and the "Mars Rover" (2006). Additional applications can be found in underwater scenarios. For instance, the communication and oil industries require the examination of pipes and cables under water. The challenging conditions of the water environments such as high pressure and poor visibility constrain the performance of divers. In contrast, underwater TPTA systems provide comprehensive access to the underwater world and improve the performance of underwater operations.

Further interest can be found in the medical field [8]. Here, TPTA systems allow the surgeon to virtually immerse into the human body. Multimodal feedback captured by the surgery robot enables the intuitive control of laparoscopic equipments and navigation within the human body. During contacts within surgery environments, haptic contact forces are sensed and displayed to the surgeon, helping to reduce tissue damage, breaks of suture material due to excessively high forces, etc. The availability of haptic feedback is particularly important for the surgeon in identifying tissue characteristics, which are often the only information for the detection of certain diseases. As the surgeon controls such a telesurgery system applied to a physically separated patient, the surgeon and the patient do not have to be at the same location and patients can access surgeons around the world without traveling beyond their local hospital. In 2001, the first completely remote surgery on a human patient was performed over a distance of 7000 km between Strasbourg (France) and New York (USA) with a latency of 135 ms [134]. Also "minimally invasive" surgery procedures benefit from this class of TPTA systems where the surgeon operates through small insertions in the human body which affect reach and manipulation. The deployment of a TPTA system enables the successful compensation of these spatial challenges for a surgeon. Furthermore, TPTA technology in the context of microsurgery operations, e.g. eye surgery and micro-assembling, offers the possibility of scaling operator movements and corresponding contact forces. This enables very precise operations with objects of small size, even in nanometer scale [173].

A variety of TPTA systems are applied in hazardous environments, particularly in the nuclear, chemical and military field. Possible applications are, for instance, the handling of radioactive or chemical materials/objects, the inspection of dangerous environments, waste disposal, ammunition disposal, etc. In the area of security as well, TPTA systems can serve for protection purposes without putting human personnel at risk. Another important application domain of TPTA systems is virtual reality (VR). Here, the human controls a virtual teleoperator which interacts with virtual objects within a simulated environment. The detection of environment contacts and the calculation of contact forces are performed by a haptic rendering engine combined with a physics engine to simulate the impact of applied forces to virtual objects [160]. Virtual TPTA systems are highly relevant in training, teaching and simulation scenarios [32, 33]. They allow the human operator to immerse into a virtual training scenario where possibly dangerous tasks can be simulated. For instance, flight simulation systems can be considered to be virtual TPTA systems for operating in a virtual world where possible pilot failures do not have immediate fatal impact.

TPTA can also be performed by multiple users interacting within a joint, collaborative environment. By exchanging the multimodal sensory information among the participants, mul-

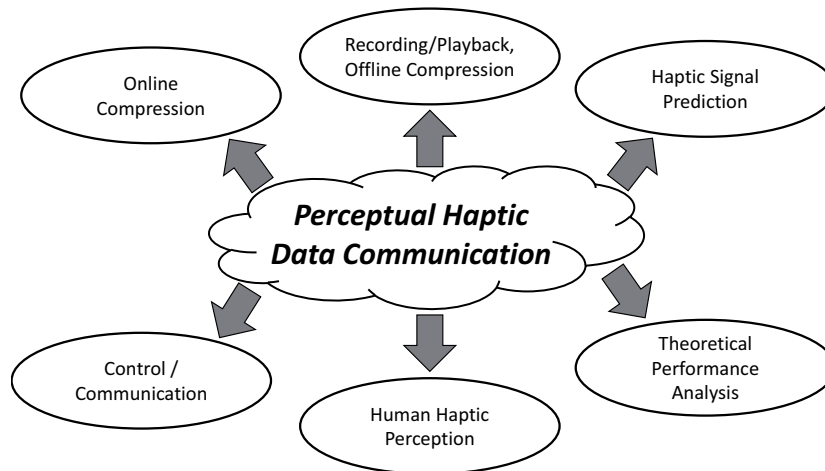


Figure 1.1: Overview of addressed research areas in this dissertation.

multiple users are able to collaborate towards a common objective. In this context, haptically enabled virtual multi-user environments are of particular interest in the gaming and entertainment industry.

1.1 Main Contributions and Outline of the Dissertation

Haptic communication plays a key role in TPTA systems. As soon as the teleoperator is located in a distant real or virtual environment, haptic signals consisting of motion commands and force sensory data must be transmitted over a communication channel. As the exchange of haptic information closes a global control loop between the human and the remote environment, the design and the development of perceptual haptic data communication methods must be carefully adjusted to expected physical and algorithmic delay. These constraints constitute a fundamental difference to standard streaming video and audio applications, where media data is typically unidirectionally transmitted. Furthermore, currently available TPTA systems deploy a large number of degrees of freedom (DoFs). As the amount of bidirectionally transmitted haptic information increases with multiple DoFs, strong interest in methods of compressing haptic data in a manner which is transparent to the human user can be found.

This thesis focuses on improving the communication and the processing of haptic signals in TPTA systems. Due to the highly interdisciplinary nature of this research topic, several fields in research are addressed in this work, as illustrated in Figure 1.1.

The outline of this thesis is shown in Figure 1.2. The scientific background and related work of perceptual haptic communication is presented in Chapter 2. It discusses the design, control, and performance evaluation of TPTA systems. Furthermore, the consideration of human haptic perception is of great relevance in the context of haptic communication. To this end, psychophysical findings on haptic discrimination thresholds are discussed which serve as the basis for the development of perceptual haptic data compression methods. Additionally, a comprehensive overview of the state-of-the-art in haptic data compression is given.

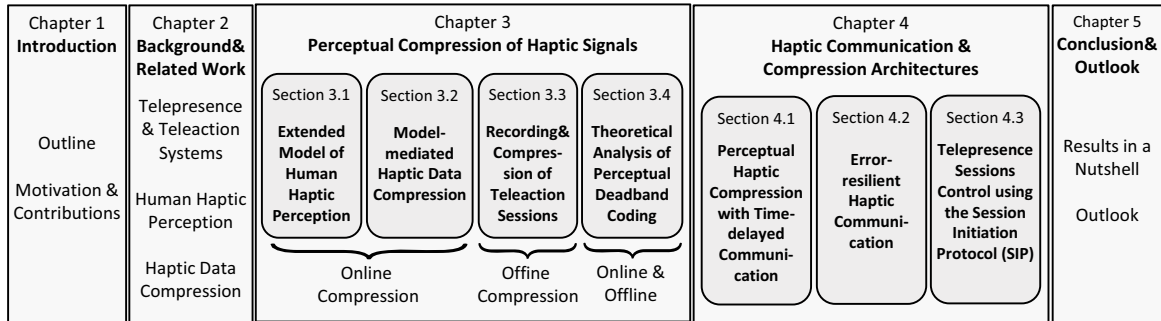


Figure 1.2: Overview of the dissertation.

Chapter 3 presents several contributions which allow for improving the performance of the perceptual haptic data compression. They are briefly discussed in the following:

- *Integrating findings from psychophysics into the perceptual haptic model:* Perceptual haptic data compression relies on a mathematical model of human haptic perception. It is used to detect imperceptible signal content that can be discarded during encoding. Accordingly, improved adaption to human haptic perception thresholds supports perceptual haptic compression in a fundamental way, as discussed in Section 3.1. Here, the concept of multi-DoF perception thresholds are introduced which exploit directional dependencies of human force-feedback perception. In addition, the influence of simultaneous movements of the human operator on haptic perception thresholds is discussed and experimentally evaluated.
- *Model-mediated haptic data compression and prediction:* During a TPTA session, motion commands are executed by the TOP. In return, force feedback is reflected during contact events with the remote environment. Hence, by associating the contact forces with the position information of the TOP, the geometry and impedance characteristics of the remote surface in contact can be estimated. In Section 3.2, the concepts of *model-mediated compression*, *prediction*, and *contact coding* are introduced which all rely on mathematical models of the remote environment. Deployed at the HSI, they can be used to locally render haptic contact forces which allows for substituting the transmission of the remote haptic sensory signals. Conducted experiments indicate that the integration of environment models into methods for perceptual haptic communication allows for improved compression performance and system transparency.
- *Recording, playback, and offline compression of TPTA sessions:* In addition to low-latency online compression of haptic data streams, the development of perceptual offline compression algorithms is also gaining in relevance. In several application scenarios, such as in training, teaching, learning, entertainment, performance analysis as well as documentation applications, the recording and playback of TPTA sessions is of fundamental interest. As soon as haptic data has to be stored on a storage device for posterior replay, the interest in offline compression for haptic data emerges. Due to relaxed delay constraints, the design of an offline compression scheme can be addressed in a fundamentally different way compared to haptic low-latency online compression, as shown in Section 3.3. In this context, the concept of deadband-based differential coding is presented which allows for exploiting knowledge about pending perception bounds. Conducted experiments demonstrate a strong data compression ability of the

presented haptic offline compression scheme while keeping introduced coding artefacts within an imperceptible range.

- *Theoretical analysis of perceptual deadband compression:* The performance of perceptual haptic communication techniques has been experimentally determined in several studies. In contrast to real-world experiments on TPTA systems, Section 3.4 presents a framework for analytically evaluating the performance from a theoretical perspective. This allows for mathematically determining the expected packet rates on the communication channel according to a stochastic model of haptic signals.

Perceptual haptic data compression methods successfully address the challenges of high packet and data rates of haptic communication. Their performance, however, also depends on the characteristics of the haptic signals to be exchanged between human operator and teleoperator. In this context, the influence of the deployed control architecture, the performance of the communication system, as well as the physical properties of the hardware components play an important role. To address these important dependencies, the development of haptic data compression techniques needs to be approached from a combined signal processing, control engineering and communication point of view.

Chapter 4 addresses the impact of network errors on perceptual haptic data compression and investigates its integration into established Internet-based communication frameworks. Particularly, the following contributions are presented:

- *Perceptual haptic compression with time-delayed communication:* Already short latency on the communication channel destabilizes the global control loop of a TPTA system. The scattering theory is known to solve these stability issues by transmitting wave variables instead of haptic signals over the communication channel. This, however, impairs the application of perceptual haptic compression techniques as transmitted wave variables do not directly represent haptic information anymore. In Section 4.1, a modification of the wave variable control scheme is presented which takes advantage of the stabilization ability of the wave variables while allowing the application of perceptual communication schemes on the haptic channel. Furthermore, a modified passivity-preserving signal encoding scheme for perceptual haptic data compression is discussed.
- *Error-resilient haptic communication:* Unreliable networks (i.e. the Internet) introduce several disturbing effects to the haptic communication system. Particularly, the communication of perceptually compressed haptic signals is highly sensitive to packet loss. The stronger haptic signals are compressed, the more vulnerable the transmitted bit-stream becomes against losses. Section 4.2 addresses the issues of unreliable communication networks in TPTA scenarios. It presents a perceptually-motivated approach for robust low-delay haptic communication. By employing a probabilistic model of the receiver, its most likely state can be used to adaptively determine the amount of redundancy which is required for compensating packet loss disturbances.
- *Telepresence sessions control using the Session Initiation Protocol (SIP):* The human-system-interface and the remote teleoperator in a telepresence and teleaction system are highly complex systems. To enable flexible and dynamic connections between multiple haptic enabled interfaces and devices, detailed knowledge of the system parameters, functional capabilities and requirements of the deployed hardware is essential. In order to enable interoperability among heterogeneous TPTA systems and platforms, a flexi-

ble framework leveraging Internet session and presence protocols for telepresence and teleaction systems is presented in Section 4.3. It uses the widely adopted Internet-based Session Initiation Protocol (SIP) to negotiate and establish real-time haptic data transport streams and to enable session control.

The thesis is concluded in Chapter 5 with a summary and a discussion about future directions in this research field.

Parts of this work have been published in [2, 3, 4, 5, 6, 8, 9, 10, 11, 13, 14, 15, 16, 17, 18, 19, 20, 21, 23, 24, 25].

2 Background & Related Work

2.1 Telepresence and Teleaction Systems

Telepresence and teleaction (TPTA) systems enable a human operator (OP) to operate within a distant, scaled, inaccessible and/or hazardous environment. Their goal is to provide a local immersion of the remote environment in order to enable the execution of remote explorative and manipulative tasks.

2.1.1 System Overview

A TPTA system can be decomposed into three main subcomponents (see Figure 2.1): the human OP connected to a human system interface device (HSI), a teleoperator (TOP) which receives control commands for the execution of remote operations, and the communication link which bidirectionally exchanges the haptic signals over a communication channel.

- *Human system interface (HSI)*: The HSI device consists of both the input device for position and orientation sensing and the output devices for displaying multiple modalities. The latter uses haptic displays for presenting force and torque as well as vibrotactile feedback, visual displays such as head-mounted displays, stereographic displays for displaying stereo-video, etc. and headphones or speakers for audio feedback. As the haptic display exchanges mechanical energy between the TPTA system and the human OP, it needs to be in physical contact with the OP. Haptic devices can provide kinesthetic as well as tactile feedback. Kinesthetic force feedback can be generated using high torque motors. Tactile feedback can be displayed with multi-pin displays attached to the human skin (see [34, 42, 69, 177, 182]) or by using small vibrators for the display of vibrotactile stimuli [52, 141]. Recent advances in tactile display technology also deploy electroactive polymers, so called "dielectric elastomer actuators" [45, 135]. A comprehensive overview of haptic devices is presented in [94]. Further aspects of the development and the control of haptic devices are discussed in [39, 95, 183]
- *Communication system*: The communication system transmits the multimodal sensory data between the HSI and the TOP. In addition to well known media types like video and audio streams which are mostly transmitted unidirectionally from the TOP to the HSI, haptic data streams need to be bidirectionally exchanged between the HSI and the TOP. They describe mechanic quantities like position, angle, velocity, angular velocity, acceleration, angular acceleration as well as force and torque feedback over time. The performance of the communication system strongly influences the overall performance of the TPTA system. Particularly, latency and data loss in the network quickly impair task performance and system transparency. Accordingly, the operation of a TPTA system over long-distance and/or wireless networks (using satellites, underwater modems, etc.) poses a particular challenge.

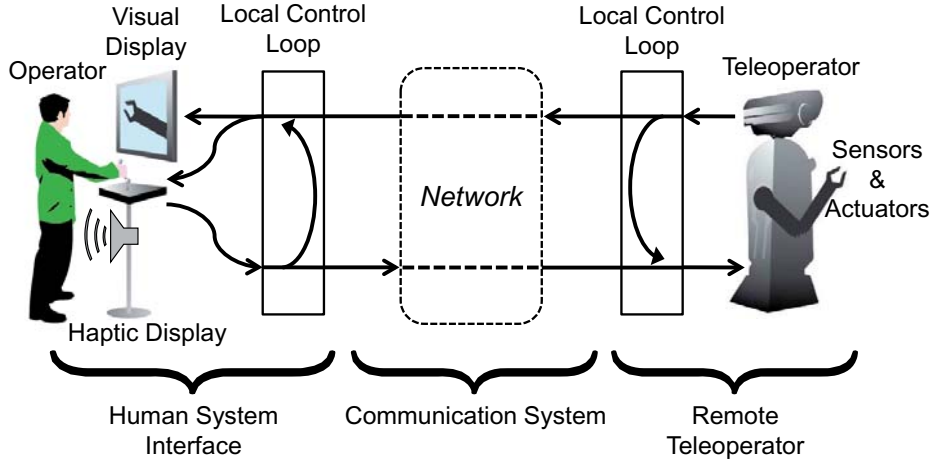


Figure 2.1: Overview of the main components of a TPTA system: the human system interface device, the communication system and the remote teleoperator (reproduced from [18]).

- **Teleoperator (TOP):** The TOP is a robot equipped with multiple sensors like contact force and torque sensors, cameras, microphones, etc. for capturing multimodal sensory information. In addition, it uses haptic actuators like grippers or other anthropomorphic limbs for physical interaction with its remote environment. In case the remote environment is virtual, physical interaction is simulated to generate multimodal feedback. During a TPTA session, the TOP receives high-level motion commands from the HSI. In complex TPTA scenarios with significant latency on the communication channel, the TOP can be also equipped with autonomous features. Both the HSI and the TOP apply a local control scheme for controlling the TOP movements and force feedback display.

The communication channel closes a global control loop between the human connected to the HSI and the TOP interacting with the remote environment. In order to maintain control loop stability, a global control scheme is of fundamental importance. One of the most commonly applied control approaches for bilateral teleoperation is the velocity-force control architecture [29], as illustrated in Figure 2.2. In this scheme, the human manipulates the HSI by moving the input device with velocity \dot{x}_h . The HSI senses and transmits its velocity \dot{x}_m to the TOP. The exchange of velocity signals is favored over the exchange of absolute position coordinates as it enables the decoupling of the coordinate systems at the HSI and the TOP system. The TOP receives a *desired* velocity signal \dot{x}_s^d , which is delayed with a communication delay T_1 . It is used to command a local control loop which controls the velocity \dot{x}_e of the TOP robot. During contacts with the remote environment, an environment force f_e is measured. The resulting force sensory signal f_s is transmitted from the TOP to the OP with communication latency T_2 . The HSI receives the *desired* force-feedback information f_m^d which becomes the reference for the local force feedback control loop at the HSI device. Consequently, the output force f_h is displayed to the human OP.

The haptic signals \dot{x}_m and f_s tend to exhibit mostly low frequency components due to the inertia and dynamics of the TPTA system. However, high sampling rates of ≥ 1000 Hz are typically applied in order to encompass the bandwidth of human perception and to reduce

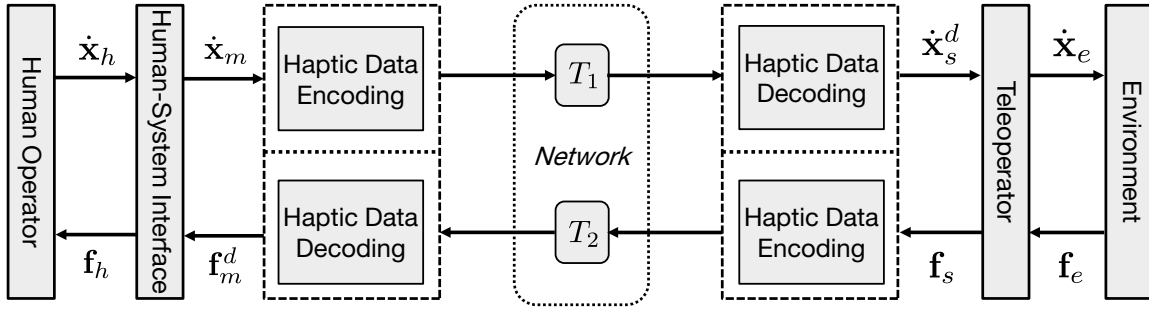


Figure 2.2: Overview of haptic signals in a TPTA system with velocity-force control and haptic data compression.

control loop instabilities originating from sampling-based discretization (see [127]).

2.1.2 Haptic Communication

Unlike the communication of audio and video signals, the haptic signals in TPTA systems are bidirectionally exchanged between the HSI and the TOP which closes a global control loop. Accordingly, any transmission delay on the haptic communication channel immediately impairs the stability of the global haptic control loop which significantly affects the immersiveness of the TPTA system [29]. Hence, for the real-time transmission of haptic signals, the introduced end-to-end delay needs to be kept at an absolute minimum. Therefore, the joint processing of haptic samples using block-based coding and transmission techniques and/or filters introducing a group delay cannot be applied. A common strategy to address this issue is to minimize the communication delay by transmitting haptic samples immediately upon their generation. This, however, leads to high packet rates up to the applied haptic sampling rates at the HSI and the TOP (typically 1000 Hz), which are particularly hard to maintain in Internet-based communication [77, 133].

The Internet provides flexible, low-cost communication with world-wide coverage and is, therefore, also of great interest in TPTA scenarios. Unfortunately, the high packet rates in haptic communication typically increase network disturbances such as jitter and packet loss effects which may destabilize the TPTA system. In addition, they lead to significant network overhead due to increased packet header information to be transmitted. Depending on the number of DoFs and the data type resolution (typically 16 bit floating point precision), the typical payload per haptic packet is between 10 and 50 bytes. Taking into account the UDP/IP header overhead of 24 bytes per packet (20 bytes IP, 4 bytes UDP), overall traffic is considerably increased by 50%-100% due to additional packet header information.

In addition to the challenging high packet rates, haptic communication in TPTA scenarios is also characterized by high data rates. In order to provide high manipulative flexibility and haptic immersion, complex human body tracking with multi-DoF position sensors and force feedback actuators is required for many joints. Modern TPTA systems therefore integrate a high amount of degrees of freedom (DoF). For instance, the human hand exoskeleton system CyberGrasp/CyberGlove by Immersion integrates 22 DoFs to enable the haptic modality for a single human hand [118]. As each degree of freedom needs to be separately sampled

and controlled, the amount of haptic data to be exchanged over the communication channel quickly increases.

In order to address the challenges of high packet rates and high network load on the haptic communication channel, compression methods that efficiently reduce packet and data rates with minimum processing delay are of great importance. Furthermore, reduced packet rates decrease possible packet congestion along the network route and enable haptic real-time communication over rate-limited (i.e., wireless) communication networks.

2.1.3 Control & Stability

A TPTA system is a robotic system which exchanges mechanical energy between the human OP and the remote environment. In this way, it closes a global control loop over the communication system which can destabilize the TPTA system [188]. Already a short round-trip delay of ≥ 100 ms leads to a noticeable lag in the position control [73] which significantly affects the OP's motion planning leading to decreased teleoperation bandwidth [187]. The applied control architecture therefore has a significant impact on the system stability and transparency. However, these two properties are typically conflicting goals as discussed in [131].

2.1.3.1 Passivity-based Control

Several bilateral teleoperation control schemes focus on the energy-based concept of passivity which was first applied in [29]. Intuitively, a passive system consumes more energy than it produces and, therefore, dissipates energy.

As long as a control loop reflects passive behavior by either storing or dissipating signal energy, it is passive which guarantees stability. The power P_{in} entering a system can be defined as the dot product between its input \mathbf{u} and its output \mathbf{y} . Accordingly, a passive system obeys

$$P_{in} = \mathbf{u}^T \mathbf{y} = \frac{d}{dt} S + P_{diss} \quad (2.1)$$

where S is an energy storage function and P_{diss} is a non-negative power dissipation function. If $P_{diss} = 0$, the system is energetically lossless, as no energy is dissipated. As a passive system cannot generate energy, its energy balance $E(t)$ (assuming zero initial energy) at time $t > 0$ is defined by :

$$E(t) = \int_0^t P_{in} d\tau = S(t) + \int_0^t P_{diss} d\tau \geq 0 \quad \forall t > 0 \quad (2.2)$$

It follows that, at any time, the energy balance of a passive system must be non-negative. This can be easily investigated in a TPTA system by observing the energy of its input and output.

Passivity-based control strategies for bilateral TPTA can be categorized into two different classes [193]:

- The first class of control architectures inherently guarantees stability by their design. In this context, the concept of *wave variables* constitutes an important framework. It guarantees passivity in TPTA scenarios with arbitrary but constant communication

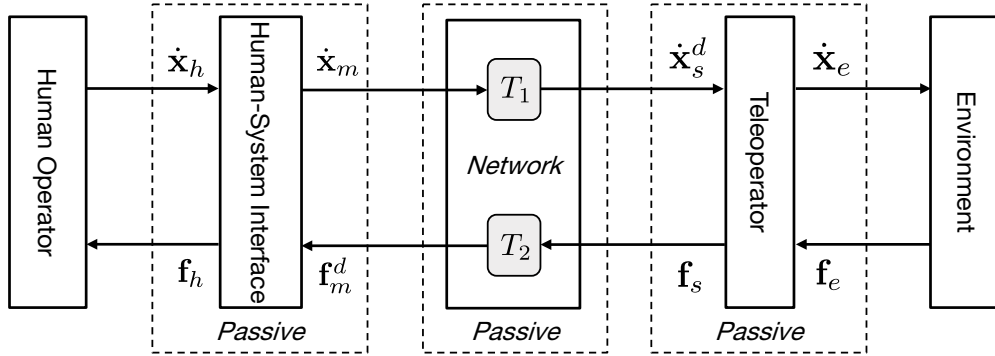


Figure 2.3: A TPTA system can be divided into a cascade of one-port and two-port subsystems. If all subsystems are passive, the overall TPTA system is proven to be passive which guarantees global control loop stability. The human and the environment are considered to always behave in a passive manner.

delay [142]. An extension of the "wave variable" approach for scenarios with time-varying communication delay has been presented in [50, 199]. Furthermore, stability issues due to packet loss during the transmission of wave variables are addressed in [35, 36, 106].

- The second class describes control methods that actively observe the input-output energy balance of the TPTA system and immediately intervene as soon as an increase in energy is detected. Typically, the system reacts with virtual damping in order to dissipate the additional energy. In this context, Hannaford *et al.* propose a framework called "Passivity Controller/Passivity Observer" which observes the relationship between the incoming and outgoing energy flows at the HSI and TOP system [91]. Another stability observation technique called "Haptic Stability Observer" is based on the frequency of the motion of the HSI device [124]. As high frequency content within the HSI motion signals indicates instabilities within the TPTA system, a stability preserving virtual damper can be adaptively controlled proportional to the detected oscillations of the HSI device.

To facilitate the passivity analysis, the global TPTA system can be split into a cascade of interconnected one-port and two-port subsystems [142, 153] as illustrated in Figure 2.3. The human OP and the remote environment can be reflected by two separate one-port subsystems. The HSI, the communication system and the TOP can be represented by individual two-port subsystems. As passive systems connected in either a feedback or a parallel configuration are again passive in their global energy behavior [164], a TPTA system operates in a passive manner, if all of its subsystems are showing a passive signal behavior. Hence, in order to prove passivity within the global control loop, the energy balances $E(t)_{in}^{HSI}$, $E(t)_{in}^{COM}$, $E(t)_{in}^{TOP}$ of all involved subsystems can be investigated, i.e., the HSI, the communication (COM) and the TOP system, respectively:

$$E(t)_{in}^{HSI}(t) = \int_0^t \dot{\mathbf{x}}_h^T(\tau) \mathbf{f}_h(\tau) - \dot{\mathbf{x}}_m^T(\tau) \mathbf{f}_m^d(\tau) d\tau \geq 0 \quad \forall i > 0 \quad (2.3)$$

$$E(t)_{in}^{COM}(t) = \int_0^t \dot{\mathbf{x}}_m^T(\tau) \mathbf{f}_m^d(\tau) - \dot{\mathbf{x}}_s^{dT}(\tau) \mathbf{f}_s(\tau) d\tau \geq 0 \quad \forall i > 0 \quad (2.4)$$

$$E(t)_{in}^{TOP}(t) = \int_0^t \dot{\mathbf{x}}_s^{dT}(\tau) \mathbf{f}_s(\tau) - \dot{\mathbf{x}}_e^T(\tau) \mathbf{f}_e(\tau) d\tau \geq 0 \quad \forall i > 0 \quad (2.5)$$

According to Hogan (see [111]), the interactions of a trained human being can be considered to be passive. In addition, the dynamics of real-world environments can be considered to be passive as well. Furthermore, the dynamics of the HSI device and the TOP robot are typically known or can be well estimated. They can also be adaptively controlled in order to assure energy consumption. The influence of the communication channel on the system's energy behavior still remains a critical factor in terms of passivity and, hence, of the stability of the overall TPTA system. Particularly, the physical propagation time of transmitted signals can quickly jeopardize the system stability of the global haptic control loop, especially in long-distance TPTA applications such as on-orbit servicing.

Note that fulfilling the condition of passivity is not the only sufficient criteria in guaranteeing system stability. For instance, non-passive behavior can be accommodated by applying strong system damping without losing the stability of the TPTA system. Similarly, controller implementations working in discrete time are also known to violate the passivity property due to signal discretization [56]. However, in typical TPTA systems with controller sampling rates of ≥ 1 kHz, sampling related instability effects are considered to be negligible [127].

A detailed discussion of control architectures for bilateral teleoperation and their influencing factors can be found in the survey articles [107, 112, 131].

2.1.3.2 Model-mediated Control

Model-mediated control schemes address the stability issue of a TPTA system by deploying models of the remote environment. These environment models are used to locally generate haptic feedback which can be immediately displayed without being affected by network latency. Consequently, the delay-critical global haptic control loop between the HSI and the TOP becomes opened since the OP perceives locally rendered forces instead of remotely captured haptic sensory signals. Model-based control schemes have been intensively discussed in literature. Their main concepts are briefly summarized in the following:

The first efforts to employ haptic models for decoupling the control loops at the HSI and the TOP have been made in [89] by introducing the so called "bilateral impedance control". Here, estimated impedances of the human OP connected to the HSI and the TOP in contact with the remote environment are bidirectionally exchanged and used for local feedback generation. In [201], this approach is further investigated in the context of space teleoperation, where significant communication latency is unavoidable and system stability of great importance. Similarly, Hashtrudi-Zaad *et al.* propose to use a remotely configured mass-spring-damper model for locally rendering environment forces [92]. The authors in [167] present a similar approach called "model predictive control" which shows improved robustness against communication uncertainties. Tzafestas *et al.* discusses "impedance-reflection

control” which is based on the exchange of simple impedance models [181]. This scheme is further extended by Achhammer *et al.* to enable six DoF haptic interactions by proposing a multi-DoF impedance estimation technique [26]. The “stiffness reflecting controller” presented in [192] reflects estimated environment stiffness to an impedance controller deployed at the HSI device. Furthermore, a model-mediated multi-operator and multi-teleoperator TPTA controller based on exchanged haptic impedance models is presented in [149].

The idea of integrating a geometric model of the remote environment is firstly presented in [144]. Here, the so called “predictive display” is proposed which consists of a virtual-reality 3D simulation of the remote TOP and its environment that is overlaid onto the remotely received and delayed visual feedback. This helps the human OP to predict the motion of the TOP during his/her active positioning control which supports an intuitive and stable operation of the TPTA system with increased fidelity and task performance. A combination of a predictive display and impedance-reflection control is proposed by Huijun *et al.* [114]. The authors in [140] suggest further improving this approach by integrating a laser range finder in order to support the model generation process. Also haptic multi-contact point sensors can be used to estimate the structure and orientation of the remote surface in contact, as shown in [27]. These approaches may also be applicable to virtual TPTA scenarios, where surface characteristics are directly obtained from the triangle in contact that is used for rendering the haptic feedback.

With increasing complexity of the environment models, the amount of model parameters to be estimated and, in consequence, the amount of required model training data increases. Hence, the application of complex environment models adds an additional lag to the haptic feedback. This drawback is an argument for the concept of *model-mediated teleoperation*, which uses rudimentary geometry and impedance models with small parameter sets [78, 138, 139]. To this end, Mitra *et al.* propose to keep the model as simple as possible by assuming fixed linear stiffness and only adapting the virtual model location to the current TOP contact position [139]. The reduced parameter set guarantees frequent model updates and quick adaptation to geometric changes of the remote surface structure. On the downside, the simpler the haptic models become, the higher is the probability of incorrect haptic predictions, leading to a trade-off between model complexity and feedback rendering performance. In order to compensate for a possible discrepancy between the locally applied environment model and the haptic properties of the remote surface in contact, the haptic models need to be estimated and exchanged at a high rate. Nevertheless, certain disturbing artifacts like “phantom walls” and “delayed contact feedback” cannot be avoided in scenarios with significant communication latency. In this context, an experimental study presented in [139] investigates the user preferences of different transition mechanisms for locally updating the environment models at the HSI device. The presented results indicate that users prefer an active slow fading from the currently applied model configuration to the updated model parameterization and dislike abrupt or passive update strategies.

Experimental studies presented in [149, 181, 189] confirm significant benefits and improvements of model-based control in terms of system transparency, i.e., increased fidelity and improved perceived realism.

2.1.4 Evaluation Methods

Methods for determining the quality of experience and task performance of a TPTA system are instrumental for the development and design of the components of a TPTA system. In the following, subjective and objective evaluation methods for multimodal TPTA systems are briefly discussed.

2.1.4.1 Subjective Evaluation Methods

Subjective evaluation methods investigate so-called human factors which reflect a subjective impression of the human OP on the perceived performance and quality of the TPTA system. A subjective measure of presence can be estimated, for instance, via post-test questionnaires containing different questions on the perceived degree of immersion and experienced quality of the displayed multimodal feedback (see [162, 195]). In contrast to direct “presence” measurement, psychophysical experiments can be performed which focus on the detection of absolute and/or relative discrimination thresholds and the identification of preferences within displayed multimodal stimuli. The general assumption of such psychophysical evaluation is that the TPTA system provides a high-degree of immersion as long as the difference between the remotely captured and the locally displayed stimuli or property stays within human discrimination thresholds.

Several techniques exist for investigating perceptual discrimination thresholds. The *method of magnitude estimation* is based on subjective ratings reflecting the intensity of perceived stimulus’ deviation/distortion. Another method called *method of constant stimuli* is based on a pairwise comparison of constant stimuli that are sequentially presented to the subject. Furthermore, the *method of adjustment* allows the subject to directly control the intensity of stimulus deviation in order to detect the discrimination thresholds in pending stimuli.

Table 2.1 illustrates the subjective rating scheme for the *method of magnitude estimation* that is used in several experiments in this dissertation. It allows for a psychophysical evaluation of the perceived intensity of introduced compression distortion during lossy haptic compression. The detected discrimination thresholds can be used to perceptually adapt the system to the fidelity of the human haptic perception system and/or the display capabilities of the deployed feedback devices. As every human is characterized by individual perception thresholds, a statistical analysis of the obtained subjective results is required to determine conservative perception bounds that apply to the majority of humans. In addition to the calculation of the expected mean and standard deviations, the univariate variance analysis (ANalysis Of VAriance, ANOVA) is often applied to investigate statistical significance.

A comprehensive overview of subjective presence measurements is presented in [117].

2.1.4.2 Objective Evaluation Methods

Objective performance evaluation methods typically focus on the task performance of the human operator. In this context, variables for an objective evaluation are for instance the task completion time, error rates and the learning factor [44]. The task completion time represents the time span from the beginning to the completion of a given task. The task error rate describes the frequency, type and size of errors that occur during the execution of a given task. Task repetitions usually lead to a decrease in task completion time and

Description	Rating
no difference	100
perceptible, but not disturbing	75
slightly disturbing	50
disturbing	25
strongly disturbing	0

Table 2.1: Rating scheme used for subjective evaluation.

error rate which can be reflected by a task learning factor. A statistical analysis of these objective variables among all subjects allows for the determination of an objective rating of system performance. Several studies show that the haptic modality has a significant impact on the task performance of a TPTA system. Both the OP's immersion as well as the task performance may improve when the OP is provided with visual-haptic feedback as opposed to visual feedback only (see [33, 55, 65, 68, 132, 180]).

Another important class of objective evaluation methods is based on the *concept of transparency*. The term *transparency* describes the degree of immersion that is provided to the human OP. If the OP feels like directly interacting with the remote real or virtual environment, the system is considered to be *transparent* (see [137, 168, 169, 192]). Several definitions and metrics for describing the transparency of a TPTA system have been proposed. According to Handlykken *et al.*, an ideal TPTA system should act as a massless and infinitely stiff mechanical system connecting the human OP with the remote environment [88]. Similarly, Yokokohji *et al.* propose an ideal TPTA system to be characterized by guaranteeing identical positions and forces at the OP (x_h, f_h) and the TOP (x_e, f_e) side during the TPTA session [200], hence

$$\forall t : \begin{cases} \mathbf{x}_e(t) = \mathbf{x}_h(t) \\ \mathbf{f}_h(t) = \mathbf{f}_e(t) \end{cases} \quad (2.6)$$

Lawrence uses the displayed impedance of contacts with the remote environment as a metric to define transparency [131]. Accordingly, the impedance felt by the human user Z_h and the environment impedance Z_e must be identical in a fully transparent TPTA system.

$$Z_h(t) = Z_e(t) \quad (2.7)$$

However, ideal transparency as defined in (2.6) and (2.7) is not achievable due to several factors, such as the influence of system dynamics, a limited amount of degrees of freedom, communication latency, unpredictable changes in system behavior, etc. In addition, TPTA systems are constrained by a fundamental trade-off between stability and transparency (see [90, 93, 131]). Therefore, a metric for transparency can only reflect the distance to an ideal but unreachable degree of transparency. This distance to the ideal point of operation can be used as an objective quality metric. It is typically obtained by integrating over the display error in \mathbf{x} , \mathbf{f} and/or Z . However, this metric of TPTA performance does not incorporate any characteristics of the human haptic perception system.

To address this issue, so called *perceived transparency* as an perceptual objective metric has been presented in [107]. It uses Weber's Law of Just Noticeable Differences (JND) to perceptually evaluate the difference between the environment impedance Z_e and the displayed impedance Z_h (see also [64]). As long as the impedance Z_h displayed to the human OP stays within imperceptible bound defined by $Z_h \in [Z_e - \text{JND}, Z_e + \text{JND}]$, the TPTA system is expected to be transparent to the human OP.

2.2 Human Haptic Perception

The development of haptically enabled systems requires a fundamental understanding of the human haptic perception system. This enables the adjustment and optimization of the performance and fidelity of haptic devices and haptic signal processing algorithms to ensure compliance with the characteristics and limitations of the human haptic perception system. In particular for the development of lossy haptic compression algorithms, detailed knowledge about perceptual discrimination thresholds is of great relevance.

2.2.1 Human Haptic Perception System

Human haptic perception describes the human sense of feeling and the sense of touch. It involves two separate perception systems, namely the kinesthetic sense (also called "proprioception") and the tactile sense (see [82]), which are briefly discussed in the following:

- *The kinesthetic sense:* The kinesthetic perception system refers to the sense of the posture of limbs, limb movements and the perception of applied forces and torques stressing on extremities. In addition, the kinesthetic sense provides information about stimulus' derivatives such as velocity, acceleration, force changes, etc. This enables the identification of physical properties such as stiffness, viscosity and inertia of currently touched objects. The kinesthetic sensory information is captured by mechanoreceptors which are located at the muscle spindles. They respond to changes in muscle length which allow for measuring muscle activity. Compared to the tactile perception system, the amount of involved mechanoreceptors is much smaller and its density and distribution depend on muscle size. A comprehensive overview of the human kinesthetic perception system is presented in [121].
- *The tactile sense:* Tactile perception refers to the sense of touch located on the skin. Several different types of mechanoreceptors enable the perception of tactile sensations, such as temperature, roughness, geometry and slippage of touched objects. Additionally, the vibrotactile sense is able to detect vibrations (repetitive pressure stimuli) within the frequency range of 3-500 Hz [85]. Psychophysical findings reveal that the sensitivity of tactile perception is not regularly distributed over the human body. The frontal face and the hand regions have the highest density of mechanoreceptors supported by a large amount of cortical space in the brain [120, 185]. Correspondingly, maximal tactile sensitivity can be found at the lip borders and the fingertips [79, 120, 170]. A detailed discussion on human tactile perception can be found in [161].

2.2.2 Limitations of Human Haptic Perception

The human perception system maps physical stimuli to sensation effects in the brain. These dependencies can be mathematically described with psychophysical functions for every sense of the biological perception system. Psychophysical functions are further characterized by absolute and relative perception thresholds.

Absolute perception thresholds describe the minimum intensity level of a just detectable stimulus. These thresholds often depend on temporal aspects of previously perceived stimuli and are therefore typically defined as a function of stimulus frequency. In addition, the relative perception thresholds describe discrimination thresholds of changes in perceived stimuli (see [59, 60, 190]). The German anatomist and physiologist Ernst Heinrich Weber was one of the first researchers who systematically and experimentally examined the relative perception thresholds of the human perception system [190]. Weber's research revealed that over a large dynamic range, the perception of relative changes in stimulus is linearly proportional to the stimulus intensity itself. This observation was found to apply to almost every biological sense (see [28, 44, 81, 84, 170, 178, 190]). Later, Fechner proposed a logarithmic scale to map a physical stimulus to the perceived intensity of the corresponding sensation in the brain [67]. Similarly, Stevens suggests using a power function to describe corresponding psychophysical dependencies [174]. Interestingly, Dohaene finds the predictions of the linear and the logarithmic model to perform essentially equivalently, and favors the linear model due to its simplicity [66].

Research in psychophysics typically uses Weber's Law of the Just Noticeable Differences (JND) to model relative discrimination thresholds. It describes a constant ratio between the intensity of a pending stimulus and the maximum change in intensity that is just not noticeable. For example, during a strong force stimulus, a small absolute change in force intensity might not be perceivable. But it becomes clearly perceivable during a smaller applied pending force stimulus.

Weber's Law of the JND can be mathematically described by the following implication

$$\frac{\Delta I}{I} = \kappa = \text{const.} \quad \text{or} \quad \Delta I = \kappa I \quad (2.8)$$

where I is the stimulus intensity, ΔI is the so called Difference Threshold or the JND and κ is the constant *Weber fraction* (also called "relative difference limen" [170]). It describes the smallest amount of change in stimulus I which can be detected just as often as it cannot be detected.

2.2.2.1 Perceptual Limits of the Kinesthetic Perception System

Psychophysical experiments on absolute detection thresholds of limb position perception reveal different results if the limb is actively moved by muscle contraction or passively moved by the experimenter [121, 148]. With active positioning, the position error of the outstretched arms is on average 0.6° , in contrast to an average position error of 2.0° if the limbs are passively moved. These thresholds differ for other joints and limbs. For instance, Taylor *et al.* report absolute detection thresholds of position changes of hand joints in a range of $4.4\text{--}6.8^\circ$ [179]. Experimental studies presented in [53, 123] investigate the relative discrimination thresholds for the perception of limb velocity. Their results reveal a Weber fraction of 8% for

Variable	Resolution	Weber fraction
Limb movements	0.5-1°(over 10-80° /s range)	8% (range 4-19%)
Limb position	0.8-7°(full range of motion)	7% (range 5-9%)
Force	0.06 N	7% (range 5-12%)
Stiffness	Not available	17% (range 8-22%)
Viscosity	Not available	19% (range 13-34%)
Inertia	Not available	28% (range 21-113%)

Table 2.2: Perception thresholds of the kinesthetic sense (reproduced from [121]).

the elbow and finger joints meaning that only changes in limb velocity with at least 8% of the magnitude of the limb movement can be perceived.

The human discrimination ability of force perception has also been intensively studied in literature. Surprisingly, relative perception thresholds of force feedback seem to be not completely independent from the intensity of force being applied. Jones reports a Weber fraction of 7-10% within large force dynamics from 0.5 N to 200 N and increased Weber fractions within the range of 15-27% for forces with low intensity below 0.5 N [121].

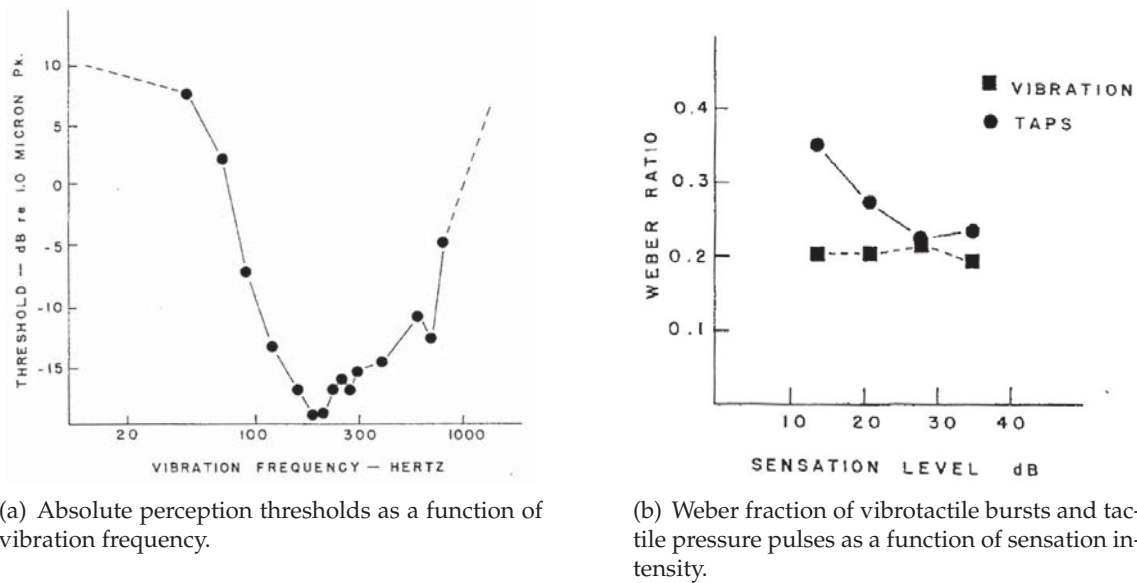
Interestingly, psychophysical studies of derived kinesthetic quantities such as environment stiffness, viscosity, inertia, etc. also revealed the existence of absolute and relative perception thresholds. For instance, experimental results presented in [64] reveal a Weber fraction of 8-12% for the discrimination of environment stiffness.

An overview of the resolution and relative discrimination thresholds (i.e. Weber fraction) for limb movement, limb position, force, stiffness, viscosity and inertia is illustrated in Table 2.2 (from [121]). A comprehensive psychophysical study of the Weber fractions of human force perception is presented in [113]. An additional collection of haptic perception thresholds reported in literature can be found in [104].

2.2.2.2 Perceptual Limits of the Tactile Perception System

The absolute detection thresholds of a tactile stimulus is strongly affected by the frequency of the stimulus (see [175, 186]). Figure 2.4(a) illustrates the absolute thresholds of vibrotactile perception as a function of vibration frequency in a range from 10 to 1000 Hz [170]. The results indicate low vibrotactile sensitivity within the frequency band from 10 Hz to 50 Hz. The highest perceptual sensibility can be found around 250 Hz which quickly degrades with rising frequency.

Figure 2.4(b) shows the relative perception thresholds (described by the Weber fraction) of vibrotactile and constant skin pressure stimuli as a function of logarithmic sensation level [170]. Interestingly, the Weber fraction for tactile stimuli varies under different conditions and at different skin locations. For instance, Craig investigates the perception of pulsed stimuli at the index finger and determines a Weber fraction of 0.2 (see [59, 60]). In contrast, the human discrimination ability of static skin pressure under same conditions is characterized by a Weber fraction of 14 % [37].



(a) Absolute perception thresholds as a function of vibration frequency.

(b) Weber fraction of vibrotactile bursts and tactile pressure pulses as a function of sensation intensity.

Figure 2.4: Absolute and relative perception thresholds of tactile stimuli (reproduced from [61] and [170]).

The authors in [119] show that also simultaneous masking effects influence human tactile perception. Their results indicate that both, absolute and relative perception thresholds increase as soon as a vibrotactile masker is simultaneously displayed. Their results show that during masking conditions, the Weber fraction raises from 13%-38% and 14%-28% to 60% and 46% for the vibrotactile and static pressure, respectively.

2.3 Haptic Data Compression

Methods to compress data for efficient storage and/or transmission have been investigated for a long time. By encoding the desired information with fewer information units (bits) than the corresponding not-encoded representation consumes, the amount of data can be reduced without any loss of information. This can be achieved by reducing any type of redundancy in the original signal representation, for instance by applying entropy coding techniques (i.e., Huffman, arithmetic, runlength coding, etc.). As no information is lost during this process, these compression methods are completely reversible; they are denoted to be lossless. By contrast, in the field of compression methods for multimedia content, the so-called lossy compression algorithms are attracting considerable interest and are widely applied in modern multimedia applications. Here, not only redundancy is removed. These systems explicitly detect and remove so called "irrelevant information" from the processed data, which either is either not perceivable by the human perception system or cannot be displayed to the human through integrated hardware and/or connected interfaces due to hardware limitations. In this context, the availability of a perceptual model becomes highly interesting. If compression is done without affecting the quality and without disturbing the performance of the underlying system, the applied signal processing methods are consid-

ered to be transparent. Perceptual lossy compression often achieves very high compression rates.

Compared to the processing of audio and video signals, the real-time processing of haptic signals is by far more sensitive to introduced latency. Due to the global control loop that is closed by the communication system, the processing of haptic signals is restricted by hard delay constraints. They disallow the use of block-based coding approaches, such as DCT, DWT, Vector Quantization, etc., which are widely used in the field of audio and image/video coding. In other words, common video and audio compression algorithm cannot be directly applied on haptic signals.

2.3.1 Related Work

Early approaches to haptic data compression can be found in [78, 146, 165, 166], where adaptive sampling and quantization techniques for haptic signals are discussed and compared with each other. In [39] and [38], predictive coding for haptic signals based on Differential Pulse Code Modulation (DPCM) and Adaptive Differential Pulse Code Modulation (ADPCM) combined with Huffman coding are used to reduce the load on the haptic channel. Similarly, a differential haptic encoding scheme with subsequent entropy coding is presented in [126]. These differential coding approaches, however, only reduce the payload on the haptic channel and do not address the challenging high packet rates of haptic communication.

First research specifically targeting the high packet rates in networked control loops can be found in [147]. Here, the concept of deadband-based data reduction is proposed. In this work, incoming sensor readings are compared to the most recently transmitted sensory information. Only if the difference in magnitude exceeds a fixed threshold, a packet transmission is triggered. Correspondingly, the signals to be transmitted are adaptively down-sampled and transmitted at an irregular rate. The receiver reacts to dropped samples by repeating the most recently received sample (hold-last-sample, HLS). This approach has been shown to successfully reduce network transmission during intervals of low frequent signal trajectories. However, it does not specifically exploit limitations of the human perception system.

First lossy perceptual compression for haptic data which explicitly incorporates a model of human haptic perception have been presented in [98, 101, 103, 108, 110] and investigated in terms of stability criteria in [50, 104, 105, 109, 108, 130]. In this work, the perceptual deadband (PD)-based compression approach (or in short "deadband approach") is introduced which successfully combines a perceptual model with deadband coding. This enables the adaptive control of the intensity of compression artifacts to ensure remaining below human perception thresholds. The PD compression scheme significantly reduces the packet rates on the haptic communication channel without adding any latency to the processed signals. Early research on the PD compression focuses on haptic signals with a single-DoF. However, most TPTA systems provide haptic interaction in multi-DoFs. An important step towards the integration of PD-based compression in multi-DoF TPTA scenarios is presented in [100]. Here, the authors propose the construction of an isotropic deadzone which is explained in detail in Section 2.3.3.

The performance of PD compression has been evaluated in a number of real-world and simulated TPTA systems. Conducted experiments in [103] reveal a packet rate reduction

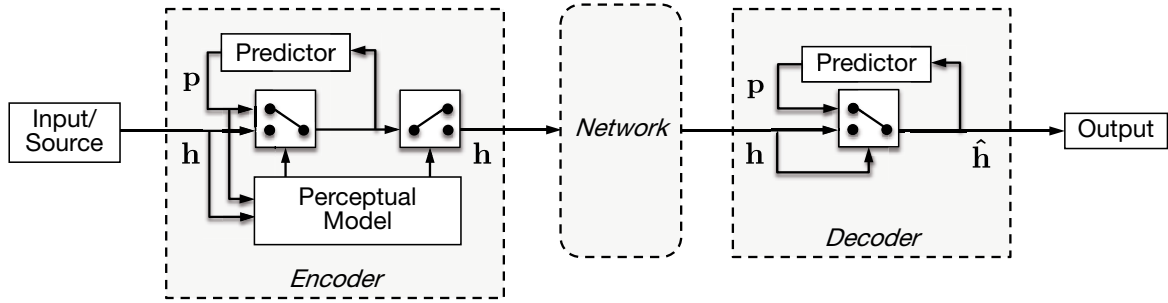


Figure 2.5: Illustration of perceptual predictive coding.

of up to 85% for a single-DoF TPTA system. Even higher reduction rates of up to 90% are reported for multi-DoF TPTA scenarios, reported in [98]. A detailed discussion of the PD compression approach can be found in Section 2.3.3.

In [54, 99, 158, 159], the PD compression approach is combined with several signal prediction algorithms. A performance comparison of haptic prediction approaches in the context of PD compression is presented in [203]. Further improvements in haptic signal prediction can be achieved if sensor noise is removed with the help of a Kalman filter, as shown in [102]. The use of an adaptive reconstruction filter for improved upsampling of PD-encoded haptic signals is discussed in [15].

A comprehensive discussion on perceptual haptic compression and communication is presented in [4, 5, 97, 98, 130].

2.3.2 Perceptual Predictive Compression Scheme

Detailed knowledge about human haptic perception is essential for determining the degree of perceived distortion when coding haptic signals in a lossy way. To this end, findings on haptic discrimination thresholds from the field of psychophysics are instrumental in perceptually evaluating changes in haptic signals (see Section 2.2.2). They can be used to construct a mathematical model of human haptic perception which combines multiple perceptual functions across different domains and modalities. In case of parallel and simultaneously interfering stimuli, masking effects can be integrated as well. In line with common lossy compression algorithms from audio and video coding, a perception model of the human haptic sense can be used to control the intensity of coding artifacts in order to keep them continuously within imperceptible ranges, as shown in the following.

The principle of perceptual predictive haptic data compression is illustrated in Figure 2.5. It consists of two key components: a psychophysical model deployed at the encoder and two signal predictors which are used at the encoder and the decoder. The prediction algorithm estimates incoming haptic samples based on previously transmitted haptic data. Both predictors at the encoder and the decoder run in parallel and are both being fed with identical signal information in order to keep them strictly coherent. At the encoder, the prediction error is psychophysically evaluated with the help of a psychophysical haptic model. As long as the difference between the incoming and the predicted haptic samples stays within imperceptible bounds, no network transmissions are required and the predicted sample at the

decoder can be output. If the difference between the incoming and the predicted haptic sample exceeds the applied perception thresholds at the encoder, additional signal information is sent over the network which also updates the predictors.

2.3.3 Perceptual Deadband Approach

Research by Hinterseer *et al.* has shown that a simple yet effective psychophysical model of human haptic perception suitable for haptic real-time communication can be built based on Weber's Law of JND (see [98, 103, 108] and Section 2.2.2). It is based on *perceptual deadbands* (PD) which describes haptic discrimination bounds according to Weber's Law of JND. In this context, the PD parameter k , which closely relates to the Weber threshold parameter κ , is introduced. It defines the relative size of the perceptual bounds. Deployed in the previously discussed perceptual predictive compression scheme, it enables to perceptually communicate the haptic signal in a lossy but to the human user imperceptible manner.

As long as incoming haptic samples \mathbf{h}_i do not violate the applied perception thresholds around the predicted samples \mathbf{p}_i , the prediction error is assumed to be imperceptible. Hence, the input sample \mathbf{h}_i can be discarded and the predicted sample at the decoder \mathbf{p}_i is output $\hat{\mathbf{h}}_i = \mathbf{p}_i$. Correspondingly, if \mathbf{h}_i violates applied perception thresholds, it is considered to be relevant for transmission and used to update the predictors and the output at the decoder $\hat{\mathbf{h}}_i = \mathbf{h}_i$. The output of the PD compression approach can be defined by

$$\|\mathbf{p}_i\|_2 \cdot k \begin{cases} < \|\mathbf{p}_i - \mathbf{h}_i\|_2 & \text{transmit haptic input sample } \mathbf{h}_i \text{ and output } \mathbf{h}_i \\ \geq \|\mathbf{p}_i - \mathbf{h}_i\|_2 & \text{discard haptic input } \mathbf{h}_i \text{ and output predicted sample } \mathbf{p}_i \end{cases} \quad (2.9)$$

In multi-DoF scenarios with multidimensional haptic sample vectors, (2.9) corresponds to the construct of an isotropic perceptual deadzone located at the tip of each haptic sample vector [100]. In the two-DoF case, this results in a circular perceptual deadzone. Likewise, the three-DoF case leads to a spherically shaped perceptual deadzone. Similar to the single-DoF perceptual compression approach, the volume of the radius of the circular/spherical deadzone in the multi-dimensional case is defined by the amplitude (i.e., intensity) of the haptic sample vector.

Figure 2.6 illustrates the multi-DoF PD for two-DoF and three-DoF scenarios. The size of the circular/spherical PD is a function of the length of the haptic vector. As long as incoming haptic sample vectors fall within the circular PD or spherical PD (as shown in Figure 2.6(a) and Figure 2.6(c), respectively), the change in haptic signal is expected to be imperceptible. In contrast, as soon as a deadband violation occurs, a perceptually noticeable change in the haptic signal is assumed, as illustrated in Figure 2.6(b) and Figure 2.6(d).

As only the samples which violate the PD bound are considered for transmission, the PD compression scheme enables to reduce the amount of packet transmissions while keeping corresponding processing latency at an absolute minimum.

2.3.4 Haptic Signal Prediction

A signal prediction algorithm estimates future haptic samples based on previous signal input. For the prediction of haptic signals, typically linear predictors of very low order (e.g.

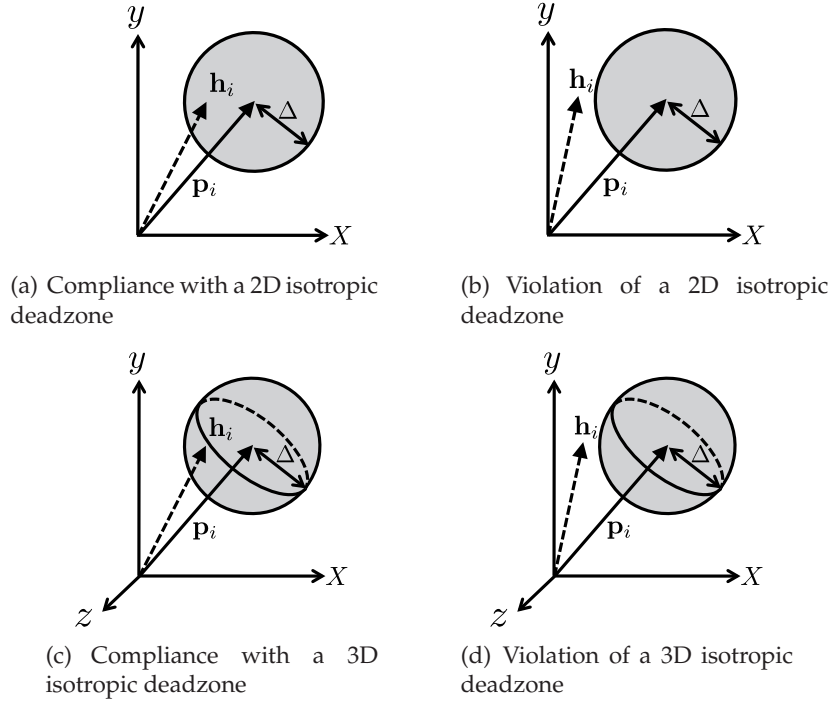


Figure 2.6: Illustration of compliance and violation events of multi-DoF isotropic perceptual deadzones. The predicted haptic sample \mathbf{p}_i defines the circular/spherical deadzone which is used to perceptually evaluate the haptic input sample \mathbf{h}_i .

order one) are deployed to comply to the strict delay constraints which are required to maintain control loop stability. They successfully model the low frequency characteristics of haptic signals while still being able to quickly adapt to transients during contact events due to their low group delay.

2.3.4.1 Zeroth-order Prediction

A zeroth-order predictor estimates future haptic samples by simply repeating its most recently received input sample (hold-last-sample algorithm, HLS).

Combined with the concept of PD compression, the size of the applied perception threshold Δ_i at discrete time i , it is a function of the PD parameter k and the signal magnitude of the most recently transmitted haptic sample $|\mathbf{h}_{i-m}|$, where m samples back in time the last violation of applied perception thresholds took place. This can be described by

$$\Delta_i = \Delta_{i-1} = \dots = \Delta_{i-m} = k \cdot |\mathbf{h}_{i-m}|. \quad (2.10)$$

This process of PD compression using a zeroth-order predictor and perceptual thresholds defined by Weber's Law of JND is visualized in Figure 2.7. Samples illustrated with solid vertical lines represent the samples that are considered to be relevant for transmission. They define discrimination thresholds represented by PDs, illustrated as gray zones. The size of the applied PD is a function of a deadband parameter k and the signal amplitude of the

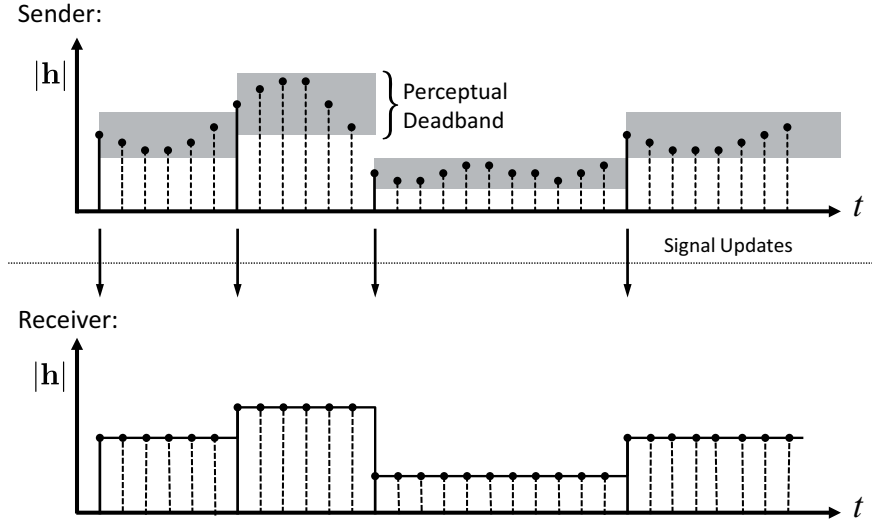


Figure 2.7: Perceptual deadband compression using a zeroth-order prediction (hold-last-sample) algorithm (adapted from [98]).

recently transmitted haptic sample value \mathbf{h}_{i-m} . Once the PD is violated by a new input sample, this input sample is transmitted and redefines the applied perception thresholds. Samples with dotted lines fall within the currently defined deadband and can be dropped as their change in signal is too small to be perceptible. In case of noisy sensors, a minimum absolute deadband size exceeding the current noise level should be defined [98].

2.3.4.2 First-order Prediction

The first-order prediction scheme as proposed in [99] takes the two most recently transmitted haptic signal updates \mathbf{h}_i and \mathbf{h}_j at time i and j into account. This allows for the calculation of a gradient \mathbf{c}_j

$$\mathbf{c}_j = \frac{\mathbf{h}_i - \mathbf{h}_j}{i - j} \quad \text{with } i > j > 0 \quad (2.11)$$

The predicted haptic sample \mathbf{p}_i at time $i \geq j$ is calculated by

$$\mathbf{p}_i = \mathbf{h}_j + \mathbf{c}_j \cdot (i - j) \quad (2.12)$$

The first-order prediction process combined with PD compression is illustrated in Figure 2.8. On the left side, the discrete predictor output is shown. The solid line illustrates the linear prediction of future haptic sample output based on the two most recently transmitted haptic samples. On the right side, the haptic input signal is visualized. With every predictor update, the PD is recalculated and applied (gray area) which enables to perceptually evaluate the perceptual quality of the predictor output. As long as the haptic input samples do not violate applied perception bounds, the haptic input samples can be discarded and the predicted sample is output. Only during events of PD violation, haptic samples need to be transmitted and are used for updating the predictors at the encoder and decoder.

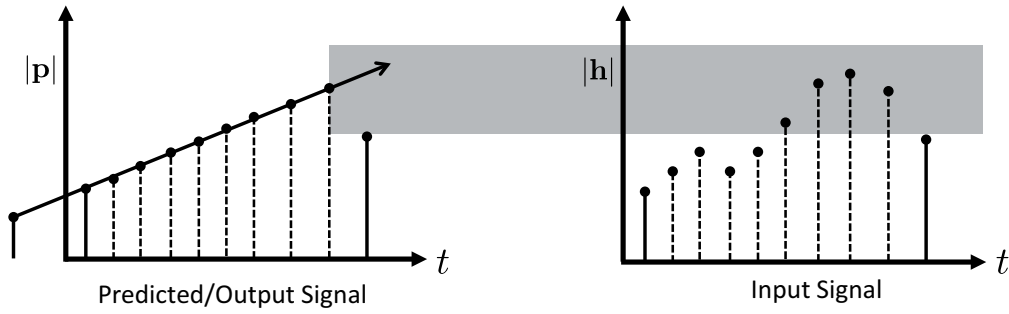


Figure 2.8: Perceptual deadband compression using a first-order prediction algorithm (adapted from [5]).

2.3.5 Perceptual Deadband Parameter k

The PD parameter k has a strong impact on compression performance and system transparency. It enables the control of the size of the applied perception bounds and, hence, needs to be carefully adjusted to match the characteristics of human haptic perception and the haptic display capabilities of the HSI device. With increasing parameter k , the amount of transmitted updates on the communication channel decreases at the cost of increased signal distortion. Optimal compression performance can be reached if the PD parameter k is set to a maximum value where compression distortion is still kept within imperceptible perception bounds. Such optimal configuration can be experimentally determined by investigating the transparency of the compression system for different values of k . As long as a loss of data is not noticeable to the human OP, the system transparency of the TPTA should not be affected.

Interestingly, an optimal configuration for k varies widely in literature. For example, Hinterseer *et al.* find a threshold for the detection of PD-induced compression artifacts in a force feedback signal at around $k = 2.5 - 7.5\%$ [103], whereas Nitsch *et al.* find no significant feedback quality deterioration with PD parameters of $k \leq 15\%$ [143]. Furthermore, Hirche *et al.* report thresholds to range between $k = 7.5\%$ and $k = 20\%$ [110]. In specialized TPTA scenarios where an accurate representation of small contact forces is of great perceptual importance to the user (such as dealing with dangerous materials or touching fragile objects), experimental results in [20] reveal significantly increased PD threshold ranges (about $k = 50\%$). It seems that the distortion introduced by PD compression is less disturbing as long as the intensity of displayed force feedback stays within small bounds. This finding is also confirmed by Jones *et al.* in [121] who identify increased Weber fractions for forces below $0.5 N$.

Although in theory JNDs for force and velocity perception are approximately similar for all healthy human OPs [122], these results indicate that the optimum size of the PD parameter k is further influenced by various other factors. For instance, cross-modal interactions, particularly those related to visual sensory input, are known to affect human perception thresholds [171]. Results in [20] indicate an impact of visual feedback on the PD parameter k . An experimental study shows that participants receiving visual-haptic feedback from the remote environment are more sensitive to the PD compression artifacts compared to subjects presented only with distorted haptic feedback.

The perception of PD coding artefacts may be also influenced by the characteristics and limitations of the deployed hardware such as the frequency response, dynamic range, precision, and noise level. For the implementation of PD-based haptic compression, these results indicate that there is no single optimum PD threshold which may be universally applicable in all TPTA systems. As the human perception thresholds are affected by many factors such as the design of the TPTA system (amount of DoFs), cross-modal feedback, the environment, specific task criteria, etc., the PD parameter k should be individually optimized for every TPTA system in order to achieve the best possible compression performance.

2.4 Chapter Summary

With various applications in industry, medicine, space operation, etc., TPTA systems are gaining in relevance. Their performance strongly depends on the bidirectional exchange of haptic signals which is restricted by hard delay constraints in order to assure system stability and transparency. Furthermore, modern TPTA systems deploy a large number of DoFs which need to be individually sampled and controlled. This leads to high packet and data rates on the haptic communication channel. The unique properties of haptic communication disallow the adaption of block-based compression techniques from the field of audio and video compression.

The challenges of haptic communication are subject to intensive research and addressed by the perceptual predictive compression schemes. These schemes employ a mathematical model of human haptic perception which maps physical stimuli to perceived sensations. These psychophysical dependencies are characterized by absolute and relative perception thresholds. By exploiting the limitations of human haptic perception, the perceptual dead-band compression scheme only transmits haptic samples that are considered to be perceptually relevant in order to reduce the high transmission rates on the haptic channel. To this end, the haptic signals are perceptually downsampled while keeping introduced compression distortion below human haptic perception thresholds.

3 Perceptual Compression of Haptic Signals

As discussed in Chapter 2, haptic real-time communication in TPTA systems is restricted by strict delay constraints to maintain control loop stability and a high degree of system transparency. To keep the processing latency at an absolute minimum, haptic samples are typically transmitted immediately upon generation. In addition, currently available TPTA systems deploy a large number of DoFs which need to be individually sampled and controlled and therefore lead to high data rates on the haptic channel. Hence, the haptic sensory and actuator control data is exchanged at the haptic sampling rate, i.e., 1000 times per second for every DoF from the HSI to the TOP (forward channel) and from the TOP to the HSI (backward channel). In packet-switched networks, this transmission behavior leads to significant network overhead and puts high demands on the deployed network resources, especially in space and underwater TPTA scenarios.

The challenges of haptic communication are addressed by the perceptual predictive haptic compression scheme. It reduces the packet rate by considering only perceptually relevant haptic samples for transmission.

In this chapter, several contributions to the perceptual predictive compression scheme introduced in Section 2.3.2 are presented. The first two sections in this chapter focus on improving the *perceptual haptic model* and the *haptic signal prediction algorithm*, which are the main components of the PD compression scheme. To this end, the integration of additional psychophysical findings into the perceptual model are discussed in Section 3.1. Furthermore, Section 3.2 proposes the use of environment models for perceptual haptic communication. They allow for substituting the transmission of remotely captured haptic sensory data with locally rendered haptic feedback.

In addition to the delay critical real-time processing of haptic signals, growing demand can also be found in the area of offline haptic data processing. In training, teaching, entertainment, and documentation applications, the recoding of TPTA sessions is of fundamental interest. As soon as haptic data has to be stored on a storage device for posterior replay, the interest in offline compression algorithms for haptic data emerges. Due to the relaxed delay constraints, the design of a haptic offline compression scheme can be addressed in a fundamentally different way, as shown in Section 3.3

Furthermore, perceptual haptic communication is analyzed and studied from a theoretical perspective. To this end, a theoretical framework is proposed which enables a mathematical performance evaluation of the PD-compression scheme. With the help of a statistical model of haptic signals, the average data rate and computational resources required for the compression of haptic signals can be expressed as a function of the PD parameter k , as shown in Section 3.4.

3.1 Extended Psychophysical Model for Perceptual Haptic Data Compression

A precise psychophysical model of human haptic perception is of fundamental interest for the development of perceptual haptic data compression algorithms. This section discusses the integration of additional findings from psychophysics into the perceptual deadband approach (see Section 2.3.3). This promises improved adaptation to human haptic perception thresholds.

The work presented in this section has been conducted in cooperation with Iason Vittorias, Verena Nitsch, and Rahul Gopal Chaudhari [3, 14].

3.1.1 Direction-dependent Multi-DoF Perceptual Deadzone

Most TPTA systems provide haptic interaction with multiple DoFs. Consequently, the haptic sensory and control signals to be compressed consist of multi-dimensional haptic sample vectors. In this context, Hinterseer *et. al* propose the construction of an isotropic deadzone (see Section 2.3.3). It assumes the human haptic perception thresholds to be independent from the direction of the pending stimulus and from the direction of stimulus change.

This is in contrast to psychophysical experiments presented in [21] which reveal that the multi-DoF equivalent of the single-DoF perceptual deadzone is not isotropic. In this study, the discrimination thresholds of pairwise presented force feedback stimuli of changing direction are investigated. The results indicate that haptic perception thresholds are a function of stimulus direction.

Interestingly, psychophysical experiments published in [31, 176] show that the human discrimination ability of changes in force direction is independent from the direction of the reference force. This effect was shown to be valid for force vectors with varying force intensity. In summary, these experimental results suggest applying individual discrimination thresholds to force direction and force intensity.

3.1.1.1 Proposed Perceptual Model

By taking both the psychophysical findings of directional discrimination thresholds for changes in force intensity and the analysis of the discrimination ability of force direction into account, a direction-dependent multi-DoF deadzone for haptic data compression can be constructed. According to [31, 176], the discrimination thresholds for changes in direction of force feedback can be isotropically defined by an angle α , hence independent from the direction of the currently applied haptic force sample \mathbf{f} . In contrast, the perception thresholds $\Delta^{\mathbf{f}}$ for changes in magnitude of \mathbf{f} are defined as a function of the pending force direction and Weber's Law of JND in order to reflect the findings from [21]. The resultant deadzone shape takes the form of a frustum of a cone, as illustrated in Figure 3.1.

Similar to the application of the Weber-based isotropic deadzone (see Section 2.3.3), this novel deadzone shape can be used for perceptually evaluating changes in haptic force feedback signals. As long as current haptic force feedback vectors \mathbf{f} fall into the adaptively constructed perceptual cone frustum, they are considered to be irrelevant for transmission. Ac-

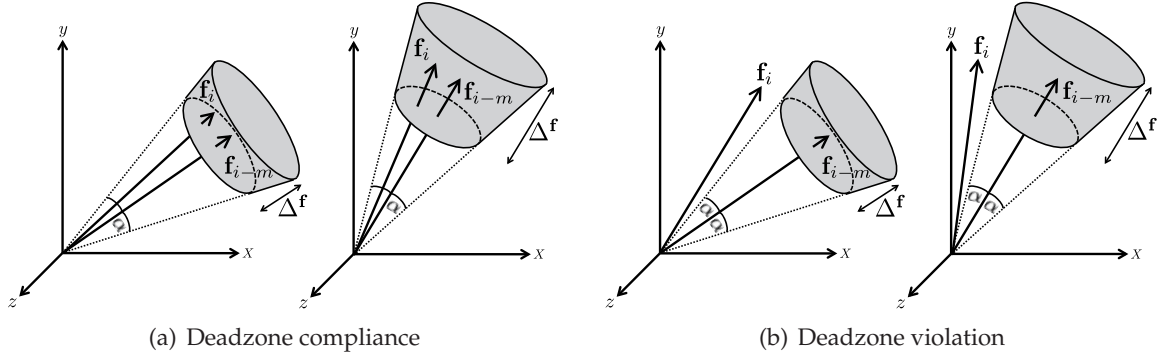


Figure 3.1: Illustration of the construction of a direction-adaptive deadzone. \mathbf{f}_i describes the current incoming haptic sample vector (adapted from [14]). \mathbf{f}_{i-m} represents the haptic reference sample vector. Discrimination thresholds for changes in force direction are defined by the isotropically uniform angle α . Perception thresholds for changes in magnitude are a function of the reference force intensity $\|\mathbf{f}_{i-m}\|$ and described by Δ^f .

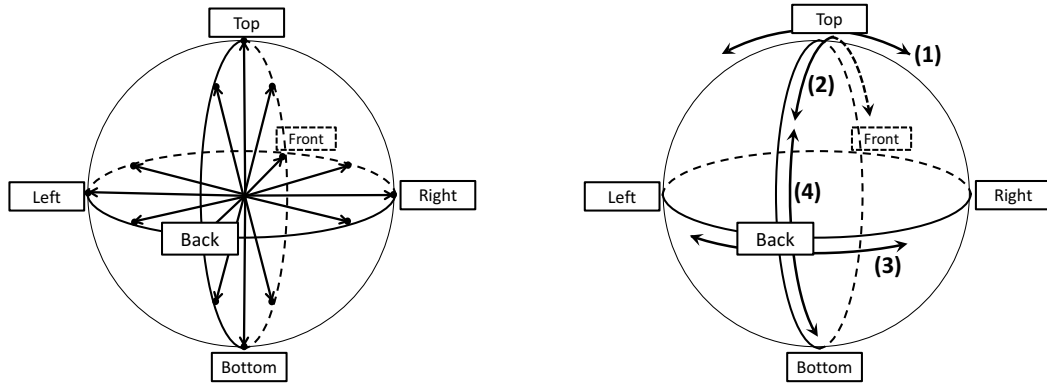
cordingly, as soon as haptic samples violate the pending PD, they need to be sent over the network and are used for redefining the perceptual thresholds.

3.1.1.2 Experimental Study

In order to investigate the performance of the direction-dependent PD model, an experimental evaluation with human subjects has been conducted. The experimental testbed consists of a Phantom Omni device by SensAble Technologies [163] and a virtual telepresence simulation that provides visual-haptic interaction with a virtual touchable sphere. During the experiment, movements by the haptic device are mapped to a spherical cursor which represents a virtual TOP. During contact with the virtual TPTA environment, contact forces are rendered and displayed using the haptic rendering routines provided by the *CHAI3D* haptic rendering library [57].

In the experiment, eleven students from the Institute for Media Technology, TUM participated. Initially, they are familiarized with the experimental setup and the expected distortion effects that are introduced by PD compression. This training phase ensures that all participants are approximately at the same level of training, as far as the detection of possible signal disturbances is concerned. Furthermore, the subjects are instructed to hold the haptic device tightly with fixed hand orientation towards the haptic device. This ensures the maintenance of a more or less consistent orientation of the hand throughout the experimental procedure. The conducted experimental evaluation consists of three parts which are performed sequentially, as explained in the following.

The first experiment investigates the PD parameter k as a function of force feedback direction. To this end, a virtual TPTA simulation is designed that provides full control of the displayed force feedback orientation without imposing limitations on haptic user interaction. This is achieved by presenting an invisible but touchable plane of infinite size in the simulated virtual environment. As no friction effects are applied during contact with the vir-



(a) Illustration of the 14 sample points on a unit sphere in the three-dimensional vector space used for investigating the dependencies of force feedback directions on the perception of PD data reduction artefacts.

(b) Illustration of the contact paths on the touchable virtual sphere object that are used for investigating discrimination thresholds of changes in force feedback direction.

Figure 3.2: Overview of sampled orientations and investigated contact paths used in the experimental study (reproduced from [14]).

tual plane, the direction of force feedback is aligned with the surface normal of the presented plane. This enables the control of the direction of displayed force feedback by modifying the orientation of the virtual plane. In the experiment, the three-dimensional space of force feedback orientations is investigated at 14 sample points, which are shown in Figure 3.2(a). They are randomly selected for each run in the experiment. During contact with the virtual plane, virtual contact forces are haptically rendered and sent to the PD compression scheme. In this way, the subjects experience distorted contact forces as a result of applied lossy PD compression. The subject can manipulate the applied PD parameter k within a predefined range of 0% to 20% and with a resolution of 0.5%. During each run, the user is instructed to tap upon the surface of the virtual frictionless plane in a direction more or less perpendicular to its surface while searching for a maximum setting of the associated PD parameter k at which no disturbance is felt in the haptic feedback. Furthermore, each of the 14 force feedback sample directions is tested twice - once by approaching the target setting of k by slowly decreasing from a maximum value of $k = 20\%$ and a second time by slowly increasing the parameter value from the minimum parameter value $k = 0\%$ to the preferred user setting. Hence, every subject performs 28 runs in total.

A second experiment is performed to determine the thresholds of perceptual sensitivity regarding directional changes of force feedback perception. The subjects are provided with a virtual TPTA scenario containing a touchable virtual sphere. They are instructed to rub on the frictionless surface of the sphere while corresponding contact forces are rendered and displayed in the direction along the vector from the sphere origin to the point of contact on the sphere's surface. In order to investigate the discrimination thresholds of changes in force direction, the orientation of the force vectors are uniformly quantized before being displayed. The quantization parameter α is controlled by the subject in steps of 0.5 degrees within a range from 0 to 5 degrees. Similar to the first experiment, the subjects are instructed to find a maximum setting of α at which compression distortion is perceptually just unno-

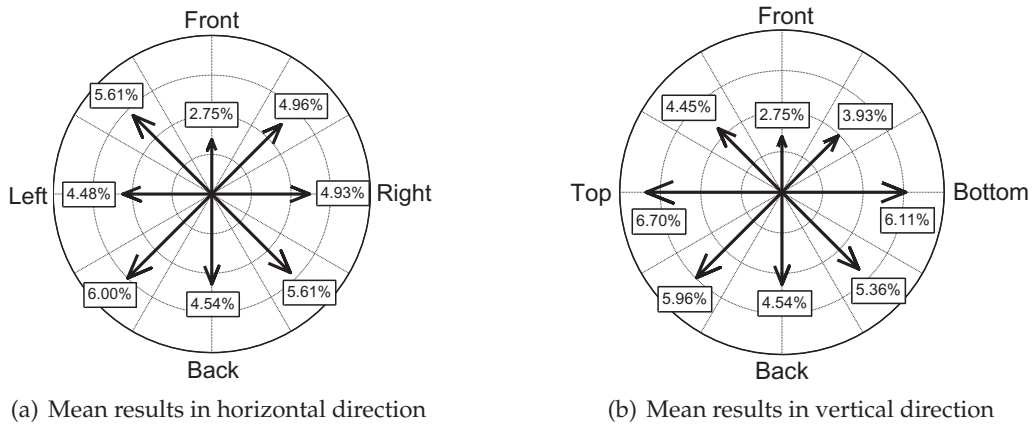


Figure 3.3: Experimental results of the first experiment investigating preferred PD parameters k as a function of force direction (reproduced from [14]). The sample points used are illustrated in Fig. 3.2(a). Note that the "front" and "back" force direction is identical in both figures.

ticeable. Furthermore, the subjects are instructed to rub along four different contact paths on the virtual sphere in order to investigate the influence of the direction of force feedback and the orientation of hand movements on the discrimination threshold of the inspected quantization parameter α . These four contact paths on the surface of the sphere are illustrated in Figure 3.2(b).

The third part of the experiment takes the results of the first two experiments into account, i.e., the direction-dependent PD parameter k and the isotropic discrimination threshold α for changes in force direction. These results are used for parameterizing the proposed adaptive perceptual deadzone with the subjective discrimination thresholds. In order to obtain a denser mesh of the direction related PD parameters, an interpolation step is applied by using the "inverse weighting distance" algorithm. This allows for estimating intermediate PD parameter values along other directions in three dimensional space. The simulated virtual environment in the third experiment again contains a touchable virtual sphere. During contact with the virtual object, rendered force-feedback is applied to PD data reduction and its output is displayed through the haptic device. The subject is given the freedom to freely switch between ten different PD configurations, i.e., disabled compression, the proposed direction-adaptive PD and eight isotropic PD configurations. The reference mode disables the haptic PD compression for displaying undistorted haptic feedback. The remaining nine selectable deadzone configurations are presented in randomized order. The configuration of the eight isotropic deadzones are $k = 1\%, 3\%, 4\%, 5\%, 6\%, 7\%, 8\%, 10\%$. During events of contact with the virtual environment, the haptic update rates are recorded for each of the provided PD configurations. In addition, the subjects are asked to subjectively rate the degree of perceived distortion between the reference (unencoded) and the lossy encoded haptic force feedback. Based on their subjective perception, they assess the influence of the applied PD configuration according to the rating scheme presented in Table 2.1 in Section 2.1.4.

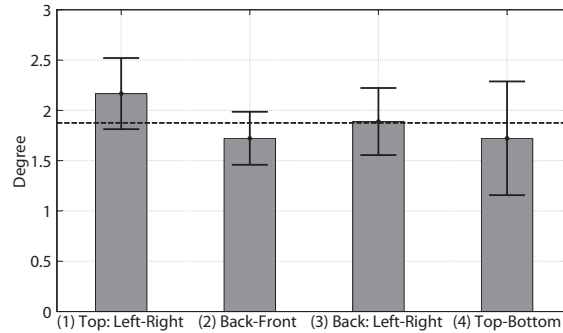


Figure 3.4: Means and standard deviations of angular thresholds quantifying the just perceptible change in the direction of force feedback for different reference force directions (reproduced from [14]). The dashed line illustrates the mean at 1.85 degrees across all test items.

3.1.1.3 Experimental Results

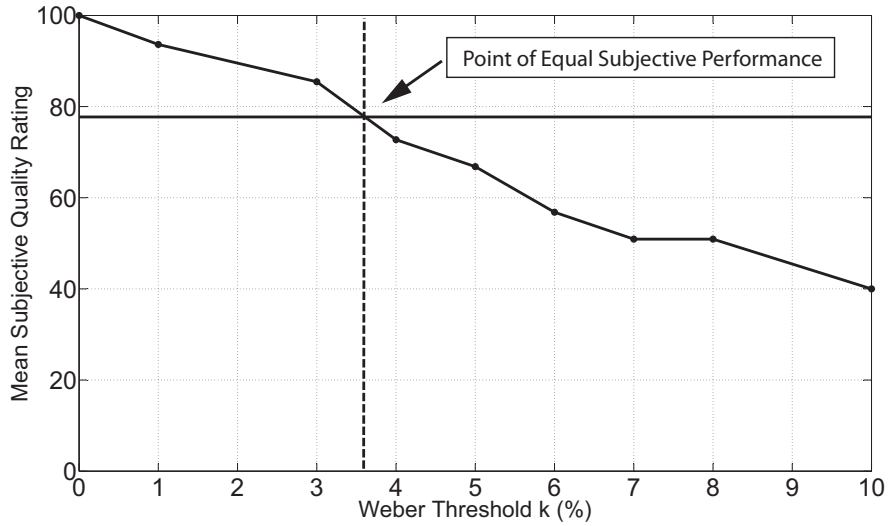
Figure 3.3 illustrates the results of the first part of the experiment. The figures show the PD parameter k determined for every force direction averaged across all the subjects and across the two runs per test-item. As is evident from this figure, the perception thresholds of disturbances arising out of the PD distortion artefacts vary for different directions of force feedback. Disturbance in force feedback with front orientation that pulls the operator’s arm towards the haptic device is detected with the highest sensitivity. Force feedback in an upward direction shows the lowest detection thresholds of PD distortion. When analyzing the results in the horizontal and vertical plane, a similar structure with increased PD threshold values in the diagonal force directions (45° , 135° , 225° , and 315°) is observed.

The results in Figure 3.4 show the mean and standard deviation of determined perception thresholds of the quantization of force direction (in degrees) for different reference forces and directions of hand movements. In contrast to the obtained results on the directional dependencies of the PD parameter, here the angular thresholds do not significantly depend on the force feedback direction. This result confirms the findings presented in [31, 176]. According to the results, a mean value of around 1.85 degrees can be assumed to be the threshold on imperceptible directional changes in the force feedback vector.

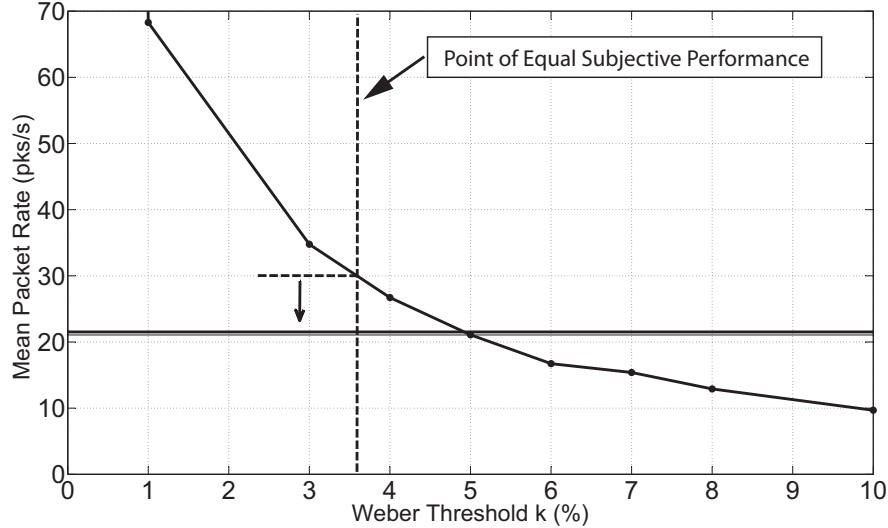
When taking the results discussed above into account for parameterizing the proposed deadzone shape, varying values for PD parameter k can be applied for different force directions to improve the encoding performance. In addition, the isotropic perception threshold α of directional changes can be further applied to the deadzone design for perceptually evaluating angular signal characteristics.

The results of the third part of the experimental evaluation are displayed in Figure 3.5. The mean subjective quality ratings for the isotropic PD shape as a function of the PD parameter k are illustrated in Figure 3.5(a). The corresponding packet/update rates on the haptic channel are shown in Figure 3.5(b). The solid horizontal lines in both subfigures represent the obtained results for the direction-dependent deadzone shape. It elicits a mean quality rating of 79 which corresponds to the quality rating that would be obtained for an isotropic deadzone configured with $k = 3.6\%$. Referring to the mean packet rate results in Figure 3.5(b) at $k = 3.6\%$, the results for the adaptive deadzone structure exhibit an improvement of

approximately 8 *pks/s* over the performance of the isotropic deadzone with 30 *pks/s*. In other words, the proposed direction-adaptive PD scheme achieves high quality data reduction with an additional gain in packet rate reduction of 26.7% compared to the isotropic PD compression scheme.



(a) Mean subjective quality.



(b) Mean packet rates.

Figure 3.5: Experimental evaluation of the compression performance in terms of subjective quality and packet rate (reproduced from [14]). The figures illustrate the results for the isotropic deadzone shape as a function of the deadband parameter k . The solid horizontal lines represent the performance of PD data reduction using the direction-adaptive deadzone shape. The results show an improvement in packet rate of approximately 8 *pks/sec* over the performance of the isotropic deadzone with 30 *pks/sec*.

3.1.2 Velocity-adaptive Perceptual Deadbands

Interestingly, very few of the empirical studies investigate the influence of dynamic movements and attentional requirements, which are both important aspects of human haptic interaction. For instance, in a typical TPTA scenario, an OP is required to plan, control and execute certain movements. These movements usually need to be executed with some degree of precision, in terms of positioning and force application. During the execution of movements and task related operations, one would speculate that less cognitive resources are available to devote attention to the perception and interpretation of displayed force feedback. Therefore, it would seem likely that task-directed movement reduces the operator's ability to perceive changes in displayed force-feedback which would be reflected by increased haptic perception thresholds.

Attentional theories from research in psychophysics support this assumption [47, 72]. Several studies suggest that attention may have a direct effect on the human haptic perceptive ability by triggering a remodulation of neuronal activity in the primary sensory cortex (see [41, 116]). Other studies found direct support for increased JNDs in the presence of multiple attentional demands. For example, the authors in [196] discover in a study on change blindness that the log of the Weber-Fechner parameter is proportional to the log of the number of targets given. Moreover, Xing-Dong et al. [198] finds that force discrimination thresholds are greater during hand movements and that this effect is independent of the speed of movement. Similarly, experimental studies in [47, 197, 198] find absolute force perception thresholds to increase when the operator's hand is in motion and the authors in [202] suggest using them in the context of haptic data reduction. However, in their work, neither difference detection thresholds nor performance and/or efficiency of corresponding data reduction architectures are investigated.

3.1.2.1 Proposed Perceptual Model

In order to reflect the reduced human force-feedback discrimination ability during the hand movements of the OP, the PD thresholds need to be dynamically adjusted to the operator's hand velocity. This allows for the exploitation of the potentially increased JNDs during task-directed hand movement for the purpose of improved, yet still imperceptible, haptic data compression. Specifically, the PD parameter can be described as a function of velocity $\dot{\mathbf{x}}$:

$$\phi = \underbrace{k}_{\text{JND (Weber)}} + \underbrace{\nu \cdot |\dot{\mathbf{x}}|}_{\text{Velocity Adaptation}} \quad (3.1)$$

where the velocity-adaptive PD parameter ϕ is determined by the sum of the constant component k and a velocity-proportional component defined by the factor $\nu \geq 0$. The parameter k represents a velocity-independent component of the JND. Adjusting ν allows for controlling the influence of the velocity on the resulting modified deadband parameter ϕ . For $\nu = 0$ the velocity independent relationship in (2.10) is obtained.

Correspondingly, the size of the applied PD bounds Δ_i at time i can be described by:

$$\begin{aligned} \Delta_i &= \phi \cdot |\mathbf{f}_{i-m}| \\ &= (k + \nu \cdot |\dot{\mathbf{x}}_i|) \cdot |\mathbf{f}_{i-m}| \end{aligned} \quad (3.2)$$

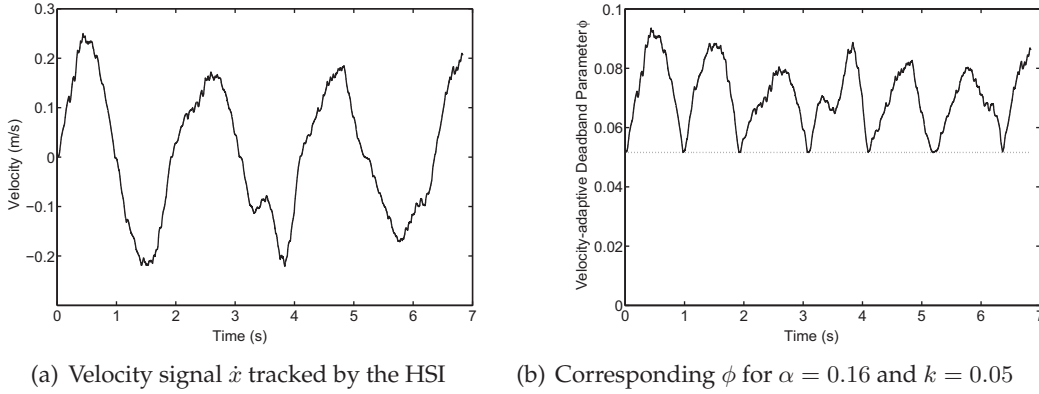


Figure 3.6: Adaptive PD parameter ϕ as a function of velocity (reproduced from [3]).

where the last PD violation of the velocity-adaptive deadband occurred at time $i - m$.

An example of the adaptive PD parameter ϕ recorded during the experimental evaluation is shown in Figure 3.6. The velocity signal \dot{x} referring to the operator's hand movements is illustrated in Figure 3.6(a). Its magnitude is used to calculate the velocity-adaptive deadband parameter ϕ which is illustrated in Figure 3.6(b).

The system architecture of the velocity-adaptive PD compression scheme is illustrated in Figure 3.7, where \dot{x}_h and f_h denote the pending velocity and the force-feedback signal at the HSI, respectively. The HSI measures the human operator's hand movements and corresponding motion commands are sent across the network. At the TOP, the received velocity signal enters the proposed adaptive PD block modifying the current deadband size according to (3.2). As changes in the haptic signal are only transmitted in case of a violation of the applied perception thresholds, the increased PD during movements of the OP's hand leads to an additional packet and data rate reduction and, accordingly, improve the performance of the perceptual PD compression scheme.

3.1.2.2 Experimental Evaluation

To evaluate whether the velocity-dependent PD compression scheme constitutes an improvement to the traditional Weber-inspired approach in terms of transparent, i.e. imperceptible, perceptual haptic data compression, an experimental study has been conducted.

Firstly, the respective PD disturbance detection thresholds are investigated with respect to the constant PD parameter k , the basis of the traditional PD compression approach. Secondly, the velocity adaptation parameter ν from (3.2) is analyzed, which forms the basis of the proposed velocity-adaptive PD extension. In addition, influential factors such as the speed of the movement performed by participants on k and ν are analyzed. Finally, the overall performance of velocity-adaptive PD in the context of perceptual haptic data compression is experimentally evaluated and compared to the standard PD compression approach from Section 2.3.2.

18 male and three female students participated in the experiment (mean age = 27 years, std. deviation = 2.5 years), all of whom are right-handed and did not know the purpose of the experiment. The experimental setup consists of a tubular linear motor, Thrusttube 2510

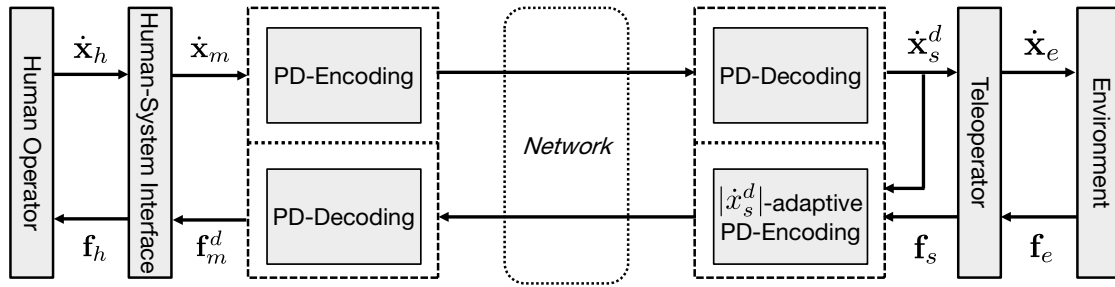


Figure 3.7: Architecture of the velocity-adaptive PD data reduction principle (adapted from [3]). The size of the applied PD adapts to the velocity signal \dot{x} .

from Copley Controls Corp. as shown in Figure 3.8(a), a Burster Corp. 8524-5500 force sensor and two computers. The linear motor displays peak forces of up to 780 N and continuous stall forces of up to 104.3 N . It is connected to a digital servo drive Xenus XTL, also from Copley Controls Corp. The digital servo operates in current control; thus, the signal input can be considered to be approximately proportional to the applied motor force. The position is captured by an optical incremental encoder with a precision of 1 μm . The force sensor provides a measurement range of $0 \pm 500 N$ with an accuracy of 0.25% in full scale. The entire haptic interface is controlled by a PC running a real-time Linux operating system. The digital servo is connected to the PC through a sensory I/O card. The overall haptic device is controlled by a high-gained force controller which compensates for viscous and Coulomb friction. This results in negligible device dynamics for the purpose of the experiment, i.e., 0.35 kg inertia and 3.01 Ns/m damping. All the control functions are implemented with Simulink from MathWorks. The sampling rate of the haptic signals and the local control loops is set to 1 kHz. A second PC also running a real-time Linux kernel receives the position information of the HSI which controls and visualizes a virtual TOP within a virtual TPTA environment. The connection between the two PCs is UDP/IP-based and time delay is on average less than 1 ms and, hence, can be considered to be negligible.

The virtual test environment consists of a simulated spring which acts as an admittance, hence it received velocity information from the HSI and provides force feedback. The proposed velocity-adaptive PD scheme is applied to the rendered force signals before being displayed to the test subject. The spring covers the entire motion range and its spring constant is set to 100 N/m . During interaction with the virtual spring, two potentiometers enable the participants to control the parameters k and ν online and allow for adjustments of k and ν to maximum settings of 0.40 and 1.20, respectively, with a resolution of 0.01.

The experimental study makes use of a two (PD type) \times three (motion speed) within-subjects design. In order to introduce a measure of task performance accuracy and to ensure that participants move the master device with similar motion speed, participants are instructed to follow a given task: They are advised to control the movement of the virtual TOP in accordance to a moving, visually-displayed cursor as closely and precisely as possible whilst perceiving force-feedback originating from the virtual spring. A screenshot of the visual feedback is illustrated in Figure 3.8(b). The motion speed with which the cursor moved from one side of the computer screen to the other is manipulated in a sinusoidal manner using three different frequency levels (2, 3 and 4 rad/sec). The maximum speed for

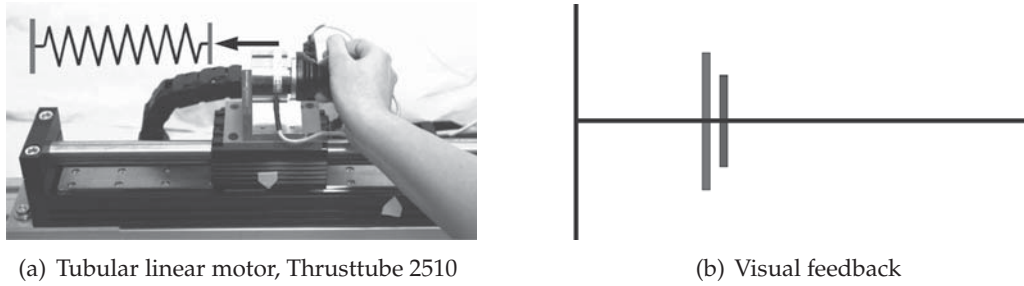


Figure 3.8: Illustration of the experimental testbed (reproduced from [3]). The left Figure 3.8(a) shows the HSI device which displays force-feedback from a virtual spring. The right Figure 3.8(b) shows a virtual teleoperator environment.

each motion level is 0.12 m/sec , 0.18 m/sec and 0.24 m/sec , respectively. During the experiment, a preferable configuration setting for the force component k and for the velocity adaptation parameter ν is determined for each speed level. In addition, the mean squared error (MSE) of the distance between the computer cursor and the TOP positions together with the corresponding compression performance of the regular and the velocity-adaptive PD compression schemes are recorded.

Firstly, the participants are given the opportunity to familiarize themselves with the experimental setup and the potentiometers affecting the control of the TOP. Furthermore, they are demonstrated the effects of the component k as well as the velocity adaptation parameter ν influencing the quality of the displayed force feedback. This training phase ensures that all participants are approximately at the same level of training as far as the detection of possible signal disturbances is concerned. They are then asked to continuously perform the task of following the moving cursor as closely as possible using the haptic device and the cursor coupled to it.

During each experimental run, the participants adjust the parameters k and ν , using the provided potentiometers until they found a maximum setting with which no disturbance is perceived. Specifically, they are asked to approach the target setting from both directions, i.e., initially starting to slowly increase from the minimum parameter value, followed by slowly decreasing from a maximum value, until they are confident that they have found the highest setting at which they feel no disturbance in the control of the TOP.

In a first step, participants are instructed to focus on an optimum configuration for k starting with its lowest setting ($k = 0$) while the velocity adaptation parameter ν is set to zero. As soon as they are confident that they have found the target setting, the corresponding compression performance is measured for 10 seconds for the preferred setting of the participants. During these 10 seconds, participants only focus on their task performance. This procedure is repeated to find an optimum velocity adaptation parameter ν while k is held to the participants' preferred configuration. Afterwards, both steps are repeated with two other speeds of movement. The order of the three speed conditions, which determine the speed of the computer cursor, and consequently participants' hand movements, is systematically randomized for each subject. In addition, participants are wearing headphones which prevent them from hearing sounds that might distract or influence them in any way.

Guided speed	Parameter k		Parameter ν	
	mean	std. deviation	mean	std. deviation
low	0.053	0.053	0.15	0.11
medium	0.064	0.056	0.15	0.10
high	0.059	0.027	0.16	0.13

Table 3.1: Preferred configuration for the parameters k and ν of the adaptive deadband coding scheme with respect to different speed levels (reproduced from [3]). Maximum settings possible are 0.40 and 1.20 for k and ν , respectively.

3.1.2.3 Experimental Results

The obtained results are inspected for outliers, as well as for normality and homogeneity of variance. In this context, z-scores are calculated which represent a normalized distance to the expected mean. Data with z-scores of $z > \pm 3.29$ are excluded from further analysis.

The results are further analyzed using the statistical *Analysis Of Variances* (ANOVA). It analyzes the statistical significance between (assumed) normally distributed dependent and independent variables. If no significance can be detected, the dependent variables do not need to be investigated further. If, however, a significant dependency can be found (so called *effects*), a so called F-test is applied to investigate the individual influence of the dependent variables. The F-test analyses the ratio of the variability between all the different variables (between-group-variability) and the variability within the variables themselves (within-group-variability). The significance of this ratio can be determined with the F-distribution, which is denoted as

$$F(x, y) = v \quad (3.3)$$

where x and y describe the between-group-variability and within-group-variability, respectively. The F-value v allows for determining the significance p in the probability table of the F-distribution. In psychophysical studies, values of $p \leq 0.05$ are typically considered to reflect statistical significance. Further information about the ANOVA can be found in [76].

In the following, the experimental results of the ANOVA are summarized. For a detailed discussion of the ANOVA evaluation, the reader is referred to [3].

Table 3.1 illustrates the results of the obtained disturbance detection thresholds. It shows the mean and standard deviations of the parameters k and ν that the participants adjusted for each movement speed to a maximum level without feeling any introduced coding artefacts. The results presented indicate that the mean preferred setting for the constant component k lies at around 0.06. The mean preferred value for the velocity adaptation parameter ν has been detected to be approximately 0.15.

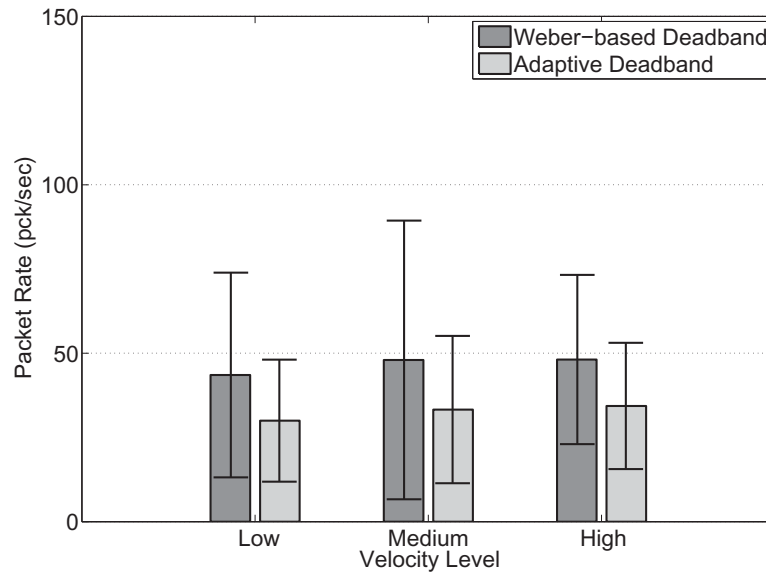
In order to determine the influence of the velocity of the operator's hand on the respective deadband detection thresholds for the Weber-based and velocity-adaptive deadband types, as indicated by k and ν , two within-subjects univariate ANOVAs are conducted with hand movement speed as independent variable and adjusted k and ν settings as dependent variables, respectively. The obtained results suggest that the effects of each component are velocity independent. In other words, the participants adjusted to very similar values for k

and ν , regardless of the speed at which they performed their movement. While the number of participants in this study would not suffice to detect small effects of speed on k and ν values, the results provide an indication that the design and the deployed psychophysical function consisting of a constant component k and a velocity-proportional component characterized by ν is a valid assumption.

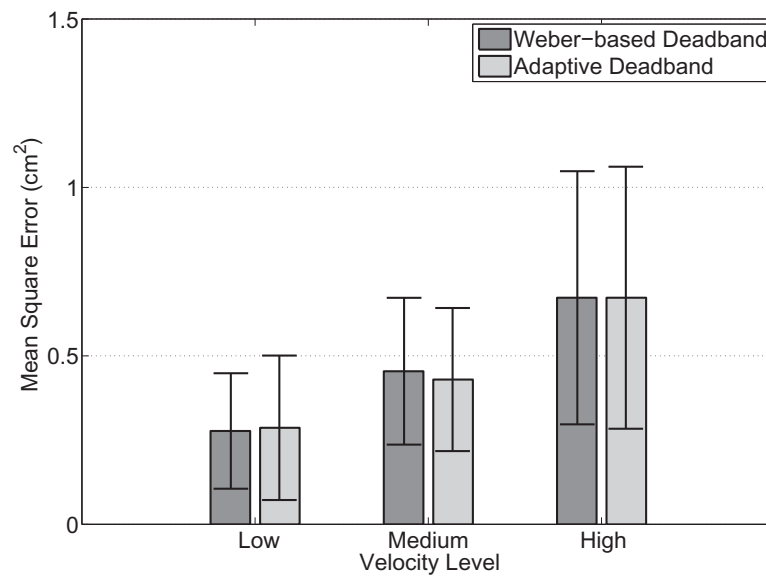
In order to determine whether or not the use of velocity-adaptive deadbands achieves greater data reduction compared to the standard PD-based haptic compression approach without deteriorating performance accuracy, two further repeated-measures ANOVA are conducted with movement speed (low, medium, high) and deadband type (non-adaptive vs. adaptive) as independent variables, and task performance accuracy (mean squared position error) as well as data reduction performance (signal updates per second) as dependent variables, respectively. Despite a trend of increasing signal updates with increasing motion speed as indicated by the mean values, the ANOVA results do not show a significant main effect of the speed on the data reduction performance. In contrast, it reveals a significant main effect of the applied deadband type. Looking at the mean values, the results indicate that the use of adaptive deadbands significantly reduce the number of signal updates performed per second regardless of the speed at which participants move their hands (see Figure 3.9(a)).

For the investigation of task performance data, the ANOVA reveals a significant main effect of speed on the mean squared position error. As no significant main effect of deadband type on position error is detected, the results indicate that task performance accuracy does not significantly deteriorate with the use of velocity-adaptive deadbands compared to the use of non-adaptive deadbands (see Figure 3.9(b)).

Overall, the results suggest that the velocity-adaptive PD approach constitutes a significant improvement to the traditional Weber-based PD compression scheme in terms of compression performance. The results indicate an optimum configuration of approximately $k = 0.06$ and $\nu = 0.15$, regardless of the speed at which participants operated the HSI device. In this configuration, an additional packet rate reduction of up to 30% compared to the Weber-based PD compression approach (total data reduction of 96%) is achieved without perceptibly impairing the quality of the force-feedback signal or significantly affecting task performance accuracy. Since this effect is observed for all three motion speeds tested, the concept of the velocity-dependent PD for perceptual haptic communication seems to be valid.



(a) Mean packet rates



(b) Task performance accuracy

Figure 3.9: Mean values and standard deviations of packet rates and subjective quality with respect to velocity level and deadband type (reproduced from [3]). The dark bars show results for the Weber-based (non-adaptive) PD approach. The light bars represent results for the proposed novel velocity-adaptive PD compression scheme. Compared to Weber-based PDs, velocity-dependent deadbands achieve an additional mean packet rate reduction of 30.1% without effects on task performance accuracy.

3.2 Model-mediated Haptic Communication

During a TPTA session, kinesthetic motion commands are executed by the TOP. In return, force feedback is reflected during contact events with the remote environment. Hence, by associating the contact forces with the position information of the TOP, the geometry and impedance characteristics of the remote surface in contact can be estimated [70]. This observation allows for the construction of surface models based on an analysis of combined position-force sample pairs (see Section 2.1.3.2).

The use of environment models in the context of haptic data communication has not been intensively addressed in literature so far. In this section, the concepts of *model-mediated compression, prediction, and contact coding* are presented which all rely on mathematical models of the remote environment.

Parts of the work presented in this section have been conducted in cooperation with Rahul Gopal Chaudhari, Xiao Xu, and Zike Chen [2, 10, 25, 48, 49]. The experimental study of the model-mediated compression scheme has been performed at the Institute of Automatic Control Engineering, TUM with support from Iason Victorias.

3.2.1 Model-mediated Haptic Data Compression

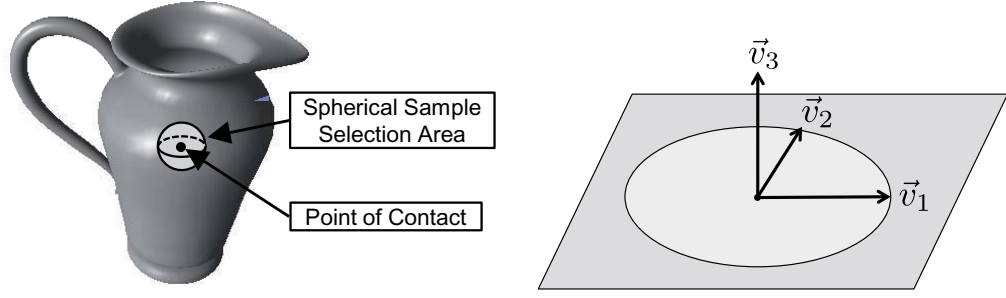
Research by Mitra *et. al* has shown that the integration of simple environment models into the control scheme of the TPTA system allows for increased system stability and transparency due to the decoupling of the global haptic control loop (see [138, 139] and Section 2.1.3.2).

In this section, an architecture for combining model-mediated control with perceptual haptic data compression is discussed. In model-mediated control, the haptic models are typically estimated and transmitted at high rates from the TOP to the HSI device in order to reduce inconsistencies between the remote environment and the locally applied haptic feedback model. Consequently, high update and data rates are observed in the network, which are addressed in this section. Note that the previously discussed methods for perceptual haptic communication cannot be directly applied to the transmitted model parameters due to missing haptic signal information on the haptic channel.

3.2.1.1 Model Estimation Process

Contacts of the TOP with the environment can be easily detected by investigating the magnitude of the pending force sample ($|\mathbf{f}_s| > 0$). In order to increase the amount of support/training data for the model estimation process, the TOP position \mathbf{x}_s , the desired TOP position \mathbf{x}_s^d and the force sensory signal \mathbf{f}_s are jointly stored in memory during the contact period.

As soon as the model estimation process is triggered, a subset of the recorded haptic sensory data is selected according to the current TOP position. Specifically, the subset consists of haptic sensory data which relates to a surface contact position closely located to the current TOP position and characterized by a similar force feedback direction. Hence, the model estimation process takes only the haptic samples into account which spatially relate to the currently touched surface area, as shown in Figure 3.10(a).



(a) Sample selection process. The current TOP position is used to query haptic sensory information from previous contact events with the remote object.
 (b) Plane fitting based on a singular value decomposition. The third singular vector v_3 with smallest singular value describes the plane normal.

Figure 3.10: Illustration of the haptic sample selection and plane fitting process.

To this end, a maximum distance r and an angle γ are defined for selecting a set of indices $M(i)$ of previously captured haptic samples which are closely located to the current TOP position $x_s(i)$ at time i and exhibit a similar contact force orientation (angle between force vectors $< \gamma$).

$$M(i) = \{j \mid 0 < j \leq i, \\ |\mathbf{f}_s(j)| > 0, \\ |\mathbf{x}_s(j) - \mathbf{x}_s(i)| \leq r, \\ \angle(\mathbf{f}_s(j), \mathbf{f}_s(i)) < \gamma\}$$
 (3.4)

The indices in $M(i)$ are used to estimate the geometric surface and impedance characteristics of the current contact with the remote surface. In this work, a rudimentary planar surface model is used, as proposed by Mitra and Niemeyer [139]. It assumes the surface in contact to be a frictionless planar structure with fixed stiffness s . Consequently, the surface plane can be expressed by the standard plane equation:

$$Ax + By + Cz + D = 0$$
 (3.5)

Its small parameter set (plane orientation and plane position) enables a quick adaptation to unknown contact locations. More specifically, at the initial contact with unknown remote objects, the parameters of this plane model can be immediately estimated in order to reflect the contact event to the human OP without introducing any algorithmic delay to the haptic feedback loop.

The current TOP position is used to query the set Q of previously captured surface contact points with indices in $M(i)$.

$$Q = \{\mathbf{x}_s(j) \mid j \in M(i)\}$$
 (3.6)

The model estimation is performed by fitting a plane into the point set Q in the least-squares sense. Accordingly, the calculation of the plane normal can be described as a linear least-

square minimization problem

$$\min_{\hat{\mathbf{n}}} \|[Q - \bar{\mathbf{q}}] \cdot \hat{\mathbf{n}}\|_2 \quad (3.7)$$

where $\bar{\mathbf{q}}$ is the mean of all contact points in Q .

By applying a singular value decomposition (SVD) on $[Q - \bar{\mathbf{q}}]$, an estimated plane normal $\hat{\mathbf{n}}$ can be determined.

$$[USV] = \text{SVD}([Q - \bar{\mathbf{q}}]) \quad (3.8)$$

Assuming a $\text{rank}(Q) \geq 3$, the first two singular vectors $\mathbf{v}_1, \mathbf{v}_2 \in V$ with highest singular values should span the plane. Accordingly, the third singular vector describes its normal, as shown in Figure 3.10(b)

$$\hat{\mathbf{n}} = \frac{\mathbf{v}_3}{|\mathbf{v}_3|} \quad (3.9)$$

In case of $\text{rank}(Q) < 3$, the direction of the current force sample is used to obtain an estimate of the surface normal

$$\hat{\mathbf{n}} = \frac{\mathbf{f}_s}{|\mathbf{f}_s|} \quad (3.10)$$

By taking estimated plane normal $\hat{\mathbf{n}}$ and the current TOP position $\mathbf{x}_s(i)$ into account, the planar surface model can be successfully parameterized:

$$\begin{aligned} A &= \hat{\mathbf{n}}_x \\ B &= \hat{\mathbf{n}}_y \\ C &= \hat{\mathbf{n}}_z \\ -D &= \hat{\mathbf{n}} \cdot \mathbf{x}_s \end{aligned} \quad (3.11)$$

The obtained model parameters are transmitted to the HSI device and used for model-based force rendering with stiffness s and the current HSI position \mathbf{x}_m

$$\hat{\mathbf{f}} = \underbrace{(\hat{\mathbf{n}} \cdot \mathbf{x}_m + D)}_{\text{distance to plane}} \cdot \underbrace{s}_{\text{stiffness}} \cdot \underbrace{\hat{\mathbf{n}}}_{\text{force direction}} \quad (3.12)$$

In order to avoid abrupt changes in the haptic feedback during model updates, a linear crossfade from the currently applied model to the recently received model is performed within a short time window (similar to the *active transition* update strategy in [139]). As in model-mediated control the haptic control loop is locally closed at the HSI, a (shortly) delayed presentation of the remote surface model does not directly impair the stability of the TPTA system.

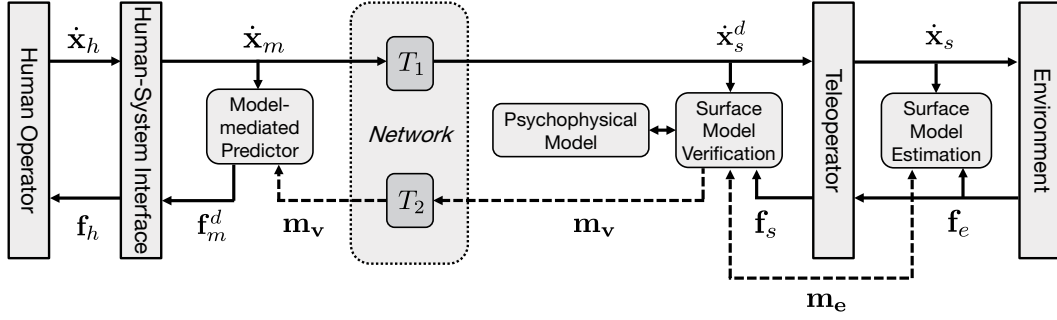


Figure 3.11: Proposed architecture for model-mediated compression.

3.2.1.2 Surface Model Verification

In model-mediated control, the estimated models are typically transmitted with high update rate. In order to reduce the network load on the haptic channel, only perceptually relevant model updates should be transmitted.

To this end, the detection of perceptually relevant model updates can be achieved by comparing the output of the most recently transmitted model with the current force sensory data at the TOP. Only if the model-based and the sensed force feedback exceed applied perception bounds, the transmission of model updates is required. However, small and probably unrecognizable displacements of the estimated planar surface and the actual contact point quickly lead to significant differences in force feedback (particularly with high stiffness s). For instance, if the model-mediated feedback displays a contact shortly before the actual contact occurs at the TOP, a PD-based evaluation would immediately invalidate the currently applied model, although the error in contact position might be too small to be perceivable and, hence, can be considered to be neglectable.

To address this issue, the distance between the plane model and the actual contact point of the TOP with the remote environment needs to be investigated, rather than directly comparing the model-based rendered and the remotely sensed force feedback signals. The distance p between the current TOP position \mathbf{x}_s and the applied plane model can be calculated by

$$p = |\hat{\mathbf{n}} \cdot \mathbf{x}_s + D|_2 \quad (3.13)$$

In order to compensate for sensor noise and small position drifts of the TOP control, a minimum distance Δ^{\min} is applied to discard small and neglectable model updates with $p < \Delta^{\min}$. However, with stronger contact forces being applied, the human perception system is assumed to be less sensitive to changes in force feedback which allows for a reduced model update rate. This is exploited by increasing the minimum plane distance threshold in accordance with Weber's Law of JND and, therefore, by taking the currently force sample \mathbf{f}_s , the PD parameter k and the stiffness s into account.

$$\Delta^p = \max \left(\Delta^{\min}, \frac{k|\mathbf{f}_s|}{s} \right) \quad (3.14)$$

Similarly to (2.9) in Section 2.3.3, this allows the perceptual detection and transmission of only those model updates which are considered to be important for transmission.

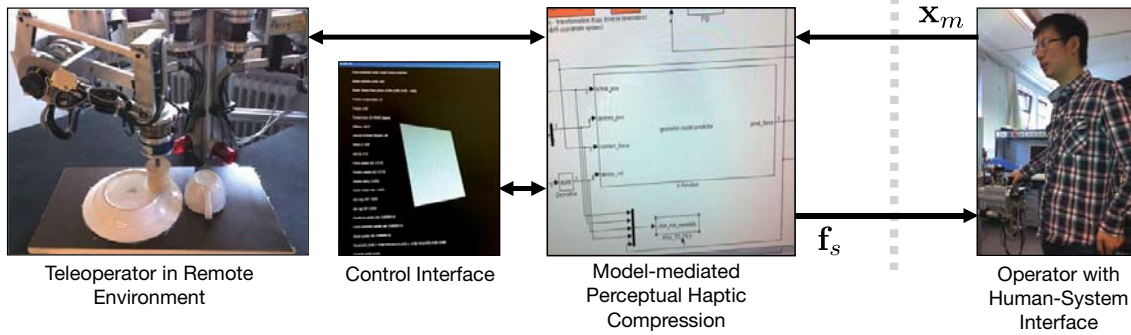


Figure 3.12: Overview of the experimental setup for model-mediated haptic data compression. The experiment has been performed at the Institute of Automatic Control Engineering (LSR), TUM.

$$p \begin{cases} \leq \Delta^p & \text{keep current surface model - discard current model estimate} \\ > \Delta^p & \text{update current surface model - trigger model update transmission} \end{cases} \quad (3.15)$$

Figure 3.11 illustrates the proposed architecture for combined model-mediated control and perceptual haptic data communication. At the TOP side, captured haptic sensory data is used to estimate the model parameters \mathbf{m}_e . They are evaluated and perceptually relevant model updates \mathbf{m}_v which are sent over the network to the HSI. The human OP only interacts with the remotely estimated and locally applied environment models. In this way, the HSI and the TOP are haptically decoupled and the haptic control loop locally closed at the HSI device.

3.2.1.3 Experimental Evaluation

In order to compare the performance of model-mediated haptic data compression with the standard PD compression approach from Section 2.3.3, an experimental study has been conducted.

The experimental setup is shown in Figure 3.12. It consists of a bimanual TPTA system using the DeKiFed (HSI) and DeKiTop (TOP) devices described in [97]. They provide high performance low-friction tracking and force feedback due to DC-motors with Harmonic Drives for every joint. The HSI and the TOP are similarly constructed and equipped with a force/torque sensor at the handle (HSI) and at the tip of the endeffector (TOP). The remote environment contains a plate and a cup which are turned around and fixed upside-down on the ground. The plate shows a slight curvature at its edges. The center of the plate is mainly planar and contains slight indentations. In contrast the cup is strongly curved at its edges and the handle. Also its top is shaped with a slight concavity.

The model-mediated compression methods are implemented in C++ and integrated into a MATLAB/Simulink environment that runs on a real-time capable Linux system (RT-Linux). Both the HSI and the TOP system run on separate PCs connected via 100 MBit/s Ethernet and communicate via the UDP/IP protocol. The robot hardware is controlled using special I/O-PCI cards.

In the experiment, the model estimation process is configured with the following parameters. The sample selection method is configured with $\gamma=45^\circ$ and selects samples within a radius of $r = 1 \text{ cm}$. The surface stiffness parameter s is set to 25000 N/m . The linear crossfading window for updating received model parameters at the HSI is set to 15 ms . The latency on the communication channel is kept at a minimum ($< 1 \text{ ms}$).

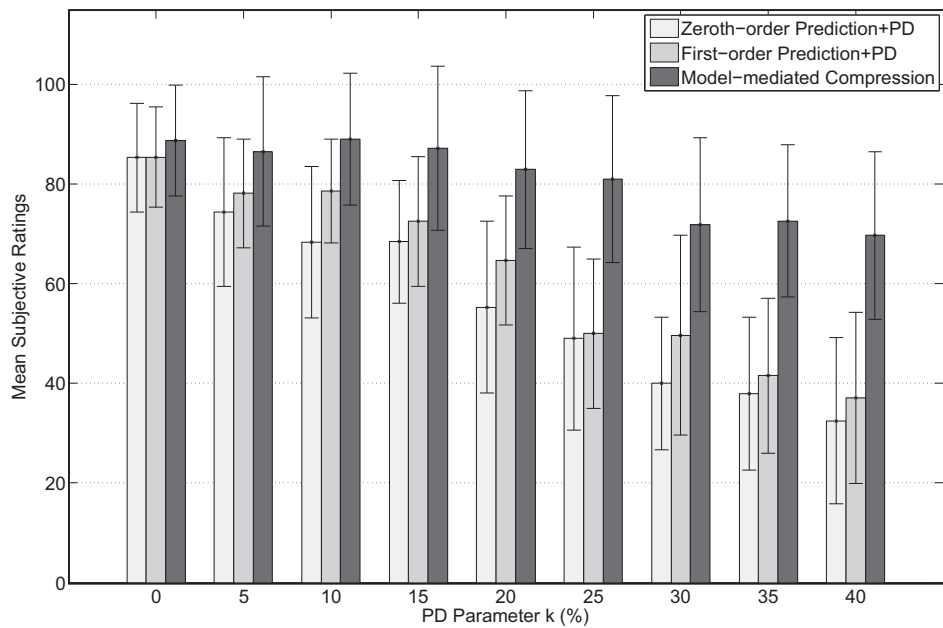
Seventeen subjects participated in the experimental study, aged from 21 to 33. Prior to each experiment, the subjects are familiarized with the experimental equipment and the expected distortion introduced by the model-based and PD compression. The participants are further instructed to haptically explore the surface of the remote environment along a fixed path they could freely choose. This fixed contact path strategy facilitates a direct comparison between different compression settings. The experiment consists of nine runs each investigating randomized PD parameter configurations ($k = 0\%, 5\%, 10\%, 15\%, 20\%, 25\%, 30\%, 35\%, 40\%$). During each run, the subjects are able to freely choose between three blindly presented compression schemes: the PD compression approach using the zeroth-order predictor (see Section 2.3.4.1), the PD compression approach using the first-order predictor (see Section 2.3.4.2), and the proposed model-mediated compression scheme. Furthermore, the subjects are provided with a reference setting which completely deactivates haptic data compression within the system. This allows for a direct subjective evaluation of the presented compression schemes in comparison to the undisturbed reference configuration. In each run, the subjects are asked to perceptually evaluate any perceived difference to the reference setting according to the evaluation scheme shown in Table 2.1 in Section 2.1.4.

3.2.1.4 Experimental Results

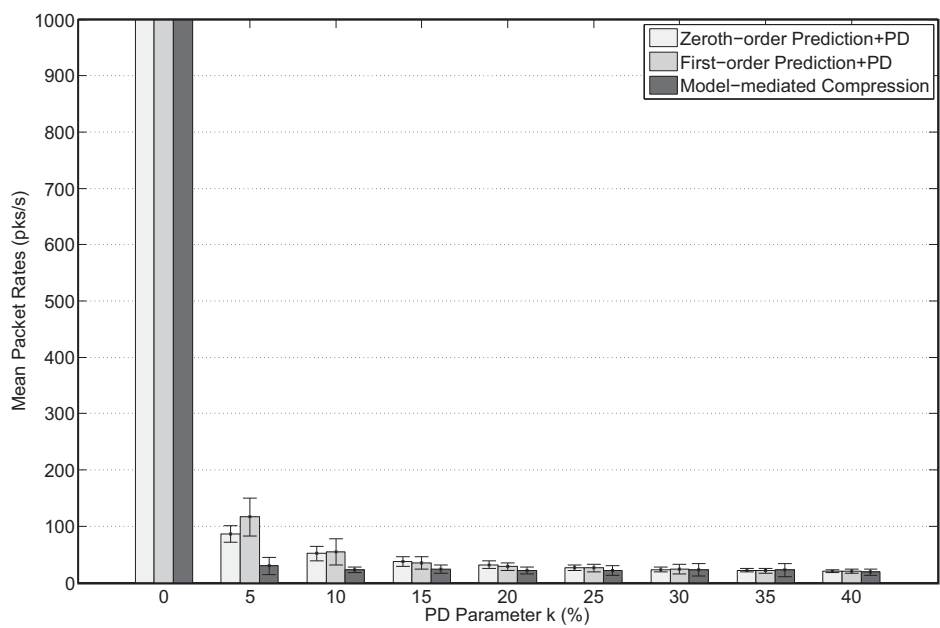
The experimental results are illustrated in Figure 3.13. The bottom Figure 3.13(b) shows the mean packet rates as a function of the applied PD parameter k for all investigated haptic compression schemes. As a PD parameter $k = 0$ deactivates the perceptual compression schemes, a maximum update rate can be observed on the haptic channel which is as high as the applied sampling rate of 1000 Hz . With increasing PD parameter k , the packet rate quickly decreases, even for small values of k . The packet rate reduction performance of the model-mediated compression scheme outperforms the signal prediction schemes already at $k = 5\%$. At a PD parameter of $k > 30\%$, the performance of all three perceptual compression techniques reaches a similar packet rate reduction performance of $> 95\%$. Figure 3.13(a) show the corresponding mean subjective quality ratings as a function of the applied PD parameter k . With increasing PD parameter k , a decrease in subjective quality of the presented haptic feedback is observed. For the PD compression approach using zeroth-order and first-order predictors, the subjective quality quickly reaches a level where the introduced distortion becomes clearly perceivable (≤ 80). In contrast, the compression artefacts for the model-mediated compression approach stay clearly below human perception thresholds up to $k \leq 15\%$. Accordingly, the results show improved subjective performance of the model-mediated compression approach compared to the zeroth-order and first-order perceptual compression.

Taking both the mean packet rates and the mean subjective quality ratings into account, the results show that the model-mediated compression significantly outperforms the first-order and second-order predictive PD compression methods. Already at a small PD parameter $k = 5\%$, strong data reduction is achieved without affecting the perceptual quality of the

haptic feedback. Here, the model-based compression approach further reduces the packet rates from 100 to 25 *pkts/s* compared to PD compression scheme. As the model-based local haptic feedback rendering provides natural force feedback to the human OP, the disturbing update steps during PD signal reconstruction can be avoided which seems to be preferable to the subjects.



(a) Mean subjective ratings.



(b) Mean packet rates.

Figure 3.13: Mean subjective ratings and mean packet rates as a function of the PD parameter k for PD compression with zeroth-order and first-order prediction in comparison to the proposed model-mediated compression approach. The model-mediated compression approach shows best performance in terms of both subjective ratings and packet rate reduction.

3.2.2 Model-mediated Prediction

Interestingly, the prediction of haptic signals does not necessarily need to be based on statistical models of the haptic signal trajectories. Inspired by the concept of model-mediated control and compression, a haptic model of the remote surface can be estimated by analyzing the bidirectional haptic data streams. This section discusses a model-mediated prediction scheme which estimates future haptic samples based on simple models of the remote environment. Particularly, it can be used to predict haptic feedback at the HSI device that otherwise would be remotely sensed and transmitted.

In contrast to model-mediated control and compression, a model-based predictor needs to be deployed at both the sender and the receiver side (see Figure 2.5 in Section 2.3.2). As both predictors need to be kept strictly coherent during all time, they must be fed with identical training data in order to assure their consistency. Accordingly, the model estimation process can only refer to the perceptually downsampled and transmitted *desired* velocity/position and *desired* force feedback signals that are available at the communication subsystem. Correspondingly, the absolute contact location of the TOP endeffector is not available and cannot be used to support the model estimation process. To address this lack of absolute TOP contact position information, the model-mediated prediction scheme must reflect the impedance properties of both the environment *and* the deployed TOP position controller in order to estimate the TOP contact position required for predicting the haptic feedback at the HSI device.

3.2.2.1 Model Estimation Process

In order to keep the amount of samples necessary for approximating remote surfaces as small as possible, simple surface models such as a plane and/or a sphere associated with linear impedance properties are used which allow for the haptical modeling of frictionless planar, concave and convex surface structures.

Plane model

A planar surface in 3D space can be defined by the plane equation:

$$Ax + By + Cz + D = 0 \quad (3.16)$$

where $\mathbf{n} = (A, B, C)$ is the normal vector of the plane, as illustrated in Figure 3.14(a). In absence of surface friction, the direction of the actual force \mathbf{f}_s is identical to the surface normal \mathbf{n} . Hence it can be estimate by $\hat{\mathbf{n}} = \mathbf{f}_s/|\mathbf{f}_s|$.

Furthermore, assuming linear stiffness of the TOP controller in contact with the environment, Hooke's law can be applied to estimate the surface contact point $\hat{\mathbf{x}}_s$ as a function of the contact force vector \mathbf{f}_s and the unknown combined controller and surface stiffness s :

$$\hat{\mathbf{x}}_s = \mathbf{x}_s^d + \mathbf{f}_s/s \quad (3.17)$$

Combined with (3.16), we obtain

$$(\mathbf{f}_s, 1) \begin{pmatrix} \frac{1}{s} \\ -D \end{pmatrix} = \hat{\mathbf{n}} \cdot \mathbf{x}_s^d \quad (3.18)$$

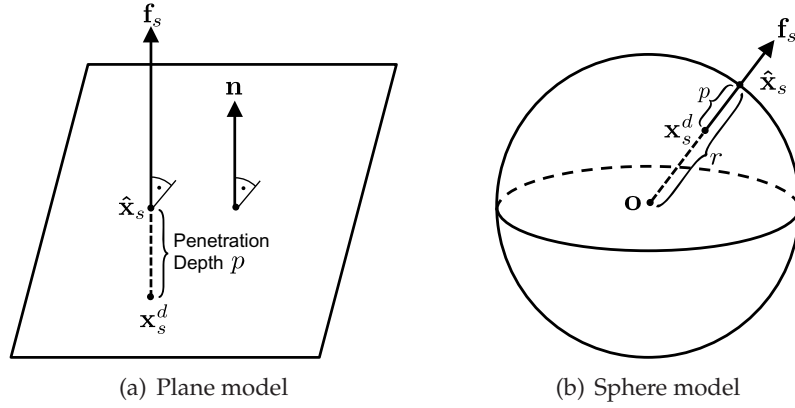


Figure 3.14: Estimation of the surface contact point $\hat{\mathbf{x}}_s$ using a planar and a spherical surface model (adapted from [49]).

In (3.18), the only unknowns are the stiffness s and plane parameter D . Hence, by collecting at least two force/position pairs, and solving a system of linear equations, the plane model in (3.16) can be estimated with associated stiffness, as shown in Figure 3.14(a).

In order to use the model for local haptic signal prediction, the penetration depth p needs to be computed:

$$p = \mathbf{x}_m \cdot \hat{\mathbf{n}} + D \quad (3.19)$$

If $p > 0$, the current device point is outside the object, the predicted force is zero; otherwise the current contact force can be estimated using Hooke's law:

$$p \begin{cases} \leq 0 & \hat{\mathbf{f}}_s = \mathbf{0} & \text{remote surface not touched} \\ > 0 & \hat{\mathbf{f}}_s = sp\hat{\mathbf{n}} & \text{remote surface touched, render haptic feedback} \end{cases} \quad (3.20)$$

Sphere Model

The sphere model is capable of modeling concave as well as convex surface structures. It is defined by the center $\mathbf{o} = (o_x, o_y, o_z)$ and the radius r , as shown in Figure 3.14(b).

Under the assumption of a frictionless surface, the actual force \mathbf{f}_s points radially outward from the center \mathbf{o} of the sphere. Hence, the surface contact point of the TOP $\hat{\mathbf{x}}_s$ can be defined by:

$$\hat{\mathbf{x}}_s = \mathbf{o} + r \frac{\mathbf{f}_s}{|\mathbf{f}_s|} \quad (3.21)$$

By assuming linear stiffness, the distance p to the surface of the sphere can be estimated using Hooke's law.

$$p = \frac{|\mathbf{f}_s|}{s} \quad (3.22)$$

Hence, the force \mathbf{f}_s can be expressed as a function of the desired TOP position \mathbf{x}_s^d :

$$\mathbf{o} + r \frac{\mathbf{f}_s}{|\mathbf{f}_s|} - \frac{\mathbf{f}_s}{s} = \mathbf{x}_s^d \quad (3.23)$$



(a) Spherical approximation in horizontal direction in(b) Spherical approximation in horizontal direction in (c) Planar approximation in vertical direction

Figure 3.15: Simulation of model-mediated prediction of haptic force-feedback based on simple geometric surface models (adapted from [5]). The little spheres represent the virtual end-effector. In (a) and (b) a spherical and in (c) a planar surface approximation are illustrated.

This can be expressed in matrix-vector notation form:

$$\begin{pmatrix} I & \frac{\mathbf{f}_s}{|\mathbf{f}_s|} & \mathbf{f}_s \end{pmatrix} \begin{pmatrix} \mathbf{o} \\ r \\ -\frac{1}{s} \end{pmatrix} = \mathbf{x}_s^d \quad (3.24)$$

where I is the identity matrix. According to (3.24), there are five unknown variables (o_x, o_y, o_z, r, s) and three equations (for each dimension). Correspondingly, at least two force/position pairs are required to solve this system of linear equations.

Once defined, the distance p between the HSI position \mathbf{x}_m and the sphere model can be calculated in order to perform model-based force prediction.

$$p = r - |\mathbf{x}_m - \mathbf{o}| \quad (3.25)$$

The sign of the estimated stiffness s tells us the surface shape. If $s \geq 0$, the surface is considered to be convex, otherwise it is assumed to be concave. So depending on convex or a concave surface structure, the predicted force $\hat{\mathbf{f}}_m$ at the HSI device can be computed as follows:

$$\hat{\mathbf{f}}_m = \begin{cases} p \cdot s \cdot \frac{\mathbf{x}_s^d - \mathbf{o}}{|\mathbf{x}_s^d - \mathbf{o}|} & \text{if } |\mathbf{x}_s^d - \mathbf{o}| < r, s \geq 0 \\ p \cdot s \cdot \frac{\mathbf{o} - \mathbf{x}_s^d}{|\mathbf{o} - \mathbf{x}_s^d|} & \text{if } |\mathbf{x}_s^d - \mathbf{o}| > r, s < 0 \\ 0 & \text{else} \end{cases} \quad (3.26)$$

3.2.2.2 Adaptive Selection of Surface Models

The performance of the planar and spherical models strongly depend on the characteristics of the remote environment. Dependant on its curvature and structure, the choice of an optimal surface model might change for different remote objects (see Figure 3.15). In order

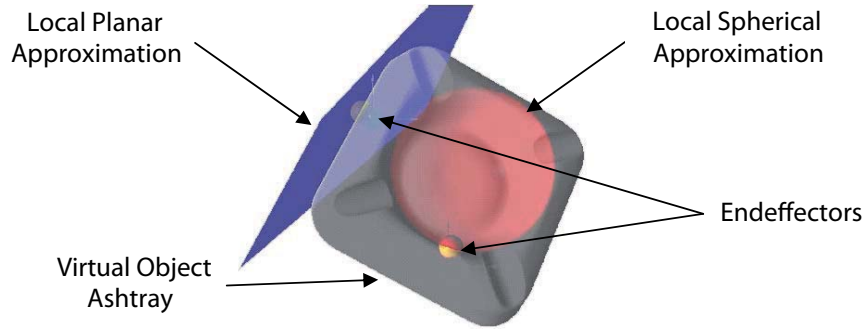


Figure 3.16: Virtual TPTA simulation used in the experimental study.

to achieve an adaptive selection of the best suited surface model, an *analysis by synthesis* approach can be applied by estimating and evaluating the performance of several surface models in parallel. By using Weber’s Law of JND, a “Weber-normalized” prediction error w_i of the i th surface model can be determined (see Section 2.2.2)

$$w_i = |(\hat{\mathbf{f}}^i - \mathbf{f})|/|\mathbf{f}| \quad (3.27)$$

where $\hat{\mathbf{f}}^i$ denotes the force estimate of the i th model-based predictor. Consequently, the model-based predictor with the smallest w_i is to be selected for predicting the current contact forces.

Note that this adaptive model selection scheme works without transmitting additional side information over the haptic communication channel. The cost function in (3.27) takes only the current force sample \mathbf{f} and the predictor output $\hat{\mathbf{f}}^i$ of the i th prediction model into account, which are both available at the HSI and the TOP side.

3.2.2.3 Experimental Study

In order to evaluate the performance of the model-mediated prediction scheme, a psychophysical experiment has been conducted [25]. The test setup consists of a virtual TPTA system developed with the *CHAI3D* haptic rendering library [57]. The simulated environment contains a virtual teleoperator and virtual 3D ashtray object which can be haptically explored (see Figure 3.16). It is slightly concave in the center and its sides are planar with curved areas in the edges. For controlling the virtual TOP, a Phantom Omni HSI by Sensable Technologies [163] is used in the experiments. The sample rate and control rate of the virtual TPTA system is set to 1000 Hz. The latency on the communication channel is kept at a minimum (<1ms).

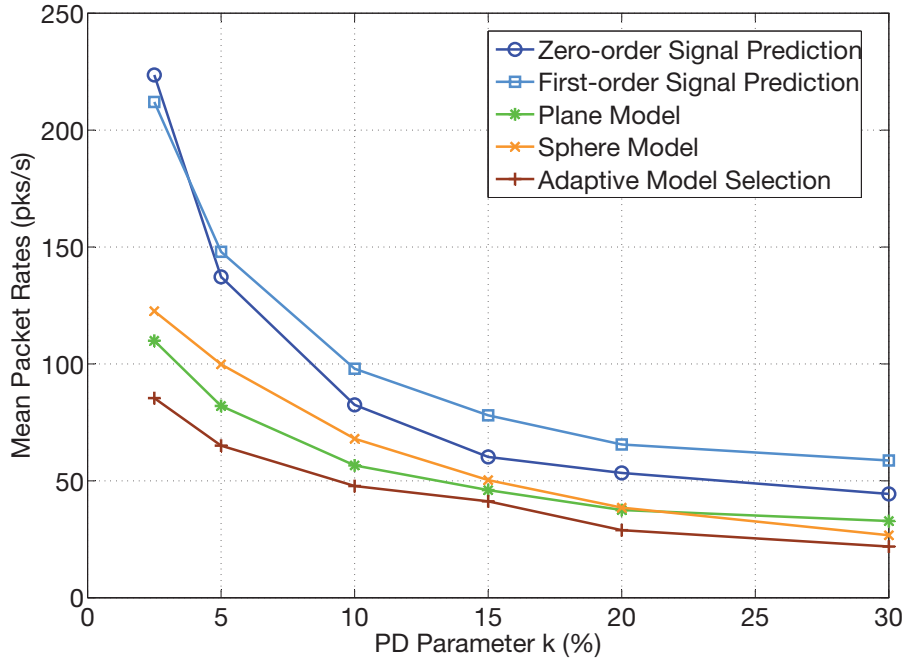
A total of 14 subjects participated in the psychophysical study, ranging in age from 23 to 32. All of them are right-handed. Ten of them had never used a haptic device before and the remaining four had used such a device on a regular basis. In order to standardize the experiments across all subjects, a fixed seating posture and hand-device configuration is instructed. The computer screen displaying the VE is placed in front of the participant while the haptic device is placed on the right. A cardboard protects the haptic device from visual observation by the subject. During the experiment, the participants wear headphones playing music to mask the noise originating from the motor of the haptic device.

At the beginning of the experiment, a training session is conducted to help the subjects familiarize themselves with the experimental setup and the task. The subjects are guided to recognize compression distortion artefacts introduced by the PD compression scheme and its influence on the applied prediction models. During the experiment, each subject is required to perform 30 test runs with different system configurations. Particularly, the performance of PD compression using the zeroth-order and first-order signal predictors is investigated (see Section 2.3.4.1 and Section 2.3.4.2). In addition, the performance of PD compression using the planar and spherical surface predictors including the proposed adaptive model selection scheme is analyzed. The PD compression scheme is configured with the following PD parameters: 2.5%, 5%, 10%, 15%, 20%, 30%. The assignment of the PD parameter k and the prediction scheme are presented blindly and in randomized order. During each test run, the subject explores the virtual object within a time interval of ten seconds while the update rate of the selected predictor is recorded. After the test run, the participants are asked to perceptually rate the quality of haptic feedback perceived by using the rating scheme shown in Table 2.1 in Section 2.1.4.

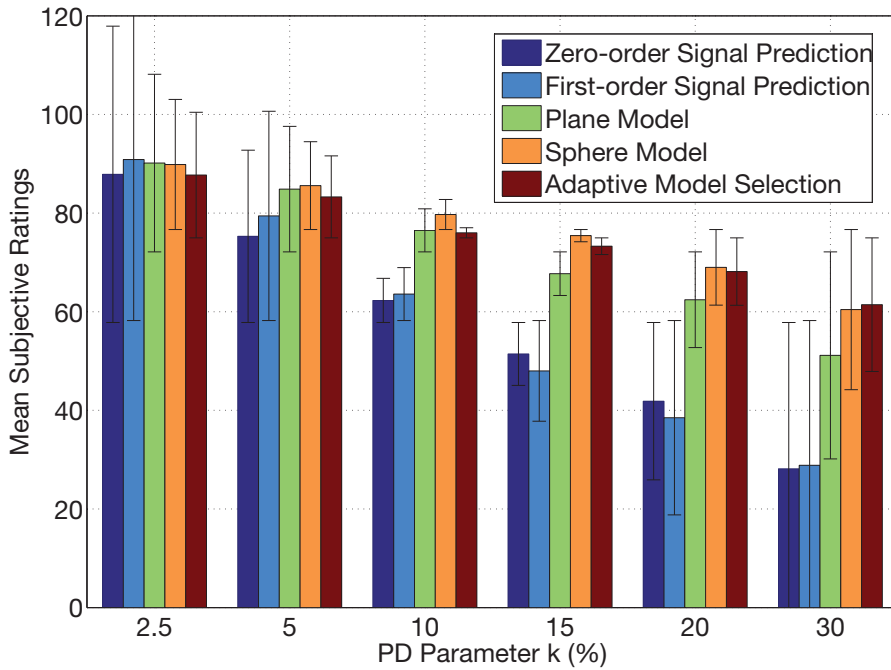
3.2.2.4 Experimental Results

The experimental results are shown in Figure 3.17. Figure 3.17(a) illustrates the mean packet rates as a function of the applied PD parameter k for PD compression using the model-mediated and the signal-based haptic prediction schemes. The results show that the model-based predictors and the adaptive prediction scheme integrated into the PD compression approach achieve best packet rate reduction performance. For all applied PD parameters, they outperform the PD compression using the signal-based zeroth-order and first-order predictors. The best packet rate reduction performance is achieved at a PD parameter of 5-10%. Here, the adaptive prediction scheme improves the packet rate reduction by a factor of two compared to the signal based predictors. The corresponding subjective ratings are illustrated in Figure 3.17(b). Similar to the results on the packet rate reduction performance, the mean subjective quality for PD compression using the model-based prediction significantly outperforms the signal-based prediction techniques, in particular with increasing PD parameter.

When taking both the mean subjective quality and the corresponding packet rates into account, the results show that best compression performance in terms of subjective quality and packet rate reduction is achieved when integrating the adaptive prediction scheme into the PD compression approach. At a similar subjective quality rating of 80 (compression distortion below perception thresholds), an additional reduction in packet rates of 54% and 60% can be achieved by the planar and spherical surface models compared to the signal-based haptic predictors, respectively.



(a) Mean packet rate results.



(b) Mean subjective ratings.

Figure 3.17: Experimental results for PD compression using signal-based and model-mediated prediction (adapted from [25]). Integrated into the PD compression approach, the model-mediated and the adaptive prediction scheme achieve best compression performance .

3.2.3 Event-based Coding using Contact Models

During a TPTA session, the human OP often targets and follows known contact points in order to navigate within the remote TPTA work space. Contact events provide important haptic information about the geometry of the remote environment. But also tactile feedback being displayed during a haptic contact event allows for perceiving highly relevant information. Wellman and Howe show that high-frequency acceleration profiles occurring during the initial contact with objects allow us to perceive important information about surface properties and impedance characteristics [191]. Ideally, displayed contacts in a TPTA scenario provide the same real-world touch experience. Unfortunately, this is not the case due to finite compliance of haptic display devices, system dynamics, network latency, etc.

The paradigm of *event-based haptics* (EVBH) proposed by Hwang *et al.* [115] and Kuchenbecker *et al.* [129] addresses this issue. They present and validate the idea that discrete events of remote contact with an object can be described by contact time and TOP velocity which allows for displaying pre-computed contact force histories. In their work, the vibration waveforms arising out of the tapping task are modeled with an exponentially decaying sinusoid whose parameters depend on the simulated material characteristics:

$$f^{acc}(t) = a|\dot{x}_s|e^{-bt}\sin(2\pi ft) \quad (3.28)$$

where $f^{acc}(t)$ is a single-DoF acceleration waveform produced by the initial contact with the object, $a|\dot{x}_s|$ is the attack amplitude which is a function of the magnitude of the contact velocity \dot{x}_s and a constant a . For a given material, b is a decay constant matched to the apparent decay of the waveform and f is the frequency of the attack portion of the wave (in Hz). Experiments performed with real world objects show that the attack frequency is typically a function of the contact stiffness. Okamura *et al.* (see [145]) further combine this empirical vibration model with a standard virtual wall controller which improves the haptic presentation of virtual stiff objects.

In addition, Kuchenbecker *et al.* present a technique for online identification and real-time matching of high-frequency acceleration profiles during remote interaction with a TPTA system [128]. During remote contacts, they extract the acceleration profiles by applying a high-pass filter to the force signal configured with a cut-off frequency just above the low-frequent tracking bandwidth. By taking the dynamics of the TOP into account, the high-frequent acceleration vibrations can be obtained. At the HSI device, the parameterized acceleration feedback is superimposed onto the closed-loop low-frequent tracking forces. The experiments of the authors show improved haptic experience when the high-frequent contact accelerations are portrayed in a TPTA system.

The concept of EVBH is also of great relevance in virtual haptic TPTA scenarios. Most conventional haptic rendering algorithms for virtual environments ignore contact acceleration feedback. Instead, they concentrate on displaying closed-loop quasi-static restoring forces to the user which are computed according to physics models, such as the well known Hooke's law. These feedback forces are proportional to the depth of penetration of the haptic device into the virtual object surface. As a result, the displayed contact forces mediate soft contacts at best and do not provide a realistic feel of haptic interaction with a rigid object.

In addition to the challenges of sensing and displaying realistic haptic contact feedback, the transmission and compression of haptic feedback signals during the initial contact event is also challenging. As soon as the remote TOP touches an object, the initial force samples

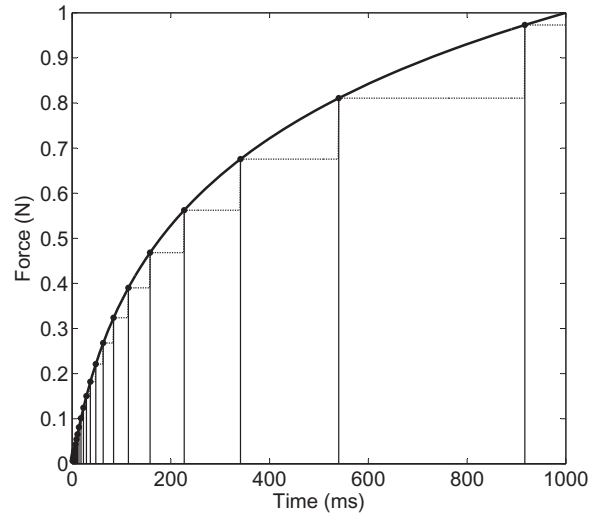


Figure 3.18: Illustration of the PD violations during contact events. High update rates can be observed during the initial contact phase.

which are used to define the perception bounds in the PD compression scheme are of small magnitude. Furthermore, the force signal tends to exhibit transient and high frequency signal characteristics which typically results in increased packet rates on the network, as shown in Figure 3.18.

The concept of event-based contact coding discussed in this section (see also [2, 10, 48]) using local contact models addresses both the impaired realism of rigid haptic contacts and the increased packet rates when applying PD compression on contact feedback signals. As the typical contact period lasts from 10 to 100 ms, it is too short for incorporating any cognitive human response. This observation can be exploited by deploying an open-loop haptic contact model at the HSI for locally approximating and displaying contact forces during the contact period. Hence, by locally rendering the initial contact forces at the HSI, the transmission of high-frequency haptic signals over the network can be avoided while the realism and quality of haptic contact feedback are simultaneously improved.

3.2.3.1 Proposed Event-based Contact Model

Figure 3.20 illustrates the proposed event-based coding scheme using contact models. Whenever initial contact with the environment is encountered, an event-of-contact message m is triggered which contains the model parameters for the local contact feedback rendering. During the short contact transient period, the transmission of the force-feedback signal f_s is substituted by locally approximated haptic contact feedback \hat{f}_s . To this end, high update rates during the initial contact phase can be avoided (see Figure 3.18).

In addition, the previously discussed Wellman contact vibration model can be used to render realistic acceleration forces f^{acc} using (3.28). Figure 3.19 illustrates the desired position \dot{x}_s^d , the commanded force f_m^d and the corresponding measured acceleration profile in \ddot{x}_m during the event of a contact. The acceleration shows the decaying high-frequency contact vibrations during a remote contact event.

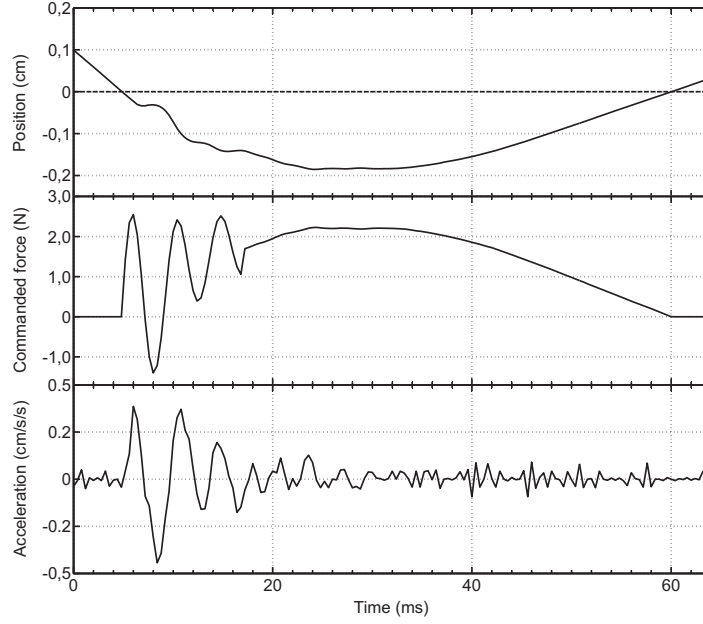


Figure 3.19: Illustration of improving contact realism by superimposing acceleration forces during contact events (reproduced from [2]). The top figure shows the trajectory of the haptic interface point as a function of time. The dashed horizontal line indicates the virtual object surface (object penetration occurs below this line). The middle figure shows the calculated and commanded force signal with superimposition of event-triggered force contact transients on traditionally rendered penetration-based feedback forces. The bottom figure illustrates the measured acceleration of the haptic interface device.

In order to completely suspend the transmission of the remote force signal, the low-frequency proportional feedback forces also need to be estimated. As these forces tend to exhibit transient signal characteristics during the initial contact phase which later decays, the rising period of a squared sine function (over $[0; \frac{\pi}{2}]$) scaled by the initial contact velocity \dot{x}_s^d has been found to be suitable for approximating the intensity of proportional force profile during the transient period. This local approximation function of force intensity is described by:

$$f^I(t) = c \cdot |\dot{x}_s^d| \cdot \left[\sin \left(\frac{(t - 0.5)\pi}{2N} \right) \right]^2 \quad \text{for } 0 \leq t \leq N \quad (3.29)$$

where \dot{x}_s^d is the initial contact velocity, c is a constant analogous to the displayed stiffness and t denotes the time during the transient period of duration N .

In single DoF TPTA scenarios, the direction of contact forces (assuming a flat wall-like object) is constrained to be exactly opposite to the direction of approach for every interaction. In contrast, in multi-DoF TPTA systems, the contact feedback can freely change direction depending upon the nature of user interaction and the physical and geometric properties of

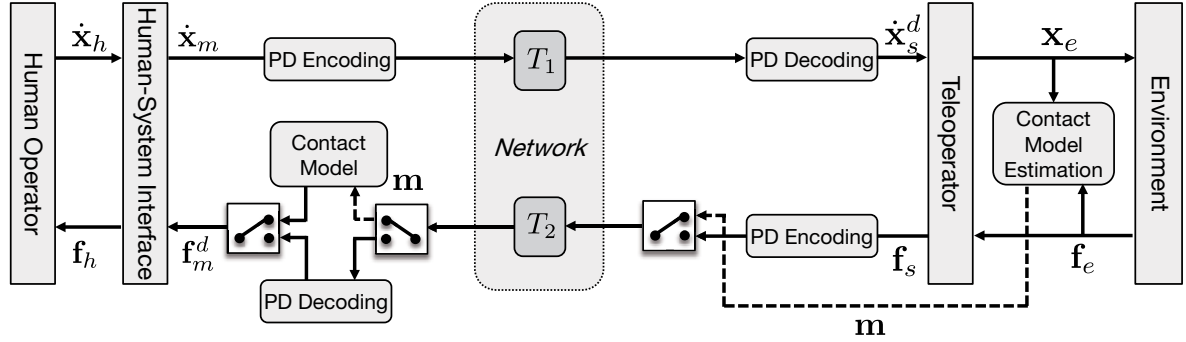


Figure 3.20: Proposed architecture for event-based coding using contact models. As soon as contact with the remote environment occurs, an event-of-contact message \mathbf{m} is sent. During the initial contact phase, haptic feedback is substituted with locally rendered contact forces. This enables the reduction of high packet rates during the initial contact phase and improves the quality of haptic contact feedback.

the object in contact. Particularly, static as well as dynamic friction significantly affect the direction of force feedback [57, 160]. In order to tackle this challenge, the local contact model needs to integrate the friction characteristics of the currently touched surface.

Typically, the direction of frictional forces is opposite to the direction of the surface slip and their intensity is a function of the surface slip velocity and the applied contact force [160]. Consequently, to model the frictional forces, the orientation of the surface in contact needs to be incorporated. Several techniques for obtaining geometric information of the remote surface are known, as discussed in the previous Section 3.2.1 and Section 3.2.2.

In order to limit the amount of model parameters to be estimated and communicated, the deployed friction model is simplified based on a few assumptions. During the relatively short contact transient time period, the TOP is assumed to slide only along a short length on a surface area of the remote object. Due to this restricted contact path, any surface asperity is neglected and a locally planar surface structure is assumed. In addition, the static and dynamic friction effects are assumed to be of comparable intensity.

The proposed friction model projects the contact velocity vector \dot{x}_s^d onto the assumed contact surface with normal \mathbf{n} . The direction of the projection vector is referred to in the following as the *direction of slip* \mathbf{d} . The corresponding friction forces are in a direction opposite to \mathbf{d} , and are applied to smoothly vary the direction of the estimated proportional feedback-forces towards the surface normal \mathbf{n} over period N . Hence, the proportional forces for $0 \leq t \leq N$ can be approximated by:

$$\hat{\mathbf{f}}(t) = \underbrace{f^I(t) \cdot \mathbf{n}}_{\text{proportional forces}} + \underbrace{d \cdot |\dot{x}_s^d| \cdot \mathbf{d} \cdot -1}_{\text{frictional forces}} \quad \text{for } 0 \leq t \leq N/2 \quad (3.30)$$

where the constant d has the physical meaning of a friction coefficient that adjusts the magnitude of the frictional forces. This contact response behavior is illustrated in Figure 3.21. The applied frictional forces lead to deceleration of the TOP on the object surface. Hence, the corresponding force orientation approaches the direction of the surface normal of the touched virtual object smoothly over time.

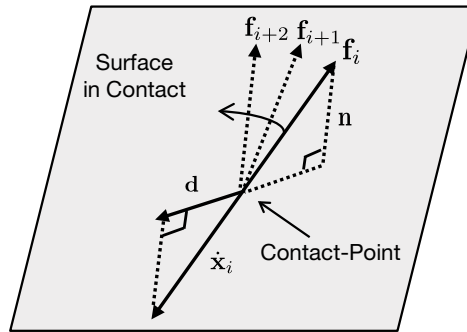


Figure 3.21: Illustration of local proportional force feedback approximation with friction compensation (adapted from [2]).

To integrate the concept of EVBH with the friction-based proportional force estimation, the contact transient force signal f^{acc} given by (3.28) is superimposed onto the magnitude of the proportional forces \hat{f} , as illustrated in Figure 3.22. After the contact period, there inevitably occurs a mismatch between the local approximation and the subsequent force sensory data received from the remote TOP. In order to avoid disturbing discontinuities arising from a hard switchover between the local contact force estimation and the remote haptic signal, a squared sinus crossfading window is applied to enable a smooth transition, as illustrated in Figure 3.23.

Note that in the proposed EVBH-based contact coding scheme, the underlying control architecture is assumed to bear the responsibility of ensuring system stability. Nevertheless, the approximated contact forces might add energy to the system which can impair the system stability (see Section 2.1.3). However, due to the relatively short contact period ($\leq 100ms$), the concept of event-based contact coding has shown to provide stable interaction. Since the human in the loop acts as an intervening compliance, the limited additional signal energy is typically not reflected back to the TOP device.

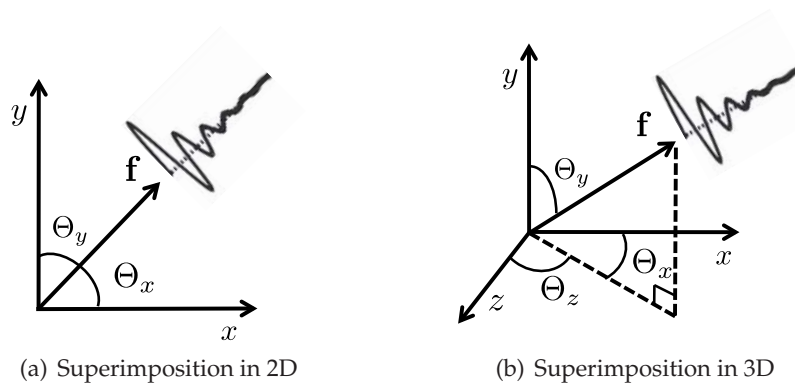


Figure 3.22: Superimposition of contact transients onto proportional forces for the local approximation of haptic contact force-feedback signals with (a) two DoF and (b) three DoF (adapted from [2]).

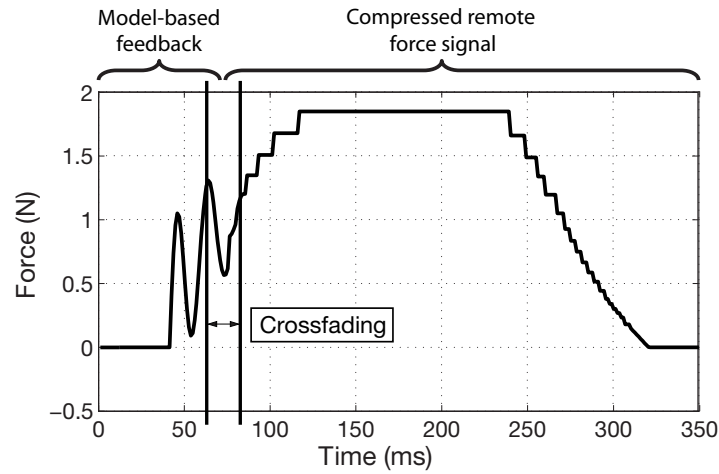


Figure 3.23: Local generation and display of proportional forces during the contact phase (adapted from [2]). A smooth transition between the locally approximated signal and the signal received from the remote side is achieved by applying a crossfading window. This window is trailed by forces which are received from the remote side with step-like artefacts due to PD compression. Note that the update step-size variation in the signal profile depends upon the instantaneous signal amplitude.

3.2.3.2 Experimental Evaluation

Perceptual tests have been carried out to investigate the performance of the proposed event-based coding scheme using haptic contact models.

The user study is based on a total of twelve subjects ranging in age from 20 to 26, all right-handed. Seven of them had never used a haptic device before. Some had used such a device a few times before and one reported using it on a regular basis.

The experimental setup consists of the SensAble Phantom DesktopTM HSI device [163] used to haptically interact within a virtual TPTA simulation rendered by the *CHAI3D* library [57]. The applied haptic sampling and control rate is 1000 Hz. The virtual workspace contains of a simple touchable spherical object with a stiffness of 540 N/m which attempts to model a solid rigid object. During contact periods, frictional forces (with static and dynamic friction of equal intensity) are rendered and displayed to the subjects. The configuration of the contact model is empirically tuned and set to the following values: $a = 4 \text{ N/m/s}$, $b = 97$ and $f = 61 \text{ Hz}$. In (3.29) and (3.30), c is set to 4.2 N/m/s , d is set to 2.25 N/m/s . The duration of the contact modeling is set to 30 ms . These parameters are hand-tuned to attribute a specific quality and feel of touch to the virtual object.

In order to ensure that the subject responds only on the basis of his sense of touch, all superfluous stimuli are removed from the experimental setting. The computer screen displaying the virtual TPTA simulation is placed on an elevated platform towards the extreme left while the Phantom is placed on the right so as to prevent visual observation of the haptic device. The subjects are instructed to hold the Phantom stylus with a firm grasp and to avoid touching the table with the other hand so as to prevent unintentional transmission of contact vibrations. In addition, headphones playing music are used to mask the noise emanating from the Phantom motors.

In the experimental evaluation, four different configurations of the proposed compression scheme are separately investigated:

- *PD compression of proportional force feedback*: In this configuration, closed-loop force feedback signals are subject to haptic PD compression before being transmitted and displayed to the OP. No high-frequency acceleration feedback is incorporated into the force signals.
- *PD compression with remote superimposition of contact acceleration forces*: The Wellman EVBH model is introduced to superimpose high-frequency acceleration feedback onto the proportional forces during the initial contact period. The EVBH scheme is remotely applied (i.e. at the virtual TOP) to render realistic haptic sensory signals of rigid contacts. Subsequently, the force signal is PD-compressed and transmitted. Its high-frequency components are expected to trigger additional haptic signal updates on the network. This configuration thus achieves improved contact realism at the expense of an increase in the number of packets on the haptic channel.
- *PD compression with local superimposition of contact acceleration forces*: In order to avoid additional packets being triggered by remotely superimposed contact transients, the EVBH contact model is shifted from the TOP to the local OP side to enable local model-based transient rendering. The proportional force signal is efficiently transmitted by applying PD compression. Hence, improved contact realism without additional network load on the haptic channel is expected.
- *PD compression with local contact acceleration rendering and local approximation to proportional forces*: Here, the performance of the local proportional forces approximation is investigated, which allows for completely substituting the transmission of the remote haptic force-feedback signal during the initial contact period. This enables further packet rate savings on the network and pushes the data reduction performance beyond what is otherwise achievable by the PD compression scheme alone.

As in this experiment the focus is on the evaluation of model-based contact rendering, no compression is applied to the position/velocity channel in the described test configurations. However, the PD data reduction schemes can also be applied on the forward position/velocity channel as shown in [98].

The experiment consists of two distinct phases; a training phase and evaluation phase. In the training phase, the subjects are familiarized with the provided haptic interaction in the virtual TPTA simulation. They are instructed to tap on the object by approaching it from different directions until they are comfortable with their movements in the virtual workspace. In order to verify the proposed contact model, the subjects experience force-feedback with and without contact acceleration forces and are asked to qualitatively compare between these stimuli. They reported improved contact perception with respect to tapping on rigid object surfaces in case of applied EVBH accelerations. In the next step, the subjects are acquainted to the distortion that the PD compression scheme introduces. For this purpose, force-feedback signals are displayed with extreme values of the PD parameter k (both for configurations with and without contact transients). The subjects are instructed to remember haptic perceptions arising out of these training interactions so that he/she would be able to identify the PD artefacts during the course of the actual experiment.

During the experimental phase, one of the previously described configurations is randomly selected and applied along with randomly changing PD parameter values between 0% to

30%. Meanwhile each setting is presented for about five to six seconds, corresponding packet transmission rates are recorded during the time interval of being in contact with the virtual object. In addition to the displayed test items, individual reference signals corresponding to the applied configuration are presented. To this end, the experimental results reflect solely the influence of the PD compression scheme on the subjective quality and does not investigate a comparison in quality between the configurations with and without EVBH contact models applied. The subjects are given the ability to switch back and forth between the distorted test configuration and corresponding reference signal. To this end, the impact of PD-based disturbances on the perceived quality is investigated regardless of the applied contact model. The subjects are then asked to subjectively assess the quality of the PD compressed haptic feedback signal with respect to the undistorted reference signal. Depending upon the degree of relative disturbance that the user perceives, a rating is obtained according to the user rating scheme shown in Table 2.1 in Section 2.1.4.

3.2.3.3 Experimental Results

Figure 3.24(a) illustrates the mean packet rate results plotted against the applied PD parameter k for each of the four test configurations. It is expressed as a fraction of the total number of packets that would have been transmitted without PD compression being applied (1 packet/sample transmission at 1000 Hz rate).

When remotely rendering contact transients, a marginal increase in packet rate of 4% can be observed due to additional packet transmissions from superimposed EVBH high-frequency signal information. In contrast, when locally approximating the proportional feedback during the contact period, a gain in packet reduction of around 8-11% is obtained independent of the applied deadband parameter (lowermost curve on the packet rate results). Here, the only overhead is the transmission of model parameters within the event-of-contact trigger messages.

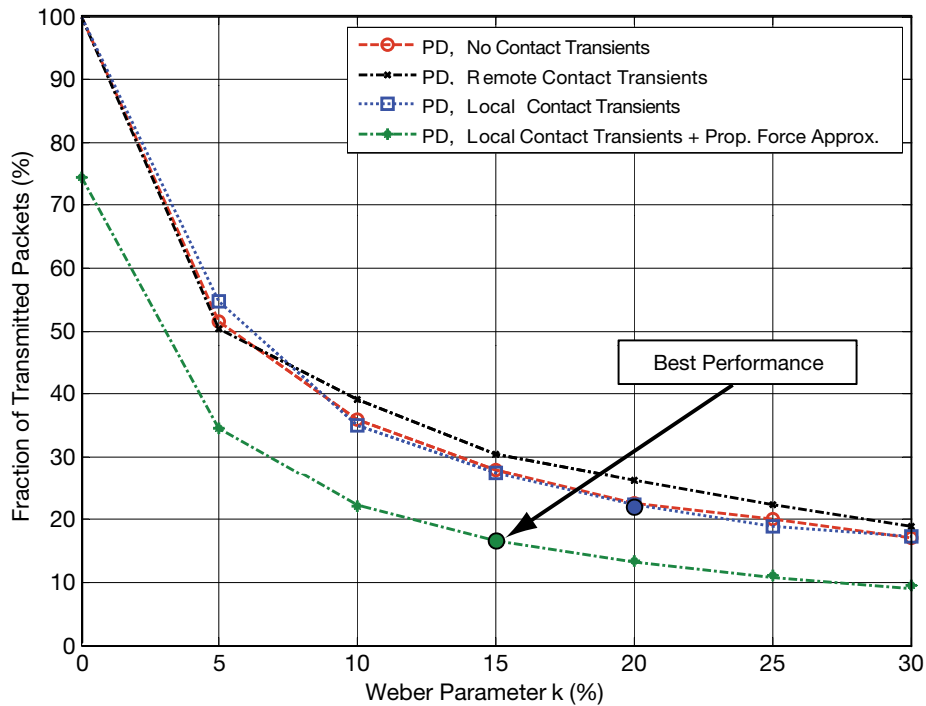
The results of the subjective quality investigation are illustrated in Figure 3.24(b) showing means and standard deviations of the subjective user ratings for the investigated configurations. The presented results on subjective quality for a given k are based on a comparison with the same configuration but disabled PD compression ($k = 0\%$). It appears that the users prefer the more crisp contact provided by the direct superimposition of contact transients. The configurations with directly applied local and remote contact transient superimposition have similar ratings.

For systems in which strong data reduction is necessary at acceptable but not disturbing presentation of the force signal, the experiments reveal the configurations with local contact acceleration to be preferable up to a deadband size corresponding to a k value of 20%. Therefore, it outperforms the plain deadband configuration without any contact transient model applied, which performs acceptably in terms of distortion for deadband sizes corresponding to k values of 15%. This is particularly surprising, as it seems that the introduction of contact transients conceals the artefacts of the perceptual PD compression scheme and therefore supports keeping introduced coding distortion below human perception thresholds, not only in the transient region but also to some extent in the post-transient interaction region.

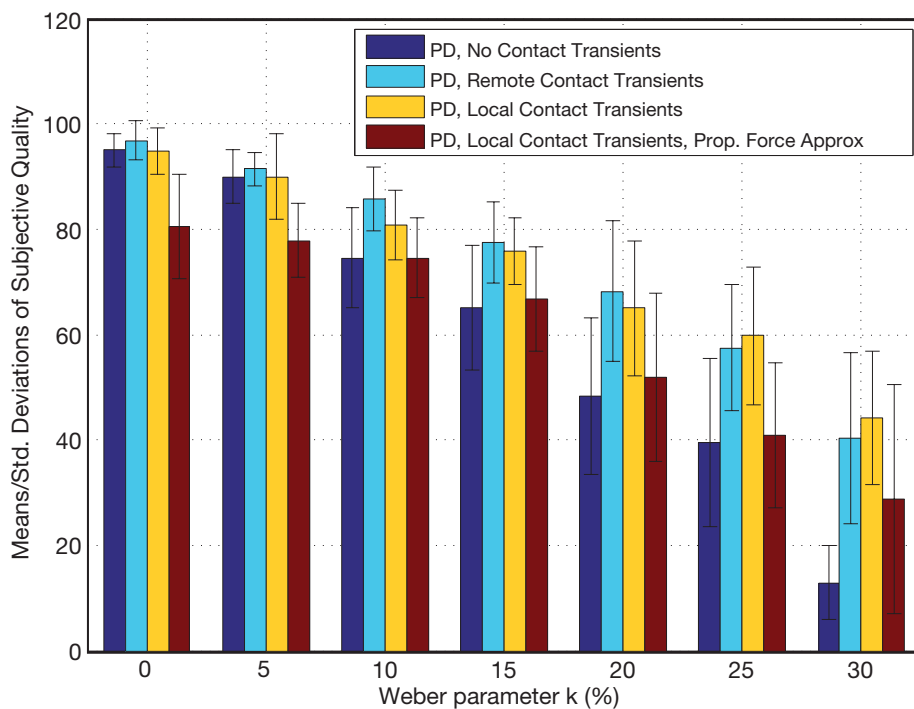
In the fourth test configuration, the proportional forces are substituted by the output of the locally deployed contact model during the contact phase. Here, an acceptable subjective quality result can be observed until a k of around 15%. Compared to this, the configurations

with local and remote superimposition of contact transients achieve similar performance at $k = 20\%$. Simultaneously consulting both the mean packet rate results and the mean subjective rating results allows for spotting points of best system performance, as marked in Figure 3.24(a). The best performance is achieved with the fourth test configuration where perceptual deadband coding with a $k = 15\%$ and locally deploying a multi-DoF contact model is combined with proportional feedback substitution. Here, the packet rate is further reduced from 28% (central curve) to 17% (lowermost curve) which results in a packet rate reduction of 83%.

In summary, the results show that with contact acceleration feedback, the PD data reduction scheme can operate with larger deadband sizes providing enhanced haptic data reduction performance. When contact forces are locally approximated for substituting the remote haptic signals, optimal performance is achieved at $k = 15\%$ on both result charts, making this point of operation the best in terms of both data reduction performance and quality of haptic force feedback. Here, an improved data reduction performance is observed as it pulls the packet rate further down (from the central curve to the lowermost curve) by roughly 11%.



(a) Packet rates for different test configurations as a function of the PD parameter k .



(b) Mean and standard deviation bars of user ratings for different test configurations across a range of k values.

Figure 3.24: Experimental results for event-based coding using contact models (reproduced from [2]). The results show that the integration of local contact models into the PD compression scheme allows for improved compression performance and enhanced quality of haptic force feedback.

3.3 Perceptual Haptic Coding of Recorded Telemanipulation Sessions

In many TPTA scenarios, the ability to record and store a haptic TPTA session is of great interest. For instance, in highly complex TPTA scenarios such as on-orbit servicing or surgery TPTA systems, recorded TPTA sessions can serve as important documentation resources of performed work steps. Furthermore, the recording and replay of TPTA sessions are an important tool in teacher-student scenarios. As complex TPTA systems require experienced and well trained OPs, the replay of recorded TPTA sessions can support skill-transfer and training tasks. In addition, a subsequent analysis of a TPTA session enables the determination of the system performance and allows for detecting important system parameters. Once haptic data has to be stored for posterior replay, the interest in compressing this kind of data emerges.

In this section, the challenges of recording and playing back TPTA sessions are discussed. In addition, a perceptual haptic offline compression scheme [17, 18, 86] is presented which exploits the relaxed delay constraints in haptic offline signal processing.

3.3.1 Recording and Replay of Multimodal TPTA Sessions

In order to record a multimodal TPTA session, all involved modalities have to be synchronously encoded and stored to a storage device. This allows for posterior replaying of the telemanipulation session by redisplaying the previously recorded media content.

3.3.1.1 Related Work

Most haptic playback systems presented in literature propose position guidance and implement a proportional-derivative position controller [62, 63, 71]. Here, the subject is kinesiologically guided through the recorded motion by the haptic interface in order to support the learning of complex movements and motion skills [75]. Similarly, Hemni *et al.* present a virtual calligraphy system which allows for the recording of the position trajectories of a teacher's writing brush for subsequently displaying the expert's data sets to a student [96]. The authors in [136] introduce haptic recording and playback in the context of a virtual haptic museum, which enables virtual "museum visitors" to haptically explore virtual exhibits by touching them. In addition, a comprehensive analysis on how sensorimotor skills can be taught through haptics is presented in [83]. Burdea *et al.* discuss a virtual reality simulator for the diagnosis of prostata cancer with integrated recording and playback functionality for performance and training purpose [43]. The potential of haptic and auditory trajectory playback as a method of teaching shapes and gestures to visually impaired people is investigated in [62, 63]. Alternatively, the authors in [157] propose using synchronized recordings of the haptic signals together with a video recording from the expert's viewpoint. During the multimodal session replay, the user is guided along the recorded position trajectory through virtual fixtures [156] while the recorded video stream is played back with dynamically adjusted speed according to the current user hand position.

However, these position guided haptic playback approaches have a major disadvantage. Position guidance in the form of virtual fixtures or proportional-derivative position con-

troller based directional forces occupy the motors of the HSI device. This means that during the playback of recorded position information of the expert's movements, the display of guidance forces excludes the ability of simultaneously displaying recorded force feedback information. Similarly, the display of prerecorded force feedback signals through the deployed haptic device does not allow simultaneously presenting force-feedback based position guidance. This haptic playback discrepancy is formally described as a control engineering problem in [58].

The ability to perceive haptic force-feedback information, however, is especially important in scenarios where information about the remote environment is presented best by the haptic modality, such as surface roughness, friction, viscoelasticity, etc. In order to overcome the playback discrepancy, Henmi *et al.* (see [96]) propose substituting competing haptic feedback signals by displaying force feedback intensity in the visual feedback represented by circles with radius proportional to the force magnitudes. Similarly, position information can be visually displayed together with the current position of the student. In this way, the student is able to follow the prerecorded trajectory of the teacher while perceiving force feedback through the device. A similar approach can be found in [194], where a virtual cursor tracing the expert's path is shown in the visual feedback. The user must actively follow the cursor to receive position feedback while the haptic device displays corresponding force feedback information. Nevertheless, the required user activity during the playback process clearly distracts the immersion into the recorded haptic session.

3.3.1.2 Proposed Recording and Replay System Architecture

In this section, a novel recording and playback scheme for interactive TPTA sessions is presented. It is based on the observation that the human perception system can associate the recorded movements and actions of the TOP from the visual content and relate simultaneously displayed force feedback to it.

Figure 3.25(a) shows a schematic overview of the proposed recording scheme for visual-haptic TPTA sessions. The human OP remotely controls the TOP and receives multimodal sensory information captured by the TOP. During TPTA operation, the OP's perception of the orientation and the position of the TOP relates to the local interaction with the HSI in conjunction with remotely sensed and locally displayed visual and haptic sensory information. In order to enable the posterior playback of the recorded multimodal TPTA session, each modality of the transmitted and displayed multimodal sensory information needs to be captured and stored on a data storage device.

During the replay of a recorded TPTA session, the previously captured and compressed multimedia content is decoded and redisplayed through the HSI as shown in Figure 3.25(b). Here, the displayed force feedback originates from the session recording and no longer relate to the user interaction. To provide a posterior immersion of the recorded multimodal TPTA session, the human OP is explicitly instructed to resist the displayed contact forces referring to the visually displayed haptic contact events. Hence, the user keeps the HSI at a fixed position during the whole visual-haptic replay, preferably at the center of its workspace and only perceives tactile contact forces. Experimental results in [17, 18, 40] show that an adequate visual presentation of the movements of the operator successfully enables an imagination of the performed actions, which is solely perceived through the presented visual information. In other words, the position perception of the haptic tool becomes substituted by the visual

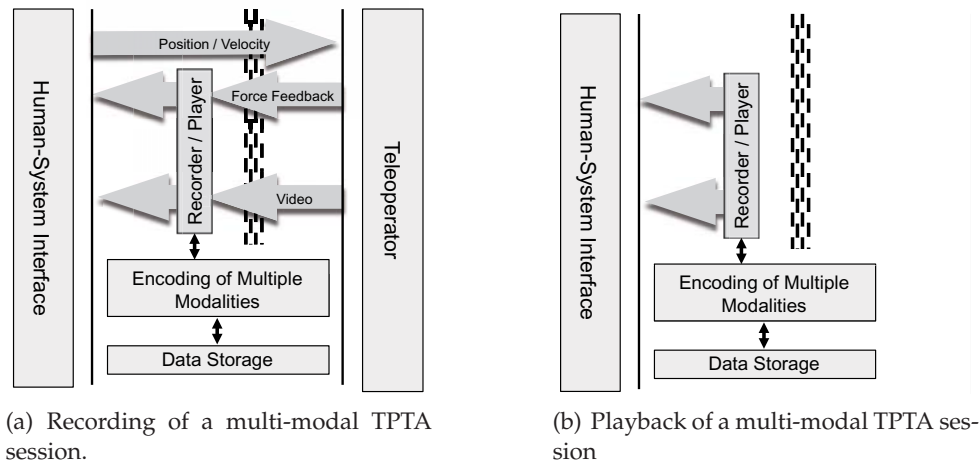


Figure 3.25: Schematic overview of recording and playback of a visual-haptic TPTA session. Multi modal feedback information to be displayed to the human OP is encoded and stored on a storage device. During playback, the previously captured and compressed multimedia content is decoded and redisplayed through the HSI.

feedback and supplemented with tactile contact forces that are displayed through the HSI, independent of the current user hand position. In this manner, the users are able to immerse into the previously recorded TPTA session.

3.3.2 Perceptual Offline Compression

When approaching haptic offline compression, one major difference in comparison to the delay-critical real-time processing of haptic data can be noted. In offline compression, haptic data is either sent from the haptic sensors to the recording device or played back from the recording device to be displayed through the human system interface. Hence, haptic signals are unidirectionally transmitted and, therefore, do not affect the stability of the delay critical control loops anymore enabling pre- and/or post-processing of the corresponding haptic data streams.

Particularly, the relaxed delay constraints enable:

- **Block-based signal encoding:** Offline compression schemes are no longer restricted to process the signals sample by sample. Instead, a comprehensive investigation of the signal at once or in parts in the time and/or frequency domain can be performed before deciding which haptic information can be considered to be irrelevant for encoding and therefore being discarded.
- **Block-based signal decoding:** The relaxed delay constraints also affect the design of the decoder algorithm. To reconstruct signal components being discarded during encoding, the decoder can reference not only previous but also future signal information.
- **Predictive coding and entropy coding:** Perceptual real-time communication mainly focuses on the reduction of high packet rates on the haptic channel. In contrast, haptic offline applications do not need to focus on end-to-end latency minimization. Here,

a reduction of data is specifically addressed by applying predictive coding techniques combined with entropy coding methods.

In the following, the PD compression approach presented in Section 2.3.2 is modified to apply to offline compression scenarios [17, 18]. In particular, a novel signal prediction approach combined with entropy coding is integrated which incorporates knowledge about applied perception bounds for additional entropy minimization. Furthermore, instead of extrapolative (predictive) signal reconstruction as performed in low-latency decoding of PD-encoded haptic signals, the offline decoding scheme uses an interpolation algorithm which takes future haptic samples into account during the signal reconstruction process.

3.3.2.1 Deadband-based Differential Coding

The perceptual predictive compression approach discussed in Section 2.3.2 deploys two coherent haptic signal predictors; one at the sender and the other at the receiver side. As long as no compressed haptic data is lost or corrupted, they keep running in parallel and provide consistent haptic sample estimates \mathbf{p} . Only if the prediction error exceeds the applied discrimination thresholds, the prediction error is considered to be perceivable and an update needs to be encoded. Instead of encoding absolute values of haptic input samples \mathbf{h} during events of PD violations (as proposed in real-time PD compression), the PD differential compression approach encodes only the deviation between the predicted \mathbf{p} and the incoming haptic sample \mathbf{h} , i.e., the prediction error $\mathbf{d} = \mathbf{p} - \mathbf{h}$, which leads to reduced entropy of the encoded haptic data. Additionally, further knowledge about the applied PD can be exploited. As only samples violating the applied perceptual thresholds are considered to be relevant for encoding, a certain knowledge about the prediction error \mathbf{d} is available: It is known that the norm of the prediction error must have exceeded the size of the currently applied PD. This observation can be exploited by transforming the prediction error \mathbf{p} to polar coordinates. Here, only the surplus of the vector norm of the prediction error $\Delta^I = |\mathbf{d}| - \{\text{size of PD}\}$ needs to be encoded which leads to additional compression gain due to reduced marginal entropy of Δ^I . As the applied perception thresholds are also available during decoding, the encoded prediction error \mathbf{d} can be fully recovered. This concept is illustrated in Figure 3.26.

The proposed architecture for PD-based differential compression is shown in Figure 3.27. During encoding, the encoder is fed with the current haptic sensory sample \mathbf{h} together with a predicted signal forecast \mathbf{p} delivered by the predictor algorithm, as shown in Figure 3.27(a). As long as the incoming signal lies within the PD of the predicted signal \mathbf{p} , the human user is expected to be unable to distinguish between the incoming and the predicted haptic samples. During the state of dropping input samples, the time interval t is clocked, which is required for later signal decoding. Correspondingly, as soon as an incoming haptic signal sample violates the pending PD of the predicted sample \mathbf{p} , a signal update $\mathbf{u} = \mathbf{d}$ together with the amount of previously dropped samples t are jointly encoded.

In the next step the proposed PD-based differential encoding technique is applied. To this end, the prediction error vector \mathbf{d} is transformed from the Cartesian domain $\mathbf{d} := (\mathbf{d}_1, \dots, \mathbf{d}_D)$ with D dimensions into the polar coordinate system $\mathbf{d} := (\varphi_1, \dots, \varphi_{D-1}, r)$. As the norm of the prediction error \mathbf{d} must have exceeded the currently defined deadzone, the corresponding deadzone size is subtracted from the norm of the prediction error to determine Δ^I . Furthermore, the direction of successive prediction errors \mathbf{d} typically shows a

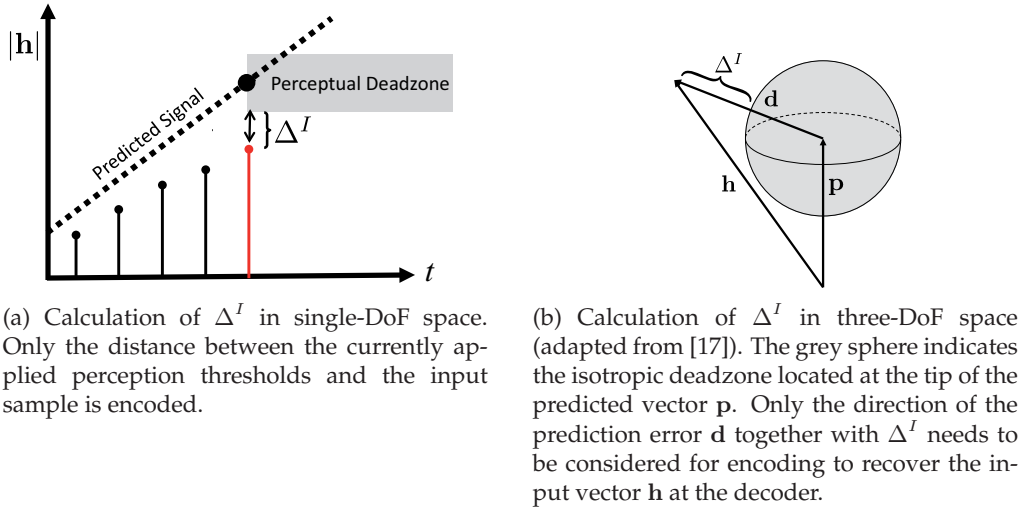


Figure 3.26: Illustration of PD-based differential encoding. Only the surplus of the vector norm of the prediction error $\Delta^I = |\mathbf{d}| - \{\text{size of deadzone}\}$ needs to be encoded which allows for a reduction of the marginal entropy of Δ^I .

strong temporal correlation, which allows for a second predictive coding stage for the polar angles. This is mainly due to the fact that the orientation of the haptic sample vectors may change slowly over time, so that the prediction process has to be updated several times in a similar manner. By differentially encoding $\varphi_1, \dots, \varphi_{D-1}$, this correlation is exploited.

The differentially encoded values $\Delta\varphi_j$ and Δ^I are furthermore uniformly quantized with individual quantization resolutions to be fed together with the time interval t to the entropy encoder. By using an end-of-sequence symbol, the individual bit streams of $\varphi_1, \dots, \varphi_{D-1}$, Δr , and time intervals t can be sequentially linked up to finally build the encoded output bit stream b . In order to keep the prediction process coherent during encoding and decoding, the predictors at the encoder are fed with the quantized signal output \mathbf{d}' .

3.3.2.2 Interpolative Signal Reconstruction

During PD-encoding, the haptic input signal is irregularly downsampled, which leads to the desired strong data reduction. The decoder needs to recover the discarded signal information and to upsample the haptic signals to their original constant sampling rate before they can be forwarded to the haptic display devices (see Figure 3.27(b)).

As previously discussed, the decoding process also benefits from the relaxed delay constraints. In contrast to haptic online compression, the decoded sample vectors \mathbf{u} can be subsequently used as the supporting points of an interpolation algorithm to estimate the discarded samples. A schematic illustration of the interpolative signal decoding process is illustrated in Figure 3.28. The assumed perception thresholds (boundaries of gray zones) in the upper graph are a function of the magnitude of the PD-defining haptic samples. Black circles represent haptic samples violating the applied perception threshold and hence are considered to be relevant for encoding. The lower graph illustrates the signal reconstruction process during decoding. Here, a first-order linear interpolation algorithm is used to

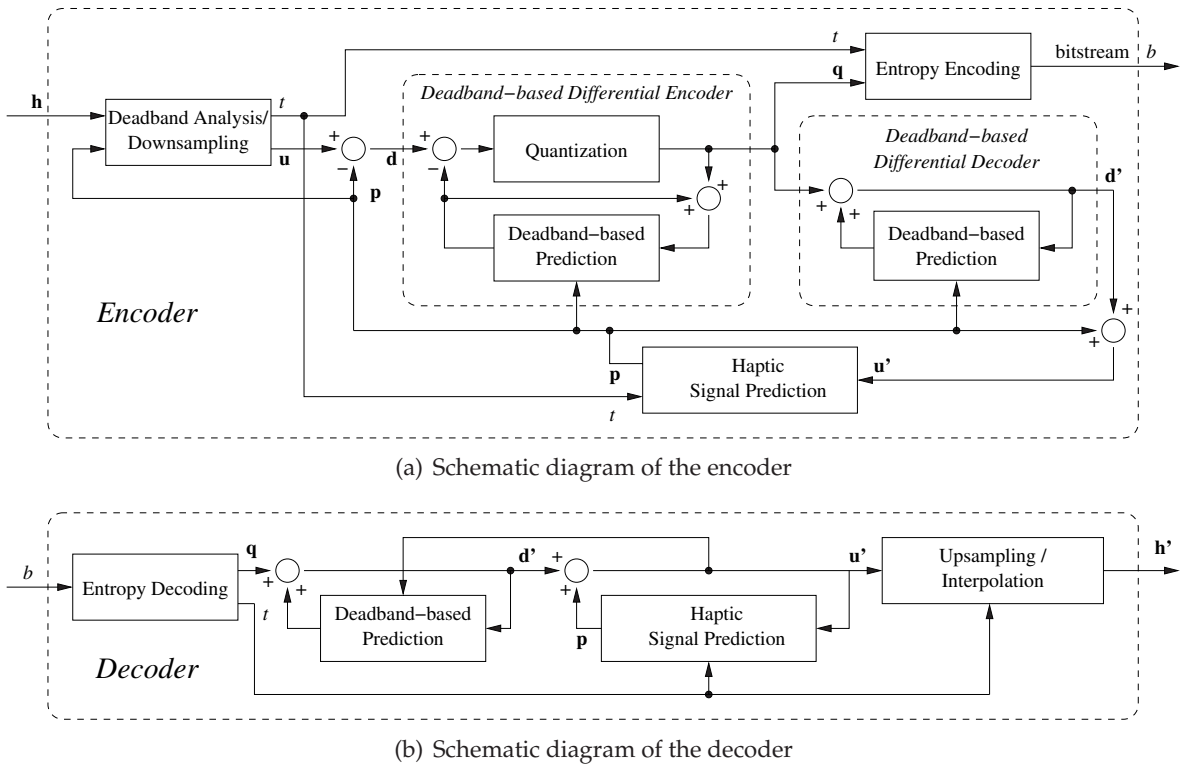


Figure 3.27: Schematic diagram of the PD-based offline data reduction scheme including the proposed signal prediction and deadband-based differential coding approach (reproduced from [17]).

estimate the missing haptic samples.

This is in contrast to the real-time PD compression which performs an extrapolative signal reconstruction in order to minimize its signal processing latency. The difference between interpolative and extrapolative signal reconstruction is illustrated in Figure 3.29. The dots illustrate the encoded haptic samples. Figure 3.29(a) shows the performance of extrapolative signal reconstruction in online perceptual haptic compression. At each predictor update, discontinuities in terms of sudden steps within the signal are observable. In offline compression, the encoded haptic signal samples can be used as supporting point of an interpolation algorithm which leads to a smooth signal trajectory, as visualized in Figure 3.29(b).

3.3.2.3 Experimental Evaluation

The goal of the proposed haptic offline compression approach is to reduce the amount of data without a noticeable impact on user perception. In particular, the PD parameter k as well as the degree of quantization puts a strong impact on the perceived quality of the encoded signal. To find points of optimal and maximized performance while maintaining a high degree of transparency of the applied signal processing methods, an experimental evaluation with human subjects has been conducted.

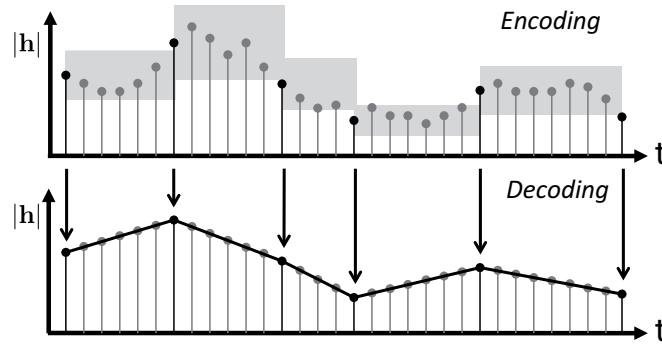


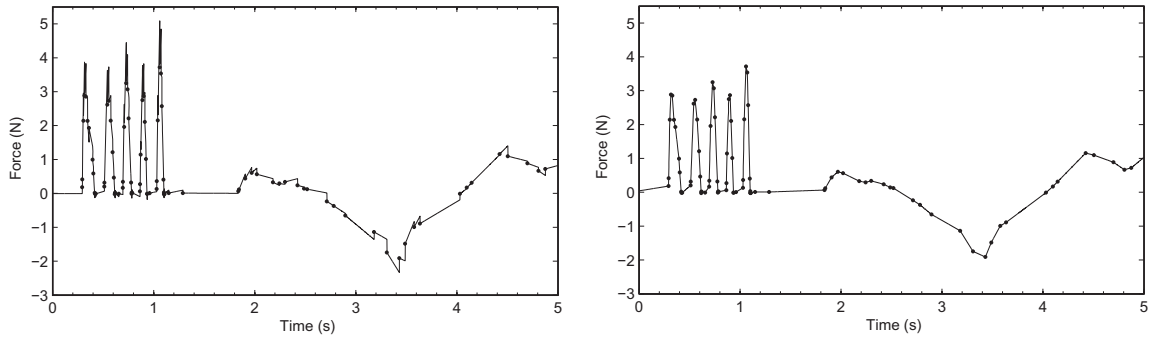
Figure 3.28: Principle of interpolative signal reconstruction (reproduced from [18]). Perceptually irrelevant samples are discarded during encoding and estimated during decoding using an interpolation algorithm.

For psychophysical evaluation, a virtual TPTA system is used. The remote environment is simulated and contains a virtual scene consisting of a touchable sphere. On the operator side, a SensAble’s PHANTOM Omni [163] HSI device is used to track the hand movements which are mapped to the virtual TOP. As soon as it encounters contact with the three dimensional sphere, corresponding force feedback is rendered and displayed to the human OP. During the recording of the TPTA session, the visual and force feedback information received from the remote (virtual) environment is synchronously stored on a local data storage device. This allows for a posterior replaying of the TPTA session by redisplaying the previously recorded multimedia content (see Section 3.3.1.2).

Prior to the experiment, a TPTA session of the described TPTA setup of 14.43 seconds in length (14432 samples) is recorded. During the recording, several actions are continuously performed to include all kinds of possible haptic force feedback characteristics, such as poking into the sphere from different directions, keeping contact while sliding along the surface, etc. As in the test scenario, haptic signal samples with three-DoF and sensed with 32 bit floating point precision are applied, the total amount of data of the unencoded haptic signal is: $3 \text{ DoF} \cdot 32 \text{ bits/smp} \cdot 14432 \text{ smp} = 173184 \text{ bytes}$.

The recorded visual data stays unmodified the whole time, while the corresponding haptic force feedback signal is modified by applying the proposed haptic offline compression scheme with different parameters. To evaluate the influence of the involved PD parameter k as well as the applied quantization resolution on performance and transparency of the proposed algorithms, 18 different parameter sets are used to configure the encoding process. That follows the generation of corresponding test signals for evaluation purposes. In six parameter sets, the quantization step is completely deactivated to investigate the sole influence of the PD parameter k . To analyze the impact of the quantization on performance and transparency, twelve additional parameter sets are applied, all with a PD parameter k set to 50% and varying quantization resolutions. The differentially encoded polar angles and Δ^I values (range 0.0-1.0N) are individually quantized with a different quantization resolution. For the test items with partly or completely deactivated quantization, the entropy coding stage and bitstream generation is also skipped due to missing quantizer indices.

Eleven subjects participated in the experiment. In the evaluation software, all versions of the recording with differently encoded force feedback content are put in random order and



(a) Online signal reconstruction based on extrapolation. (b) Offline signal reconstruction based on interpolation.

Figure 3.29: Differences between online and offline signal reconstruction of PD-encoded haptic signals (reproduced from [17]).

presented in a blind manner. Additionally, the original unmodified TPTA recording is clearly marked and made selectable for replaying. The subjects are able to switch freely between all presented versions of the TPTA session recording without knowing the explicit encoding parameter set. For each presented recording, they are asked to rate the degree of perceived deviation between the unencoded and the lossy encoded haptic force feedback signals. Based on their subjective perception, they assess the influence of the proposed encoding scheme on a scale from 0 (strong perceived difference) to 100 (no perceivable difference), as shown in Table 2.1 in Section 2.1.4.

The results of the conducted subjective evaluation show a strong data reduction ability while keeping introduced coding artefacts within an acceptable range. In order to investigate the impact of the PD parameter k on transparency and performance, six test items derive from applying a varying PD parameter k while disabling the quantization step during encoding. The mean ratings and the amount of dropped input samples during encoding can be seen in Table 3.2. The subjective mean evaluation ratings with respect to the PD percentage k are shown in Figure 3.30. The obtained results reveal an interesting system behavior. Already at a small PD of 10%, more than 95% of the incoming sample vectors are dropped during the PD analysis stage. The rate of dropped samples slowly increases even more up to 99% at a PD parameter k of 95%. When investigating the mean evaluation ratings with respect to the applied deadzone size, the test subjects report a high degree of transparency of the applied signal processing steps. Up to a deadband percentage of 50%, the evaluated mean ratings range between 80 and 90. This is in contrast to online PD compression, where already small PD parameter values of ≤ 15 lead to noticeable artefacts (update steps) originating from extrapolative signal reconstruction. Most subjects report that the only difference they could feel is a little reduction in force intensity of the force feedback signal. This can be explained by the fact that in case of an already pending strong haptic stimulus, temporary peaks in amplitude often fall within the deadzone and therefore are discarded during encoding. By this means, the PD analyzer tends to slightly reduce the energy of the haptic signal, leading to an impression of a globally reduced intensity of the decoded haptic information.

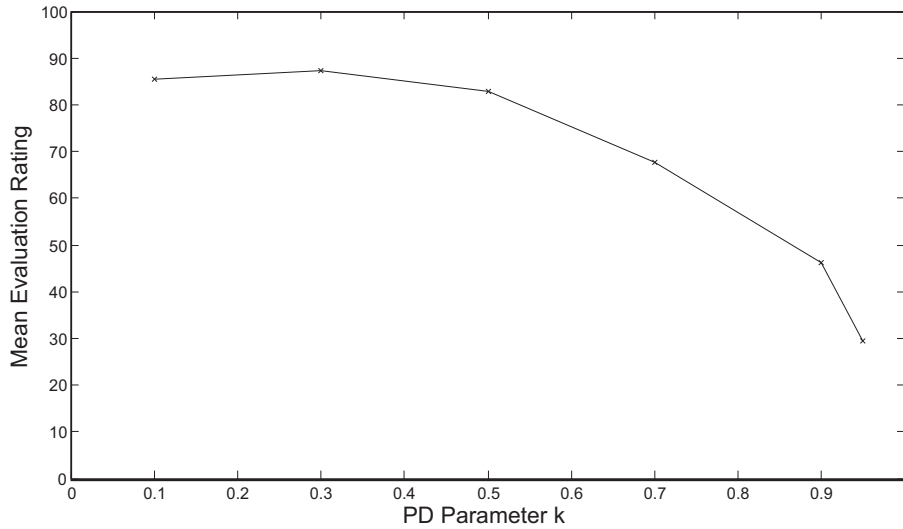


Figure 3.30: Experimental results showing the mean subjective ratings with respect to the deadband threshold parameter k (reproduced from [17]).

Additionally, the influence of the quantization settings on performance and transparency is investigated. For this analysis, a PD of 50% is used for all test items as it shows optimal performance in the previously described experiment. In a first step, the impact of quantization noise on the representation of the polar angles is analyzed, followed by a quantization of the encoded Δr norm values. The results are presented in Table 3.2. In both cases, the disturbances induced by the quantizer have a similar impact. The results show that with strongly reduced quantization precision, the mean subjective evaluation ratings are not significantly affected, while the amount of encoded samples increases slowly. During encoding, the quantization noise clearly affects the performance of the applied prediction algorithms, as the prediction filter coefficients are redefined at each encoding instance according to the encoded signal update information. Due to the quantized signal representation, bigger prediction errors are more likely leading to an increased number of deadzone violations which are generating additional haptic signal updates. Nevertheless, the results reveal acceptable ranges for quantizing the differentially encoded polar coordinates to be 6-8 bits per angle value and 2-4 bits per polar norm. When applying quantization on both the differential encoded polar angles and the PD-based norm values corresponding quantization indices are forwarded to the applied adaptive arithmetic encoder for entropy encoding. The total length in bytes of the entirely encoded haptic force feedback signal of the test item is also shown in Table 3.2.

In the experiments, best performance in data reduction and transparency is achieved with a PD of $k = 50\%$ when assigning 8 bits to the quantization of the polar angles and 4 bits for the corresponding vector norm Δ^I . Applying this configuration enables the compression of the recorded haptic force feedback signal with 173184 bytes in length to a reduced size of only 1819 bytes, which results in a data compression factor of about 95. In other words, the proposed coding scheme is able to encode recorded haptic force feedback data streams with only 0.0105% of the original data size.

Weber k	Quantization φ	Quantization r	Compression	Encoded Samples	Subjective Rating	Bitstream (bytes)
10 %	off (float)	off (float)	96.4 %	519	85.5	-
30 %	off (float)	off (float)	98.0 %	288	87.2	-
50 %	off (float)	off (float)	98.4 %	231	82.7	-
70 %	off (float)	off (float)	98.7 %	187	67.7	-
90 %	off (float)	off (float)	98.9 %	158	46.1	-
95 %	off (float)	off (float)	99.0 %	144	29.4	-
50 %	off (float)	8 bit	98.4 %	228	82.3	-
50 %	off (float)	6 bit	98.3 %	237	84.5	-
50 %	off (float)	4 bit	98.2 %	259	85.0	-
50 %	off (float)	2 bit	97.8 %	310	85.0	-
50 %	8 bit	off (float)	98.4 %	226	81.5	-
50 %	6 bit	off (float)	98.2 %	247	84.0	-
50 %	4 bit	off (float)	98.2 %	259	84.0	-
50 %	3 bit	off (float)	97.8 %	304	77.5	-
50 %	6 bit	2 bits	97.7 %	319	75.5	1585
50 %	6 bit	4 bits	98.1 %	268	77.5	1511
50 %	8 bit	2 bits	97.8 %	318	88.8	2045
50 %	8 bit	4 bits	98.2 %	257	88.5	1819

Table 3.2: Experimental results of the perceptual haptic offline compression scheme (reproduced from [17]). The influence of the quantization resolution on the encoding performance and the perceived quality can be observed.

3.4 Theoretical Analysis of Perceptual Deadband Coding

In the previous sections, several contributions to haptic online and offline compression have been presented. In this section, the PD compression scheme is further analyzed from a theoretical point of view. The presented mathematical framework allows the iterative determination of the signal statistics of the update behavior for a random input signal model. More specifically, a stochastic Gaussian first-order random walk model is used to simulate haptic signals and mathematically determine the relationship between the PD parameter k and its combined transmission rate savings. In the following, the PD compression approach is investigated in terms of an adaptive sampler.

The presented research work in this section has been conducted in cooperation with Dr. Peter Hinterseer and Prof. Subhasis Chaudhuri [11, 16, 97].

3.4.1 Perceptual Deadband Sampler

The PD compression scheme using perceptual bounds (see Section 2.3.2) can be mathematically modeled as an adaptive sampling process. In contrast to regular sampling where the amplitude of a continuous signal is measured at a fixed rate, the PD sampler samples the input only if a change in signal is considered to be perceivable according to pending perception thresholds. This leads to a non-uniform or adaptive sampling process. In accordance with the PD compression approach, the PD sampler investigated in this section aims to select only perceptually relevant samples which lead to the desired perceptual lossy compression.

In the following, the method of operation of the zeroth-order PD compression algorithm is mathematically described (see Section 2.3.4.1).

A discrete single-DoF haptic input signal h can be defined as:

$$h_i \in (-\infty, +\infty) \quad (3.31)$$

where i is the sequence number of a sequence of discrete input samples.

The output signal of the PD sampler \hat{h}_i is generated by the following rules:

$$\hat{h}_1 = h_1 \quad (3.32)$$

$$\hat{h}_i = \begin{cases} \hat{h}_{i-j} & \text{if } \frac{|h_i - \hat{h}_{i-j}|}{|\hat{h}_{i-j}|} < k \\ h_i & \text{else} \end{cases} \quad \text{where } i > 1 \quad (3.33)$$

and

$$\hat{h}_{i-1} = \hat{h}_{i-2} = \dots = \hat{h}_{i-j} = h_{i-j} \quad (3.34)$$

where j samples back in discrete time, when the last threshold violation took place. The PD parameter k controls the applied perception threshold based on Weber's Law of the JND (see (2.8) in Section 2.2.2). The sample h_{i-j} is called the *reference value* from now on.

Based on the PD parameter k , the corresponding PD bounds are defined by:

$$\text{PD interval } \mathcal{W}(\hat{h}_i) = \begin{cases} [\hat{h}_i(1-k), \hat{h}_i(1+k)] & \text{if } \hat{h}_i \geq 0 \\ [\hat{h}_i(1+k), \hat{h}_i(1-k)] & \text{if } \hat{h}_i < 0 \end{cases} \quad (3.35)$$

Note that the size of the PD bound only depends on the magnitude and not on the sign of the input value of the haptic sample. This leads to symmetry at the origin which allows for some simplifications, such as focusing on positive sample values in the upcoming derivations.

3.4.2 Stochastic Input Model for Haptic Signals

Haptic signals are influenced by many highly nonlinear factors and physical properties of the human operator, the TPTA system and the remote environment. Accordingly, the design of a stochastic model for simulating the trajectories of haptic signals in TPTA systems is a challenging and complex task. Nevertheless, some important characteristics of haptic signals in TPTA systems can be observed. Firstly, the haptic signals mostly exhibit low frequency signal characteristics. Especially during free space motions, the inertia of the human body and the haptic devices leads to smooth and relatively slow changing signal trajectories. Therefore, adjacent haptic signal samples are typically strongly correlated. Only during the events of contact with the remote/virtual environment, the haptic signal typically shows a transient signal behavior due to the sudden force feedback and/or sudden change in velocity [15, 128, 129, 191].

These signal trajectories show a certain similarity to so-called "random walks" known from the field of stochastic processes. To mathematically simulate haptic signals with similar characteristics, a first-order autoregressive (AR) random process is chosen, which is closely related to random walk models.

A first-order AR random process for modeling haptic signal input can be described as:

$$h_1 = \eta \quad (3.36)$$

$$h_i = \theta h_{i-1} + \eta \quad \text{where } i > 1, |\theta| \leq 1 \quad (3.37)$$

It implements the regression of the output signal on its own past values. By these means, the AR coefficient θ influences the degree of correlation in the output signal and can be used to adjust it to the characteristics of observed haptic signals. The random increment variable η is an independently distributed random variable. Hence, at every time instance, the random process refers to a fraction θ of the previous signal output which is added to the outcome of a real-valued random variable η . If the coefficient θ equals one, it results in a classic random walk / Wiener process. If θ equals zero, it reflects a process of order zero, i.e., an independent and identically distributed (i.i.d.) random signal.

3.4.3 Theoretical Analysis

At each time i , the PD sampler tests if the human is able to perceive the change in the signal amplitude. The signal sample h_i lies either within the PD defined by \hat{h}_{i-j} , i.e., $h_i \in \mathcal{W}(\hat{h}_{i-j})$ or not, i.e., $h_i \notin \mathcal{W}(\hat{h}_{i-j})$. In case of a PD violation, the output of the PD sampler adapts to the current sample amplitude and, consequently, the applied perception thresholds are redefined. To this end, the perceptual evaluation affects the output of the PD sampler in a non-linear manner and puts an impact on future PD bound evaluation results. To model these non-linear dependencies, a binary tree structure is built to derive the conditional probabilities of a particular sampler output value \hat{h}_i with respect to a previously occurred PD violation/compliance event history s (see Figure 3.31).

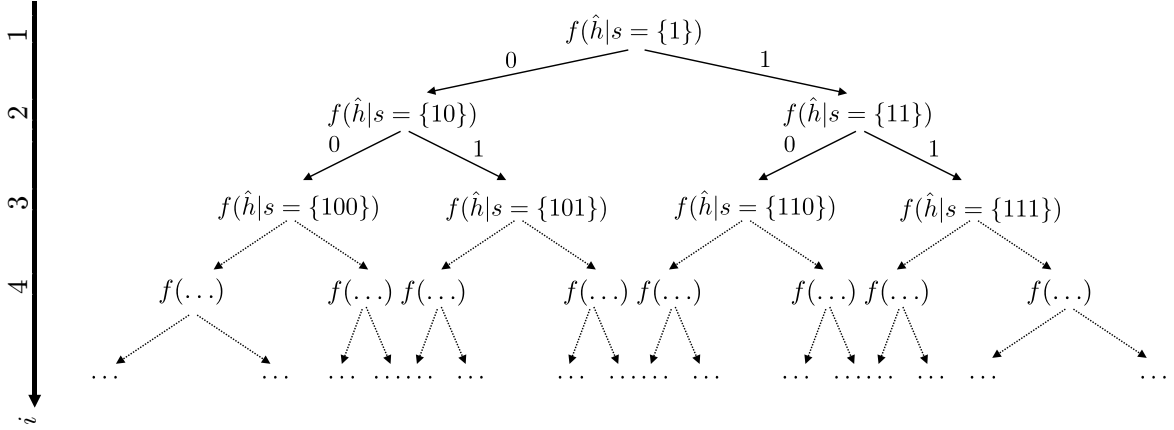


Figure 3.31: Schematic diagram of the proposed binary tree structure. Each node represents a conditional probability distribution function $f(u|s)$, which represents the probability of the occurrence of a specific event sequence s resulting in a particular output sample u .

Starting at the root of the binary tree at h_1 , the conditional probability distribution functions $f(\hat{h}|s)$ are sequentially determined. They address the probability of occurrence of a specific event sequence s resulting in a particular output sample \hat{h} . The first incoming sample initializes the PD-based perception thresholds $\mathcal{W}(h_1)$ and leads to a first output sample $\hat{h}_1 = h_1$. For sample h_2 it is either possible to lie within the PD of \hat{h}_1 or not. These two possibilities have to be considered individually and therefore constitute the first two branches of the tree. This approach enables the observation of all possible event sequences of previously occurred PD violations or PD compliances where the path back to the root of the tree represents a specific PD test sequence s . All nodes in the binary tree refer to corresponding conditional density distribution functions. In the following, the notation of the sequence s refers to either being in compliance with the respective PD (0) or not (1). Accordingly, the length of the sequence denotes the time instance i of the input sequence, which corresponds to the depth of the binary tree.

The binary tree structure considers all possible event sequences affecting the output distribution as well as the update rate behavior of the PD sampler. Integrating $f(\hat{h}|s)$ over \hat{h} at node s results in the probability of the occurrence of a specific PD event sequence s :

$$\Pr[s] = \int_{-\infty}^{+\infty} f(\hat{h}|s) d\hat{h} \quad (3.38)$$

The overall probability that a PD bound violation occurred at time i consists of all conditional probabilities referring to a PD violation event at tree depth i . As every node within a certain tree level describes an individual state of the Weber sampler, the conditional probability functions within a particular depth level of the binary tree have to be independent from each other with respect to the sequence argument s . This enables the union of corresponding conditional probabilities and, therefore, the determination of the overall probability of a PD violation event:

$$\Pr\{\text{Bound violation at time } i\} = \sum_{s=\{0,1\}^{i-1}\{1\}} \int_{-\infty}^{+\infty} f(\hat{h}|s) d\hat{h} \quad (3.39)$$

with $\{0, 1\}^{i-1}\{1\}$ indicating any binary sequence of length i where the last bit is equal to 1. In a similar manner, the overall probability of a PD compliance at time i can be determined. By taking into account any binary sequence of length i where the last bit is equal to 0, we are able to calculate the overall probability of a PD compliance at time i :

$$\begin{aligned} \Pr\{\text{Bound compliance at time } i\} &= 1 - \Pr\{\text{Bound violation at time } i\} \quad (3.40) \\ &= \sum_{s=\{0,1\}^{i-1}\{0\}} \int_{-\infty}^{+\infty} f(\hat{h}|s) d\hat{h} \end{aligned}$$

Note that the probability of a particular PD sampler output value \hat{h} is influenced by the PD event sequence s . This means, although the applied random input model is generated by a Markov process according to (3.36), the corresponding probabilities of the signal output of the PD sampler at various nodes of the proposed binary tree structure do not constitute a Markov chain. Correspondingly, one has to travel from the root node to the given node to compute the probability of that particular state. Processing the nodes backwards towards the root by taking conditional density functions of the sibling nodes into account in order to determine the distribution function at a parent node is also not possible.

$$f(\hat{h}|s\{0\}) + f(\hat{h}|s\{1\}) \neq f(\hat{h}, s) \quad \forall s \in \{0, 1\}^i \quad (3.41)$$

This means the mathematical analysis has to start at the root of the binary tree propagating to the child nodes in order to consider the conditional density functions $f(\hat{h}|s)$ of all possible PD bound event sequences. In the following, a method to iteratively derive $f(\hat{h})$ to finally investigate the PD sampling behavior with respect to its update rate is presented.

3.4.3.1 Initialization

The first signal sample h_1 needs to be sampled, as it defines the initial PD bounds. Hence, the first output sample is $\hat{h}_1 = h_1$ which defines the PD bound $\mathcal{W}(\hat{h}_1)$. The probability density functions of h_1 and \hat{h}_1 have to be identical $f_{\hat{h}_1} = f_\eta$. This distribution is used to initialize the conditional probability distribution function at the root node: $f(\hat{h}|\{1\}) = f_\eta(\hat{h})$. From there on, the conditional density distribution functions of its siblings can be iteratively determined and, consequently, all future event sequences s of the PD evaluation procedure can be systematically taken into account.

3.4.3.2 Perceptual Deadband Compliance

Whenever a PD compliance event occurs, the change in signal is considered to be too small to be perceivable. Therefore, the internal PD sampler state is maintained and its output does

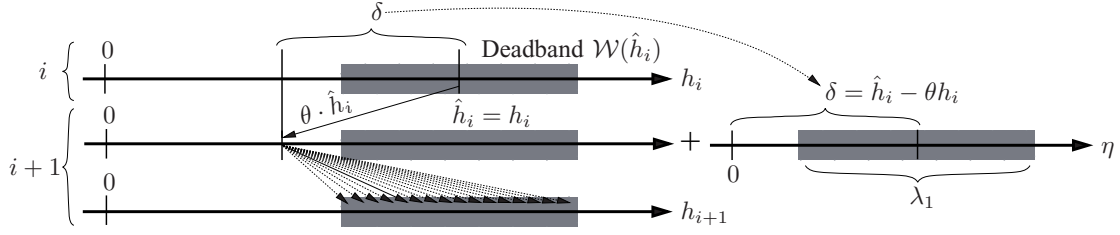


Figure 3.32: Illustration of finding an acceptable value range λ_1 for the random summand η to assure that the AR process output continuously stays in compliance with the currently defined PD bound. The center of λ_1 is shifted by $\delta = \hat{h}_i - \theta h_i$. The size of λ_1 corresponds to $\mathcal{W}(\hat{h}_i)$

not change. Only at the event of a PD violation, the sampler state is updated to the current input sample h_i and redefines the assumed human perception boundaries. Hence, every sampler state therefore has a certain "survival" probability until becoming updated and replaced by an input value. To investigate the effect on the conditional density distribution functions during a PD bound compliance event, the probability of the PD sampler state not being replaced by the current input sample is analyzed.

A PD violation happens at time i at PD event sequence $s = p\{1\}$ with previous PD event history p , which leads to a redefinition of the PD sampler state ($\hat{h}_i = h_i$). The distribution of the output value \hat{h}_i is at this point identical to the distribution of the current input value h_i . Accordingly, the problem can be narrowed to the question: What is the probability of j successive input samples falling into the deadband $\mathcal{W}(\hat{h}_i)$:

$$\Pr \left[h_{i+1}, \dots, h_{i+j} \in \mathcal{W}(\hat{h}_i) \right] = ?$$

A deadband compliance event at time $i + j$ is only assured if the outcome of the AR process contains appropriate sample values within a certain interval λ . As the regression of previous sample output by the autoregressive factor θ must be taken into account, the influence of θ has to be mapped to λ , which provides valid summands η . The interval λ_j is defined by:

$$\lambda_j = \left\{ \eta \mid \hat{h}_i - \theta h_{i+j-1} - k \hat{h}_i \leq \eta \leq \hat{h}_i - \theta h_{i+j-1} + k \hat{h}_i \right\} \quad (3.42)$$

In Figure 3.32 and Figure 3.33, the finding of the interval λ and the influence of the autoregression factor θ are illustrated. During successive PD compliance events, the intervals $\lambda_1 \dots \lambda_j$ are all of the size of the PD $\mathcal{W}(\hat{h}_i)$. However, the center of each λ shifts accordingly to the random signal input $h_{i+1} \dots h_{i+j}$ and the autoregression factor θ . The probability of obtaining a valid summand from the random variable η can be derived by partially integrating over f_η within the PD ensuring range λ_j :

$$\begin{aligned} \Pr\{\eta \text{ not inducing a bound violation at step } i + j\} &= \\ &= \Pr\{\eta \in \lambda_j\} \\ &= \Pr\{(\hat{h}_i - \theta h_{i+j-1}) - k \hat{h}_i \leq \eta \leq (\hat{h}_i - \theta h_{i+j-1}) + k \hat{h}_i\} \\ &= \int_{(\hat{h}_i - \theta h_{i+j-1}) - k \hat{h}_i}^{(\hat{h}_i - \theta h_{i+j-1}) + k \hat{h}_i} f_\eta(v) dv \end{aligned} \quad (3.43)$$

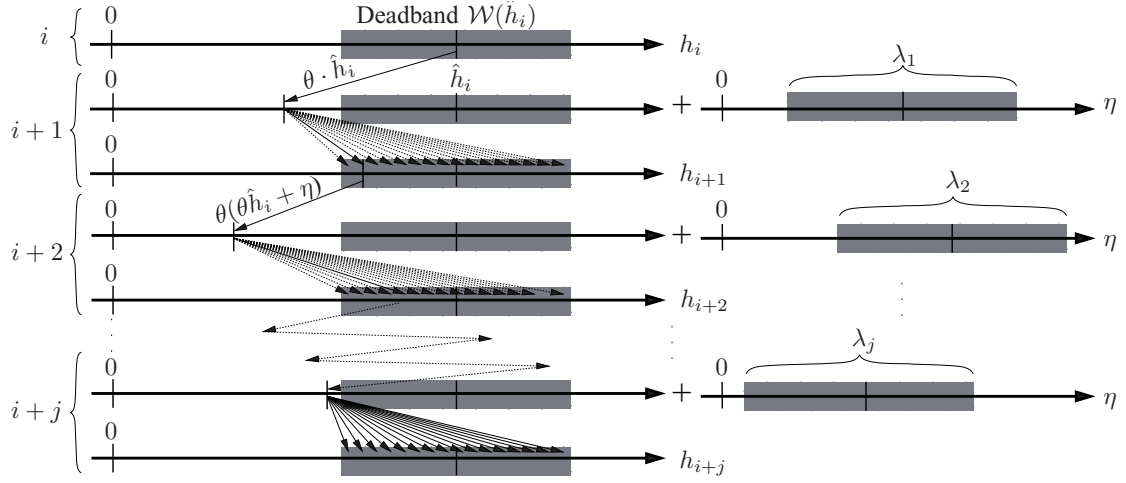


Figure 3.33: Illustration of possible signal trajectories and value ranges λ for the random summand η leading to a PD compliance during a period of j samples with autoregression factor $\theta = 0.5$.

In case of multiple successive deadband compliance events, these dependencies require taking all possible signal trajectories of future AR process output values into account which do not violate the PD during an interval of j samples. In other words, the probability of "survival" of a certain PD sampler state \hat{h}_i during a period of j samples consists of the conditional probability of occurrence of sampler output value \hat{h}_i with event history $s = p\{1\}$ multiplied with nested partial integrals of the probability density function f_η of the random variable η over the corresponding intervals $\lambda_1, \lambda_2, \dots, \lambda_j$:

$$\begin{aligned}
 f(\hat{h}_{i+j}|s\{0\}^j) &= \\
 &= f(\hat{h}_{i+j}|s) \cdot \int_{v_1 \in \lambda_1} f_\eta(v_1) \int_{v_2 \in \lambda_2} f_\eta(v_2) \cdots \int_{v_j \in \lambda_j} f_\eta(v_j) dv_j \dots dv_2 dv_1 \quad (3.44) \\
 &= f(\hat{h}_{i+j}|s) \cdot \int_{\hat{h}_{i+j} - \theta \hat{h}_{i+j} - k \hat{h}_{i+j}}^{\hat{h}_{i+j} - \theta \hat{h}_{i+j} + k \hat{h}_{i+j}} f_\eta(v_1) \int_{\hat{h}_{i+j} - \theta(\theta \hat{h}_{i+j} + v_1) - q \hat{h}_{i+j}}^{\hat{h}_{i+j} - \theta(\theta \hat{h}_{i+j} + v_1) + k \hat{h}_{i+j}} f_\eta(v_2) \cdots dv
 \end{aligned}$$

The proposed procedure is illustrated in Figure 3.33. Starting at the event of a PD violation, the discussed iterative method considers the influence of multiple PD bound compliance events on the development of corresponding conditional probability functions within the binary tree. It allows the definition of the conditional density function $f(u|p\{1\}\{0\}^j)$ by referring to the conditional density function $f(u|p\{1\})$ while recursively investigating all possible signal trajectories staying in PD compliance. For every additional PD compliance event, an additional nested integral is necessary to determine the conditional probabilities.

3.4.3.3 Perceptual Deadband Violation

If an incoming sample h_i violates the currently defined PD, the change in signal has to be sampled, which leads to an adoption of the incoming sample $\hat{h}_i = h_i$. To determine

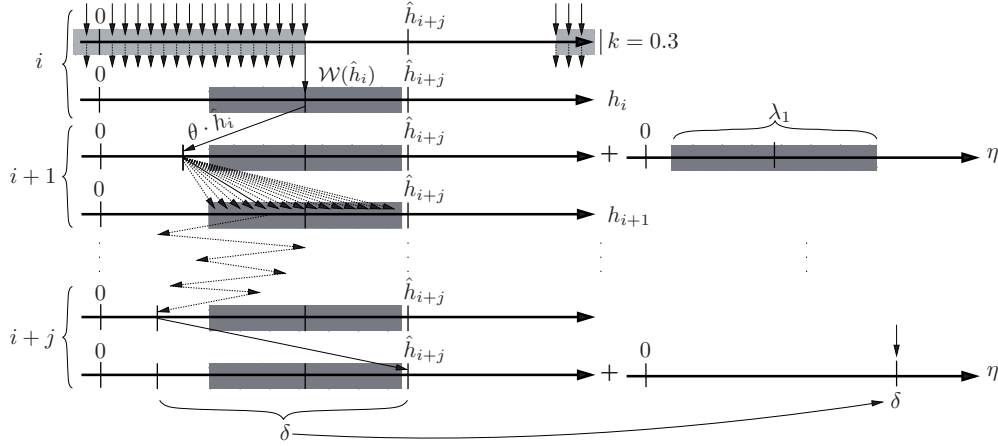


Figure 3.34: Illustration of possible signal trajectories and value ranges λ for the random value η ensuring a PD compliance during a period of $j - 1$ samples, followed by a PD violation event at time $i + j$ ($\theta = 0.5$).

the corresponding conditional probability function $f(\hat{h}_i|s)$ at the event of a PD violation described by a PD event sequence $s = p\{1\}\{0\}^{j-1}\{1\}$ with history p , the derivation has to be approached from a different perspective.

In contrast to the analysis of PD compliance events, the output sample \hat{h}_i does no longer directly refer to a fixed value defined in the past. This is due to the current update event $\hat{h}_i = h_i$ at time i . Hence, all possible signal trajectories generated by the AR process must be considered, which finally result in a particular bound violating sample value $h_i \notin \mathcal{W}(\hat{h}_{i-j})$. The PD bound to be violated has been defined during a previous violation event at time $i - j$ with PD event sequence $s = p\{1\}$. The binary tree model helps to following the path back to the root node until the first node referring to a PD bound violation event is reached, i.e., its corresponding conditional distribution function $f(\hat{h}_{i-j}|p\{1\})$.

In order to investigate all possible AR process signal trajectories which are $j - 1$ times in compliance with the PD bound $\{h_{i-j+1}, \dots, h_{i-1} \in \mathcal{W}(\hat{h}_{i-j} = h_{i-j})\}$ followed by a final PD violation event at time i , i.e. $\{h_i \notin \mathcal{W}(\hat{h}_{i-j})\}$, the value range within \hat{h}_{i-j} needs to be known within which samples define a deadband that is violable by the current input sample h_i .

As this signal range is disjunctive from the interval within which input samples are in compliance with $\mathcal{W}(\hat{h}_{i-j})$, this derivation can be simplified by focusing in a first step on possible sample values of \hat{h}_{i-j} , which comply with $h_i \in \mathcal{W}(\hat{h}_{i-j})$.

$$\hat{h}_{i-j}(1 - k) < h_i < \hat{h}_{i-j}(1 + k) \quad (3.45)$$

$$\frac{h_i}{(1 - k)} > \hat{h}_{i-j} > \frac{h_i}{(1 + k)} \quad (3.46)$$

For a particular input sample h_i , (3.46) describes the interval $[\frac{h_i}{(1+k)}; \frac{h_i}{(1-k)}]$ within which \hat{h}_{i-j} defines a PD that *cannot* be violated by the current input value h_i . Accordingly, assuming h_i lies outside that interval, it must violate the corresponding perception threshold $\mathcal{W}(\hat{h}_{i-j})$. Hence, every sample value of \hat{h}_{i-j} assuring $\hat{h}_{i-j} \notin [\frac{h_i}{(1+k)}; \frac{h_i}{(1-k)}]$ is a possible candidate to reach h_i at time i under the discussed assumptions. In line with the PD bound

compliance analysis, the consideration is in the following a PD bound defined at time $i - j$, which stays active during the following $j - 1$ input samples until it becomes violated at time i . To include the event of the final deadband violation into the analysis, the random value η within the AR process is assumed to be exactly $\delta = h_i - \theta h_{i-1}$ at time i , which happens with probability $f_\eta(\delta)$. This assures that the assumed signal trajectories of the autoregressive input signal reach the destination value $h_i = \hat{h}_i$ in the last step and therefore trigger a PD bound violation. The corresponding conditional density distribution function for the tree node $s = p\{1\}\{0\}^{j-1}\{1\}$ can be therefore written as:

$$\begin{aligned}
 f(\hat{h}_i, p\{1\}\{0\}^{j-1}\{1\}) &= \\
 &= \underbrace{\int_{-\infty}^{\frac{\hat{h}_i}{(1+k)}} f_\eta(u)}_{u \notin \mathcal{W}(\hat{h}_i)} \underbrace{\int_{\lambda_1} f_\eta(v_1) \cdots \int_{\lambda_{j-1}} f_\eta(v_{j-1})}_{h_{i-j+1}, \dots, h_{i-1} \in \mathcal{W}(u)} \cdot \underbrace{f_\eta(h_i - v_{j-1})}_{h_i \notin \mathcal{W}(u)} dv_{j-1} \dots dv_1 du \\
 &+ \underbrace{\int_{\frac{\hat{h}_i}{(1-k)}}^{+\infty} f_\eta(u)}_{u \notin \mathcal{W}(\hat{h}_i)} \underbrace{\int_{\lambda_1} f_\eta(v_1) \cdots \int_{\lambda_{j-1}} f_\eta(v_{j-1})}_{h_{i-j+1}, \dots, h_{i-1} \in \mathcal{W}(u)} \cdot \underbrace{f_\eta(h_i - v_{j-1})}_{h_i \notin \mathcal{W}(u)} dv_{j-1} \dots dv_1 du \quad (3.47)
 \end{aligned}$$

This procedure is illustrated in Figure 3.34.

3.4.4 Experimental Evaluation

In the following, the analytical derivations are compared to extensive simulations of the PD sampler with a numerical solution of the aforementioned formulas. In the experiments, the random increment η is a normally distributed random variable with variance 1 and zero mean:

$$\begin{aligned}
 h_1 &= \eta \\
 h_i &= h_{i-1}\theta + \eta \quad \text{where } \eta \in \mathcal{N}(0, 1); i > 1
 \end{aligned} \quad (3.48)$$

Due to the high computational complexity of numerically solving the nested integrals, only the conditional density functions for the first five tree levels of the binary tree structure are sampled at intervals of 0.02 within the range of -6 to $+6$ for different configurations of autoregression factors θ and PD parameters k . To determine the probability of a PD bound violation event at time instance i , the conditional density functions up to tree level i (2^i binary tree nodes) are numerically evaluated in order to calculate the overall probability of a PD bound violation using (3.39). How strongly different parameter sets affect the outcome of the experiments is illustrated in Figure 3.35. When applying different parameter configurations, varying conditional density distributions of the Weber sampler's signal output can be observed. The analytical derivation (black lines) and the simulation (grey line) are in perfect agreement.

The results of our conducted experiments are shown in Figure 3.36. The four plots illustrate the analytically derived probability of a deadband sampler update event for values of k from 0.1 to 0.9 for the first five steps in the input sequence and corresponding simulation

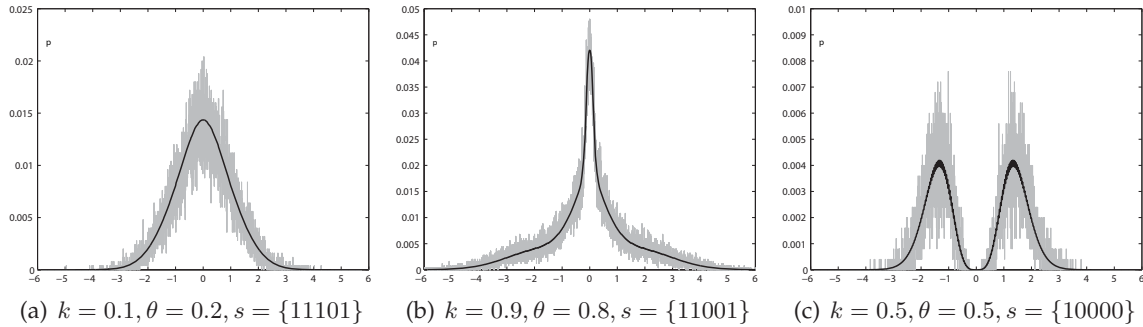


Figure 3.35: Examples of conditional density functions $f(\hat{\mathbf{h}}|s)$ for different configurations of the PD parameter k , the autoregression factor θ , and the PD event sequence s .

results. Although a strong agreement can be observed, the slight deviations for steps later in the sequence originate from the fact that 2^{i-1} discretely sampled and recursively derived conditional density functions, each with some error coming from the finite resolution of the value axis, have to be summed up.

The results show that the displayed probabilities quickly converge to a steady state. This state represents the average probability of a PD violation event after processing an infinite number of input samples. Especially for small values of the autoregression coefficient and/or higher values of the PD parameter, this state is almost reached after the very first steps in the sequence. For $\theta = 1$, the applied random input process equals a random walk model with unbounded signal evolution. Hence, the probability of a PD bound violation is asymptotically converging to zero as the variance increases with every step of the input sequence. Figure 3.36(d) shows the first five steps of the strictly monotonic decreasing probability of the PD bound violation.

Although the applied random walk models generate at first glance similar signal trajectories compared to recordings of haptic signals within real-world telepresence experiments, the obtained update rates from the analytical derivation differs from typical real-world haptic telepresence experiments. For instance, applied on a haptic force-feedback signal, haptic PD compression is able to reduce the amount of samples considered to be necessary for transmission by approximately 90% (see Section 2.3). This difference mainly originates from the huge amount of complex non-linear factors based on physical properties of the remote environment and the arbitrariness of the human operator's actions which are not reflected by the normally distributed random variable used in the experiment. However, the presented theoretical work successfully reveals how the haptic PD compression approach can be investigated from a theoretical point of view and it provides a solid framework for the analysis of more complex stochastic input signal models.

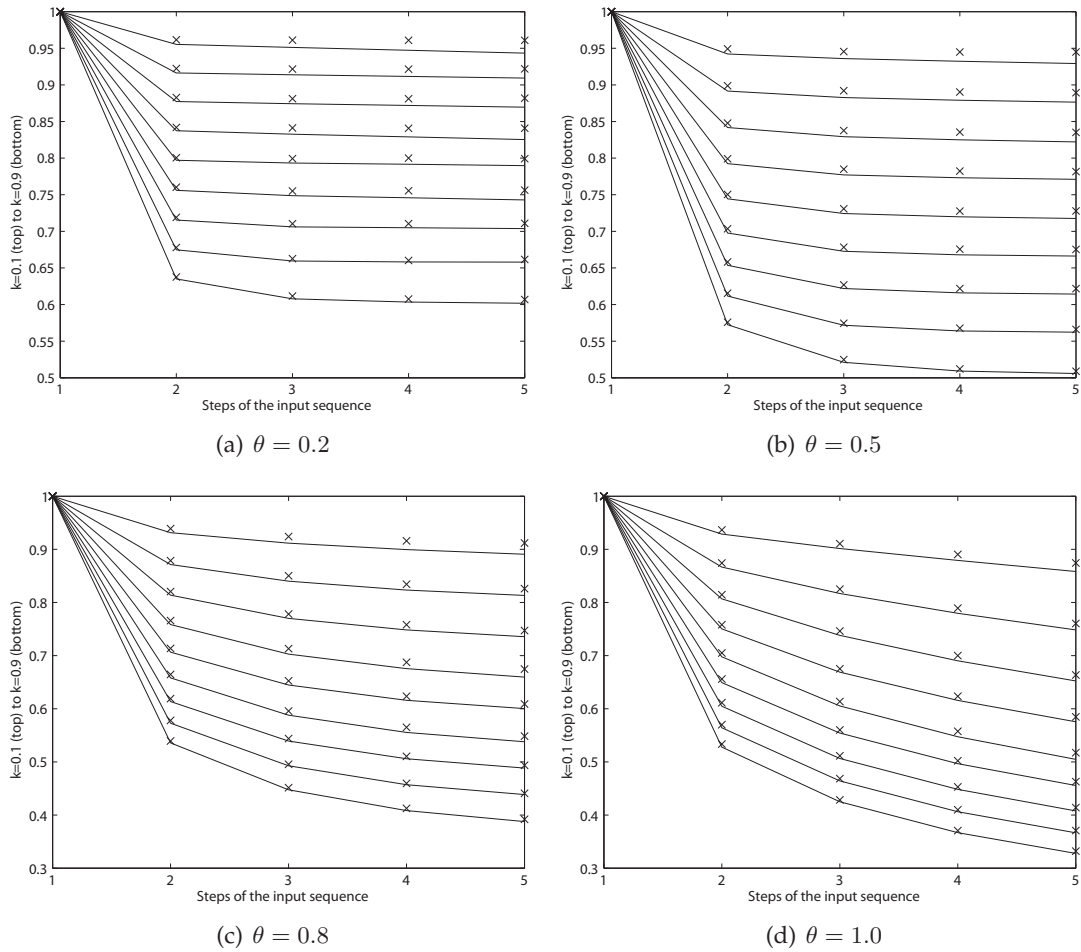


Figure 3.36: Simulation (black lines) and analytical derivation (black crosses) of the probability of a perception threshold violation for different configurations of autoregression factors θ and PD parameters k . The slight deviations with higher time originate from the limited resolution capacity when numerically solving the nested integral formulae. The figures show that the average probability that a new input value violates the active PD quickly tends to reach a steady state (steady state probability).

3.5 Chapter Summary

In this chapter, several contributions to perceptual haptic online and offline data compression have been presented. In the following, their concepts are briefly summarized.

Perceptual haptic data compression relies on a precise model of human haptic perception. Research in psychophysics reveals that the perception of artefacts arising from PD data reduction is influenced by the direction of force feedback. These psychophysical findings suggest the construction of a direction-dependent deadzone for the perceptual compression of haptic signals. Deployed in the PD compression scheme, an improved compression performance of 26.7 % compared to the isotropic PD compression scheme can be observed.

Similarly, research in psychophysics shows that active movements of the human OP have a significant impact on the haptic force feedback discrimination ability. Particularly, increased perception bounds are discovered during active movements of the OP's hand which can be exploited in the context of perceptual haptic data compression. Conducted experiments reveal that integrating velocity-adaptive PD into the predictive haptic compression approach leads to greater compression without affecting the task performance and transparency of the TPTA system. Specifically, the experimental evaluation of the velocity-adaptive PD scheme show an additional transparent packet reduction ability of 30% compared to the isotropic PD model.

Furthermore, several architectures for integrating environment models into perceptual haptic communication schemes have been proposed. In model-mediated control, the haptic model parameters are typically estimated and transmitted at a high rate over the haptic channel in order to minimize possible inconsistencies between the remote environment and the locally applied haptic feedback model. To reduce the high packet rates in the communication system, a model verification method has been developed which is able to detect perceptually relevant model updates. Psychophysical experiments performed on a real-world TPTA system show that the model-mediated compression approach leads to improved transparency and compression performance compared to the PD compression approach. The results further demonstrate that already at a small PD parameter $k = 5\%$, an improvement of 75% in transparent packet rate reduction can be achieved.

Similarly, the concept of model-mediated prediction has been presented which extends the class of signal-based haptic prediction methods. It estimates future haptic feedback based on current and previous contact events of the TOP with the remote environment. Here, the absolute contact location of the TOP endeffector is typically not available and needs to be estimated by taking the impedance of the TOP controller and the corresponding force sensory information into account. When integrated into the perceptual predictive compression approach, the conducted experiments reveal an improvement of 31% in packet rate reduction performance compared to PD compression using linear signal-based haptic prediction.

Additionally, the concept of model-based coding of haptic contact events has been proposed. The transmission of haptic feedback during contacts with the remote environment is challenging due to increased haptic update rates. By transmitting only a single event-of-contact message, a local contact model can be applied to substitute the transmission of remote haptic signals with locally rendered contact feedback. Furthermore, by integrating the concept of *Event-based Haptics*, the quality and realism of displayed contact feedback can be significantly improved. Combined with the PD compression approach, the high packet

rates during the initial contact phase can be avoided which further improves the packet rate reduction performance by 28% .

In addition to the delay critical real-time perceptual communication of haptic signals, the development of perceptual offline compression algorithms has also been addressed. In this context, a TPTA session recording and playback scheme has been presented, which allows the replaying of a prerecorded TPTA session without the need for active involvement of the user. Once haptic data needs to be stored on a storage device, methods for haptic offline compression become relevant. Interestingly, haptic offline compression algorithms can be design in a fundamentally different way to haptic online compression schemes. Due to relaxed delay constraints, the application of block-based signal processing and entropy coding techniques become feasible. To this end, the concept of deadband-based differential coding applied to the successively encoded prediction errors has been presented. It allows the exploitation of knowledge about pending perception bounds enabling an additional entropy minimization. Conducted experiments demonstrate a strong data compression ability of the presented haptic offline compression scheme while keeping introduced coding artefacts within an imperceptible range.

Furthermore, to investigate the PD compression approach from a theoretical point of view, the concept of a PD sampler has been proposed. The presented theoretical framework allows the analytical analysis of the gain in update rate savings in accordance with a stochastic model of haptic signals. Specifically, a first-order autoregressive input model is used to mathematically simulate the performance of perceptual haptic data compression. The analytical derivations show a strong agreement with the simulation results of the PD sampler performance.

4 Haptic Communication and Coding Architectures

Perceptual haptic data compression discussed in the previous chapters successfully addresses the challenges of high packet and high data rates on the haptic communication channel. Its compression performance, however, depends on the properties of the hardware components, the communication network as well as the physical properties of the remote objects being touched as they significantly influence the haptic signals that are exchanged between the OP and the TOP.

This chapter focuses on the integration of the developed perceptual haptic data compression methods into the haptic control and communication systems from a combined signal processing, control engineering and networking point of view. In particular, the impact of communication uncertainties such as latency and packet loss on the haptic communication channel are discussed. Additionally, a flexible framework leveraging Internet session and presence protocols is presented in order to enable interoperability among heterogeneous TPTA systems and platforms.

In real-world telepresence scenarios, communication latency on the haptic channel is often not avoidable due to physical propagation time, protocol, network congestions, etc. In order to solve the stability issues of time-delayed communication, the wave variable control approach can be applied which, however, excludes the applicability of perceptual haptic compression methods. To this end, a modification of the wave variable control scheme is presented in Section 4.1 which takes advantage of the stabilization ability of the wave variables while allowing for the application of perceptual communication schemes on the haptic channel.

In addition, the issues of bit errors or packet loss on the haptic channel are discussed in Section 4.2 which presents a low-delay packet loss compensation scheme for perceptual haptic communication. It employs a probabilistic model of the receiver to adaptively control the amount of redundancy required to compensate for packet loss on the haptic channel.

Furthermore, an Internet-based communication framework for TPTA session control is presented in Section 4.3 which takes advantage of synergies between the Internet-based teleconferencing technology and the TPTA system domain. This framework enables flexibility and interoperability among different types of TPTA systems and provides standard interfaces for the developed perceptual communication and control methods.

4.1 Perceptual Haptic Compression with Time-delayed Communication

Latency on the haptic communication channel impairs the stability of the global control loop closed between the HSI and the TOP [29]. The previously discussed haptic compression and processing techniques address this issue by keeping introduced time delay as short as possible. However, communication latency on the haptic channel is often not avoidable, particularly in large-distance TPTA scenarios [188].

The scattering transformation presented in [29], later referred to as the wave variable (WV) approach in [142], has become a popular control approach for addressing the stability issues of time-delayed communication. It provides a control framework that ensures stability of the global haptic control loop under the assumption of an arbitrarily long but constant time delay on the communication channel. It is based on the concept of passivity (see Section 2.1.3.1) which proves system stability as long as all components of the TPTA system dissipate or store more energy than they create. By transmitting so called *wave variables* instead of haptic velocity and/or force signals (power conjugated signals), the communication subsystem is proven to behave in a passive manner. These wave variables represent linear transformations of the local and remote haptic sensory data. Hence, the transmission of mathematically combined velocity and force signals makes it difficult to apply perceptual arguments for data compression in the wave variable domain. Furthermore, research results presented in [108] indicate that perceptual resolution limits like the Weber fraction do not directly apply to the wave domain.

In this section, a novel control scheme is presented which allows the combination of perceptual haptic data compression with wave variable-based control for time-delayed TPTA scenarios. In addition, a modified signal reconstruction approach is presented which guarantees passivity during the decoding process of PD compressed signals. The presented work has been conducted in cooperation with Iason Vittorias [24].

4.1.1 Wave Variable Control

Figure 4.1 illustrates the wave variable control architecture proposed by [142]. Instead of the exchange of the velocity signal $\dot{\mathbf{x}}_m$ and force feedback \mathbf{f}_s , the wave variables \mathbf{u}_m (on the

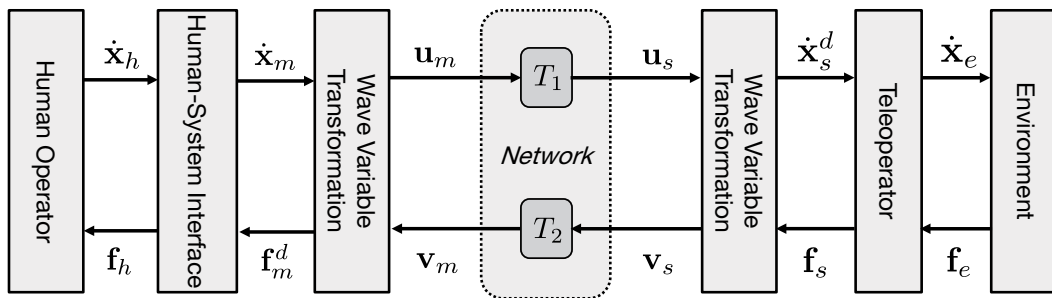


Figure 4.1: Signal diagram of the wave variable approach.

forward path) and \mathbf{v}_s (on the backward path) are transmitted. They are calculated by

$$\begin{aligned}\mathbf{u}_m &= \frac{1}{\sqrt{2b}}(\mathbf{f}_m^d + b\dot{\mathbf{x}}_m), & \mathbf{u}_s &= \frac{1}{\sqrt{2b}}(\mathbf{f}_s + b\dot{\mathbf{x}}_s^d), \\ \mathbf{v}_m &= \frac{1}{\sqrt{2b}}(\mathbf{f}_m^d - b\dot{\mathbf{x}}_m), & \mathbf{v}_s &= \frac{1}{\sqrt{2b}}(\mathbf{f}_s - b\dot{\mathbf{x}}_s^d),\end{aligned}\quad (4.1)$$

where $b \geq 0$ defines a *characteristic impedance* which represents a tuning parameter for controlling the dynamics of the TPTA system.

By taking the two-port network theory into account (see Section 2.1.3.1), the power inflow into the communication subsystem is determined by:

$$P_{in}(t) = \dot{\mathbf{x}}_m(t)\mathbf{f}_m^d(t) - \dot{\mathbf{x}}_s^d(t)\mathbf{f}_s(t) \quad (4.2)$$

After rearranging (4.1), inserting it into (4.2), and integrating, the total energy stored in the communication line during the signal transmission of the wave variables is obtained:

$$\int_0^t P_{in}(\tau)d\tau = \int_0^t \mathbf{u}_m^2(\tau) - \mathbf{u}_s^2(\tau) + \mathbf{v}_s^2(\tau) - \mathbf{v}_m^2(\tau)d\tau. \quad (4.3)$$

The communication channel delays the transmitted wave variable \mathbf{u}_m and \mathbf{v}_s with a time delay of $T_1 > 0$ and $T_2 > 0$, respectively.

$$\mathbf{u}_s(t) = \mathbf{u}_m(t - T_1) \quad \text{and} \quad \mathbf{v}_m(t) = \mathbf{v}_s(t - T_2). \quad (4.4)$$

Since the L_2 norm of a constantly delayed operator is always smaller than the L_2 norm of its undelayed input, the delay operator does not lead to increased signal energy and follows the *small gain property* [142]. Consequently, the integral in (4.3) is always positive which proves passivity of the communication two-port subsystem for constant network delays $T = T_1 + T_2$ (see passivity conditions in Section 2.1.3.1).

$$\int_0^t \mathbf{u}_m^2(\tau) - \mathbf{u}_s^2(\tau)d\tau \geq 0 \quad \text{and} \quad \int_0^t \mathbf{v}_s^2(\tau) - \mathbf{v}_m^2(\tau)d\tau \geq 0. \quad (4.5)$$

For more details on the passivity analysis of the wave variable control scheme, see [142].

4.1.2 Local Computation of Wave Variables

The transmission of wave variables in TPTA systems guarantees passivity of the communication subsystem. However, it excludes the applicability of perceptual haptic compression techniques as haptic sensory information is not directly exchanged anymore. In order to address this issue, a modification of the wave variable control architecture [24] is described in the following, which allows for the direct transmission of perceptually encoded haptic signals while ensuring wave variable-based stabilized TPTA operation.

By expanding (4.1), the desired force \mathbf{f}_m^d at the HSI can alternatively be obtained as

$$\begin{aligned}
 \mathbf{f}_m^d(t) &= b\dot{\mathbf{x}}_m(t) - \sqrt{2b}\mathbf{v}_m(t) \\
 &= b\dot{\mathbf{x}}_m(t) - \sqrt{2b}\mathbf{v}_s(t-T) \\
 &= b\dot{\mathbf{x}}_m(t) - \sqrt{2b} \left[\frac{b}{\sqrt{2b}}\dot{\mathbf{x}}_s(t-T) - \frac{1}{\sqrt{2b}}\mathbf{f}_s(t-T) \right] \\
 &= b\dot{\mathbf{x}}_m(t) - \left[b \left(\sqrt{\frac{2}{b}}\mathbf{u}_s(t-T) - \frac{1}{b}\mathbf{f}_s(t-T) \right) - \mathbf{f}_s(t-T) \right] \\
 &= b\dot{\mathbf{x}}_m(t) - \left[\sqrt{2b}\mathbf{v}_m(t-2T) - \mathbf{f}_s(t-T) - \mathbf{f}_s(t-T) \right] \\
 &= \underbrace{b\dot{\mathbf{x}}_m(t) - [b\dot{\mathbf{x}}_m(t-2T) + \mathbf{f}_m(t-2T)] - 2\mathbf{f}_s(t-T)}_{\text{all variables locally known at the HSI device}} \tag{4.6}
 \end{aligned}$$

Accordingly, the desired force at the HSI only depends on the pending HSI velocity and delayed TOP velocity and force signals which are all locally accessible at the HSI device assuming some storage element that stores the HSI velocity and force within the interval of the round-trip time delay $2T$. Hence, by rearranging the wave variable operations, haptic sensory data $\dot{\mathbf{x}}_m$ can be directly transmitted while maintaining an equivalent input/output behavior of the standard wave variable control architecture.

Similarly, this can be applied for the transmission of the desired velocity signal \mathbf{x}_s^d :

$$\begin{aligned}
 \mathbf{x}_s^d(t) &= \sqrt{\frac{2}{b}}\mathbf{u}_s(t) - \frac{1}{b}\mathbf{f}_s(t) \\
 &= \sqrt{\frac{2}{b}}\mathbf{u}_m(t-T) - \frac{1}{b}\mathbf{f}_s(t) \\
 &= \sqrt{\frac{2}{b}} \left(\frac{b}{\sqrt{2b}}\dot{\mathbf{x}}_m(t-T) + \frac{1}{\sqrt{2b}}\mathbf{f}_m(t-T) \right) - \frac{1}{b}\mathbf{f}_s(t) \\
 &= \dot{\mathbf{x}}_m(t-T) + \frac{1}{b}(b\dot{\mathbf{x}}_m(t-T) - \sqrt{2b}\mathbf{v}_m(t-T)) - \frac{1}{b}\mathbf{f}_s(t) \\
 &= 2\dot{\mathbf{x}}_m(t-T) - \frac{\sqrt{2b}}{b}\mathbf{v}_s(t-2T) - \frac{1}{b}\mathbf{f}_s(t) \\
 &= \underbrace{2\dot{\mathbf{x}}_m(t-T) + \mathbf{x}_t(t-2T) - \mathbf{f}_s(t-2T) - \frac{1}{b}\mathbf{f}_s(t)}_{\text{all variables locally known at the TOP}} \tag{4.7}
 \end{aligned}$$

Hence, by locally simulating the global wave variable loop, the direct transmission of the haptic signals $\dot{\mathbf{x}}_m$ and \mathbf{f}_s is enabled without losing the passivity property of the wave variable control scheme. The computation of these locally computed wave variable (LCWV) loops refer to local haptic signals that have to be stored for the round-trip time delay $2T$. Accordingly, the round-trip time delay needs to be known, which poses a limitation compared to the original wave variable approach where the exact knowledge of the communication latency is not required. However, recent telepresence experiments between Germany and Japan over the Internet showed that the time delay can be considered constant even over this long-distance interconnection [150]. Additionally, the round-trip time delay is rather simple to measure using time-stamps.

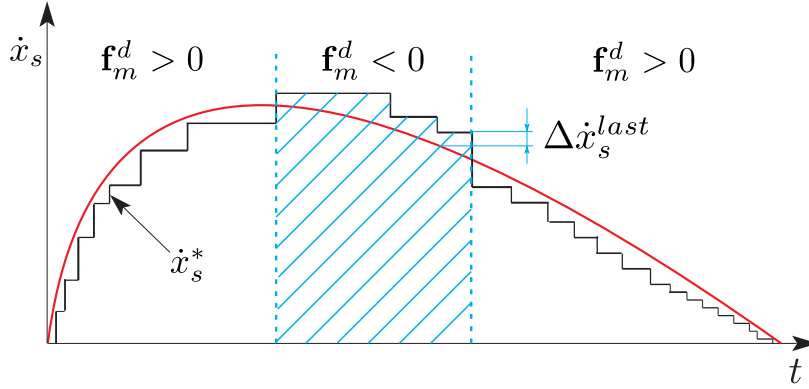


Figure 4.2: Illustration of the passivity-preserving perceptual deadband compression scheme applied at the HSI device (adapted from [24]).

4.1.3 Passivity-preserving PD compression

The previously discussed modified wave variable control approach guarantees passivity of the communication component within the TPTA system. In contrast, the signal modifications occurring during PD compression are not passive [56, 106]. Particularly, the signal upsampling step during PD decoding may lead to an active system behavior and, consequently, violate the passivity constraints, discussed in Section 2.1.3.1.

The energy balance of a passive communication subsystem must satisfy:

$$E(t)^{COM}(t) = \int_0^t \dot{\mathbf{x}}_m(\tau) \mathbf{f}_m^d(\tau) - \dot{\mathbf{x}}_s^d(\tau) \mathbf{f}_s(\tau) d\tau \geq 0 \quad \forall t > 0 \quad (4.8)$$

In case of lossless encoding and optimal channel conditions, the transmitted haptic signals are identical to the received haptic signals, hence $\dot{\mathbf{x}}_s^d(t) = \dot{\mathbf{x}}_s(t - T_1)$ and $\mathbf{f}_m^d(t) = \mathbf{f}_m(t - T_2)$.

However, applied lossy PD compression introduces coding noise in the form of imperceptible prediction errors that occur during decoding. To avoid additional signal energy during PD compression, the PD-based signal modifications in \mathbf{f}_m^d and $\dot{\mathbf{x}}_s^d$ need to be actively observed at the PD encoder side. Specifically, a modified desired velocity signal $\dot{\mathbf{x}}_s^*(t)$ at the HSI and the modified desired force signal $\mathbf{f}_m^*(t)$ at the TOP are calculated, which assures that no additional signal energy is added to the transmitted haptic signals. Depending on the sign of incoming signal energy, the haptic signals are modified towards the upper or lower end of the imperceptible PD interval in order to continuously dissipate energy from the communication system. To comply with (4.8), the passivity-preserving PD compression scheme increases the input energy and decreases the output energy of the communication subsystem, hence

$$|\dot{\mathbf{x}}_m \mathbf{f}_m^*| > |\dot{\mathbf{x}}_m \mathbf{f}_m^d| \quad (4.9)$$

and

$$|\dot{\mathbf{x}}_s^* \mathbf{f}_s| < |\dot{\mathbf{x}}_s^d \mathbf{f}_s| \quad (4.10)$$

This process is illustrated in Figure 4.2 for the HSI side. Figure 4.3 illustrates the architecture for combined perceptual haptic compression and wave variable control. The local

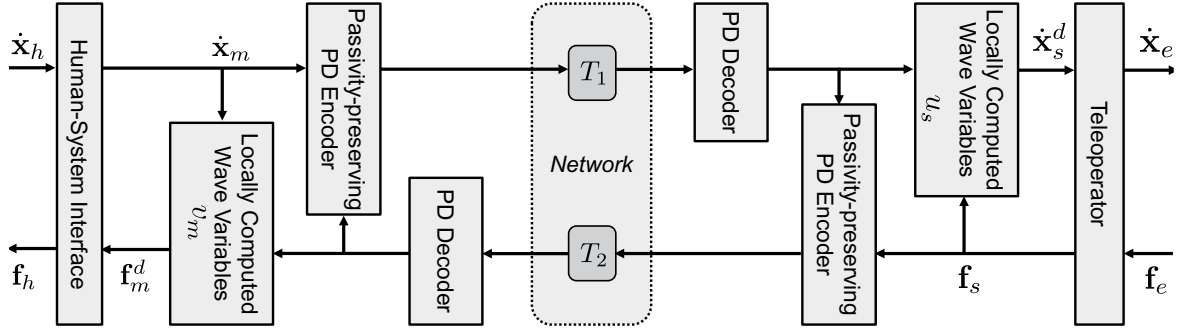


Figure 4.3: Schematic overview of the architecture for combined PD compression and wave variable control (adapted from [24]).

signals \dot{x}_m , f_m^d at the HSI device and the local signals \dot{x}_s^d , f_s at the TOP are used to locally simulate wave variable control in accordance with (4.6) and (4.7). The haptic signals are further perceptually compressed to reduce the packet rate in the network. In order to assure passivity during PD compression, the haptic samples that are considered to be perceptually relevant for transmission are further modified to the upper or lower end of the imperceptible PD interval.

4.1.4 Experimental Evaluation

In order to evaluate the performance of the modified wave variable control combined with the passivity-preserving PD compression scheme, an experimental study has been conducted. Specifically, the packet rate reduction ability and the system transparency of the proposed system are investigated in a simulated environment consisting of a virtual spring (spring constant of 200N/m). The latency on the communication channel is set to 30ms which is considered to be a realistic assumption in TPTA scenarios using Internet-based communication. The sampling rate of the control loop is 1 kHz.

According to Lawrence et al. (see [131]), absolute transparency is achieved if the displayed impedance Z_m is equal to the actual impedance of the environment contact Z_e , hence $Z_m = Z_e$ (see Section 2.1.4). Accordingly, integrating over the impedance error provides a weighted impedance fidelity measure,

$$\int_{\omega_{min}}^{\omega_{max}} \frac{|Z_m(j\omega) - Z_e(j\omega)|}{|Z_m(j\omega)|} d\omega < \epsilon \quad (4.11)$$

where $\epsilon > 0$ is the accuracy. The PD compression approach affects the dynamics of the system in a non-linear manner. However, to facilitate the analysis, a linearized impedance is assumed which allows the estimation of its frequency response. In the conducted experiments, the TPTA system is excited with sinusoidal inputs within a frequency window $[\omega_{min}, \omega_{max}] = [10^{-2} \ 10^3]$ rad/s. The gain and phase relation between the exciting velocity signal and the resulting force feedback, i.e. the frequency response of the displayed impedance, is computed using standard cross-correlation methods.

The experimental study focuses on a comparison of the performance of deadband compression using a deadband of fixed size directly applied to wave variables (proposed in [108])

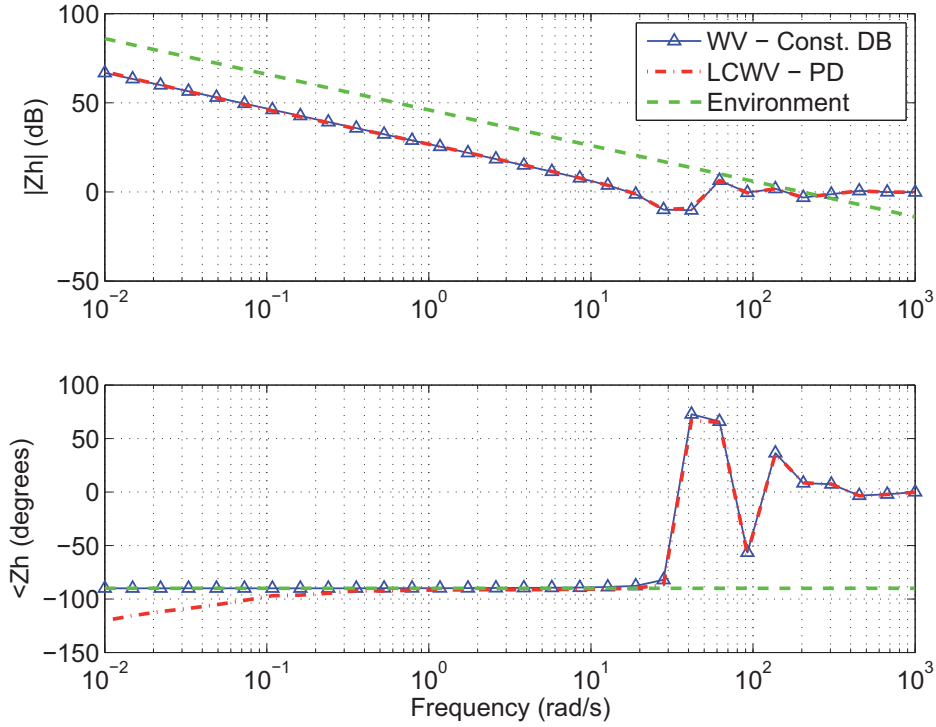


Figure 4.4: Displayed impedance for stiff environment (reproduced from [24]). The LCWV approach applies a PD with $k = 10\%$. The WV data reduction uses a constant deadband of size $0.02\sqrt{W_{att}}$.

and the local simulation of wave variables combined with the passivity-preserving PD compression approach. This comparison is divided into two parts. Firstly, the packet rate is analyzed in a stiff environment when both compression schemes are configured to operate with a similar degree of transparency. Here, the locally computed wave variable approach with the passivity-preserving PD compression is configured with a PD parameter of $k = 10\%$ which is an empirically preferable value for transparent haptic data compression, as shown in [98]. A similar degree of transparency is achieved, when the transmitted wave variables are compressed using a constant deadband of size $0.02\sqrt{W_{att}}$. This value has been identified in multiple simulations to achieve a similar displayed impedance ($\epsilon = 0.0015$). In the second part of the experiment, this configuration is used again to compare the compression performance during free space motions of the TOP within the simulation environment.

The Bode plots of the first experiment are shown in in Figure 4.4. It can be seen that both compression techniques operate at similar impedances. The simulated impedance of the remote environment $Z_e(s) = \frac{200}{s}$ is illustrated by the dashed line. The corresponding mean packet rate results on the \uparrow forward channel and the \downarrow backward channel are:

Constant Deadband Compression on Wave Variables: \uparrow 544 pks/s, \downarrow 525 pks/s

Local Wave Variables + Passive PD Compression: \uparrow 324 pks/s, \downarrow 332 pks/s

The results show that the mean packet rates of the local wave variables with PD compression outperforms the constant deadband compression scheme (original packet rate:

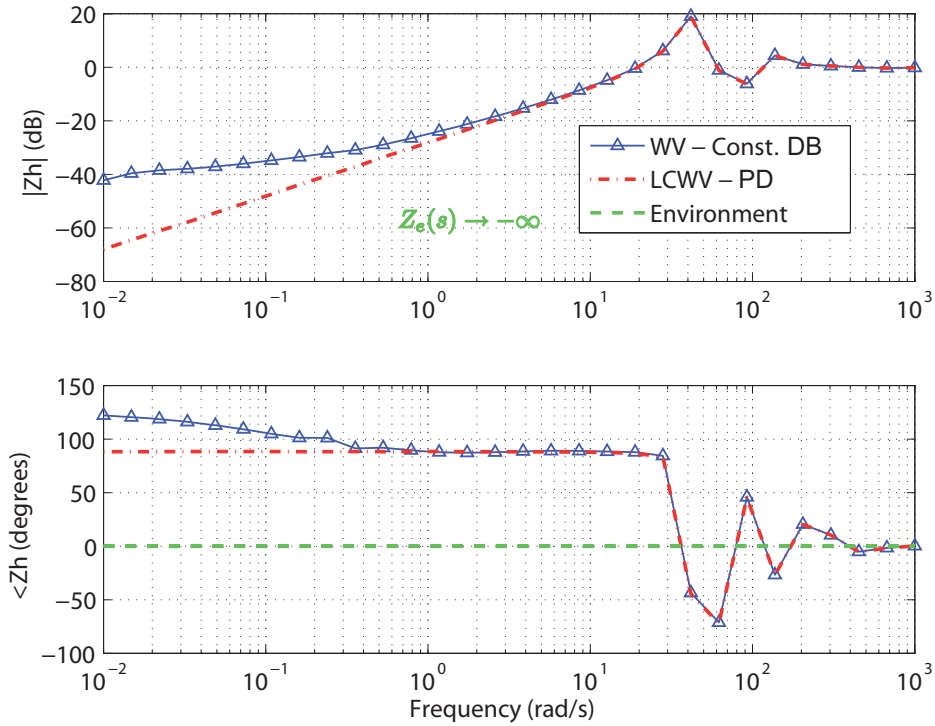


Figure 4.5: Displayed impedance for free space motion (reproduced from [24]).

1000 pks/s).

In the second part, the experiment is repeated during simulated free space motions of the TOP. Figure 4.5 shows the corresponding impedance plots. For both architectures a deviation from the ideal displayed impedance, $Z_h(s) \rightarrow -\infty$, is observed as the bilateral control dynamics and the time delay degrade the degree of transparency. However, the LCWV approach does not transmit packets when there is no contact with the environment (on this velocity-force architecture) which leads to a large gain in compression efficiency for teleoperation scenarios with mostly free space motion. Qualitatively similar results are obtained for different deadband thresholds k , i.e. different compression rates.

Constant Deadband Compression on Wave Variables: \uparrow 352 pks/s, \downarrow 334 pks/s

Local Wave Variables + Passive PD Compression: \uparrow 265 pks/s, \downarrow 0 pks/s

The experimental results show that by locally simulating the wave variable control loops at the HSI and TOP side, the global wave variable loop can be successfully decoupled. This allows the direct transmission of perceptually encoded haptic sensory data over a time-delayed communication channel while preserving the stabilization ability of the wave variables approach. The packet rates for stiff environments and TOP free space motions indicate that the LCWV control architecture with the modified PD compression achieves improved compression performance reflected by higher transparency/packet rate ratios compared to the standard wave variable architecture.

4.2 Error-resilient Haptic Communication

Haptic data transmission in real-world networks might be disturbed by bit errors or packet losses with varying probability and burstiness. Consequently, failures occurring during the transmission of haptic signals may impair the performance and transparency of the TPTA systems [172].

Particularly, the exchange of compressed haptic signals in TPTA systems is sensitive to data loss on the haptic channel. As the perceptual haptic data compression approach removes redundancy in the signal by transmitting only perceptually relevant haptic samples, lost network packets consequently impair the system's transparency. Furthermore, in predictive coding schemes, failed haptic data transmission leads to inconsistent predictor states which also results in disturbing artefacts in the decoded haptic signal.

A common strategy for detecting and compensating packet loss on the communication channel is to acknowledge successfully transmitted packets to the sender. If the sender does not receive an acknowledgement message (ACK) from the receiver within a fixed period of time, it assumes the packet to be lost and triggers a transmission until a successful transmission is achieved. However, the strict latency constraints of haptic real-time communication prevent any acknowledgement-based waiting strategy. Furthermore, since the transmission of compressed haptic packets is temporally irregular, the receiver does not know when it is supposed to receive a network packet. This poses a serious challenge for the detection and corresponding concealment of network errors on the haptic channel.

This research work has been conducted in cooperation with Fernanda Brandi and Florian Schweiger [13].

4.2.1 Architecture for Perceptually Robust Haptic Communication

Network latency and delayed feedback prevent the sender from obtaining exact information about the receiver state. Interestingly, research from the field of real-time video streaming proposes a technique for robust low-latency video streaming, which has been shown to also

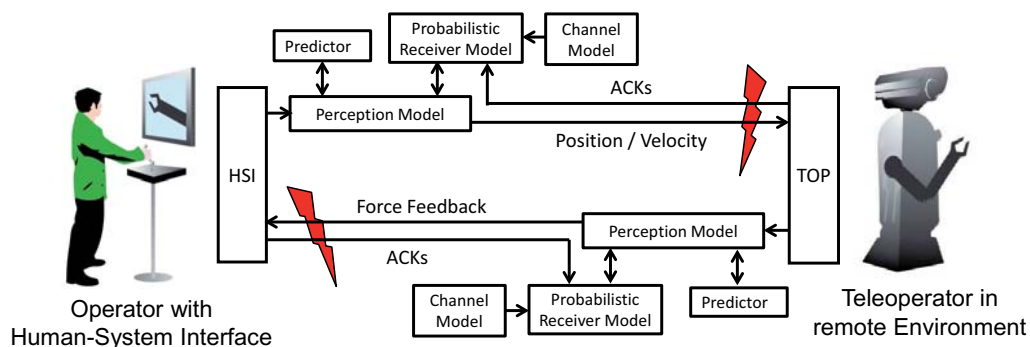


Figure 4.6: Architecture for error-resilient haptic communication. A probabilistic model of the receiver is used to estimate the receiver state. If a disturbing deviation at the receiver becomes likely, additional redundancy is added to the communication channel. Receiver feedback can be used to support the receiver state estimation process.

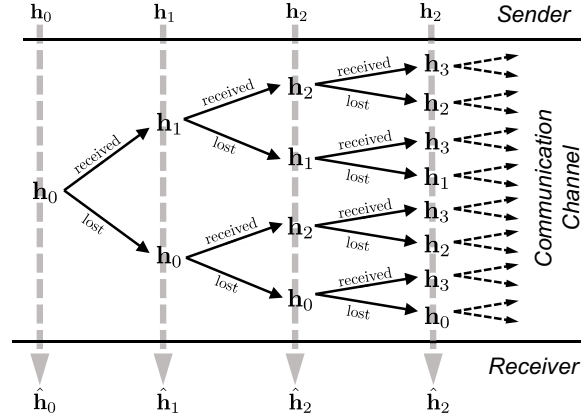


Figure 4.7: Markov decision tree considering cases of successful and unsuccessful transmissions of haptic packets (adapted from [9]).

apply to the challenges of erroneous haptic communication [9, 46, 51]. An illustration of the proposed architecture for error-resilient haptic communication is shown in Figure 4.6. The haptic signals are perceptually compressed and communicated over the haptic channel. The probabilistic receiver model at the sender considers every triggered network transmission to either successfully arrive at the receiver or to be lost. To this end, it allows for incorporating all possible states the receiver might be in. If likely receiver states deviate by more than the applied perception thresholds, additional redundancy has to be added to the transmission of the haptic signals. As every transmission on the haptic channel decreases the probability of disturbed receiver output, this scheme allows for signal-adaptive packet loss compensation without introducing any additional processing latency to the haptic signals.

4.2.2 Receiver State Estimation using Markov Decision Trees

Whenever a haptic signal transmission is triggered, the corresponding data packet either successfully arrives at the receiver or it is lost due to a network error. Accordingly, a transmitted haptic packet either updates the receiver state with probability p or, in case of packet loss, it holds its current configuration with probability $(1 - p)$. This process can be modeled with a Markov decision tree [46], as illustrated in Figure 4.7. Here, the following channel model for the transmission of a haptic sample \mathbf{h}_i at time i is assumed.

$$\underbrace{\mathbf{h}_0, \mathbf{h}_1, \mathbf{h}_2, \mathbf{h}_3, \dots}_{\text{samples } \mathbf{h} \in \mathbf{R}^D \text{ to be sent}} \longrightarrow \underbrace{\text{Channel}}_{\text{Pr}\{\text{Successful Transmission}\}=p} \longrightarrow \underbrace{\mathbf{h}_0, \hat{\mathbf{h}}_1, \hat{\mathbf{h}}_2, \hat{\mathbf{h}}_3, \dots}_{\text{receiver state } \hat{\mathbf{h}} \in \mathbf{R}^D}$$

where the sender and the receiver are initialized with \mathbf{h}_0 . From then on, haptic updates \mathbf{h}_i are transmitted and arrive at the receiver with probability p . The estimated receiver state is denoted by $\hat{\mathbf{h}}_i$ with $i > 0$.

The Markov decision tree describes all possible event sequences of successful and unsuccessful packet transmissions. Combined with a probabilistic model of the communication

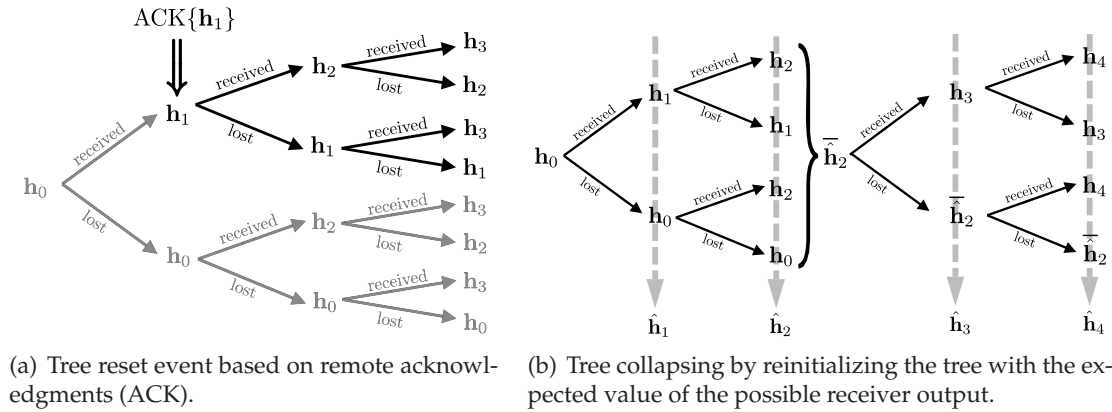


Figure 4.8: Size limitation techniques of the Markov decision tree.

channel, it allows the determination of the possible receiver states after n transmissions together with their corresponding probabilities of occurrence. This allows for the consideration of all possible signal output of the receiver which can be perceptually and probabilistically evaluated. To this end, a probabilistic decision over the transmission of possibly lost packets can be obtained.

Note that the number of branches and, hence, number of possible receiver states to consider exponentially grows with every triggered haptic data transmission. For n transmitted update packets, the total number of branches is 2^n . The exponential growth of the Markov decision tree rapidly results in a large tree size requiring increased computation and memory resources. Furthermore, as every possible receiver state in the Markov tree needs to be individually analyzed at every sampling instance, the simulation and evaluation of all possible receiver states at the haptic sampling frequency of 1 kHz becomes computationally expensive after a few iterations. Hence, techniques for reducing and limiting the size of the Markov tree model are of great interest.

This can be achieved, for instance, by transmitting additional state acknowledgement information from the receiver back to the sender. In this way the sender obtains delayed but exact receiver state information which is reflected by one of the nodes in the Markov tree model. Consequently, remote receiver feedback can be used to remove all parent and sibling nodes of the acknowledged tree node by resetting the root of the Markov decision tree to the most recently acknowledged receiver state. An alternative approach for reducing the size of the Markov tree is to collapse branches in the tree as soon as a certain tree size is reached. The procedure of resetting and collapsing the Markov tree are illustrated in Figure 4.8.

A comprehensive performance study of robust haptic communication using the Markov decision tree models is presented in [9].

4.2.3 Receiver State Estimation using Multivariate Gaussian Models

In this section, an alternative approach to the previously discussed Markov tree is presented. Conducted experiments reveal that the distribution of the signal error in the PD compression scheme originating from packet loss exhibits a Gaussian-like distribution, as illustrated in

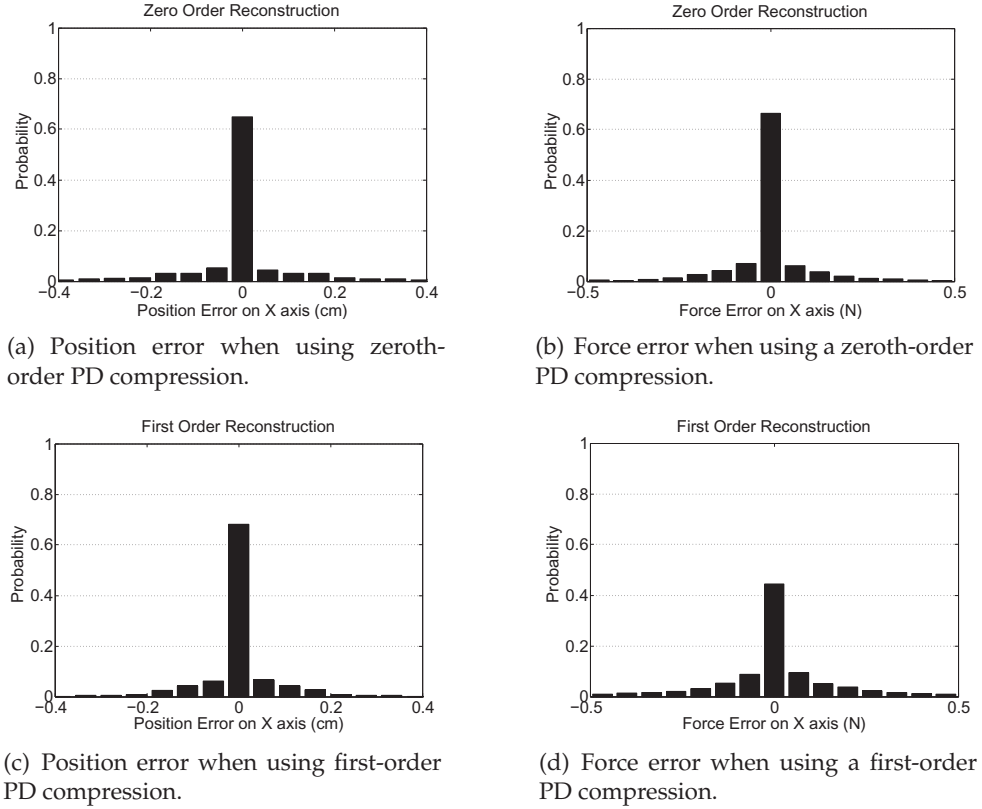


Figure 4.9: Distribution of haptic signal errors originating from packet loss. In this experiment, a uniform packet loss with probability 0.5 and PD compression with $k = 10\%$ is used. The results show that the signal error induced by lost packets exhibits a Gaussian-like distribution.

Figure 4.9. This motivates to probabilistically model the uncertainty of the receiver state with a multivariate normal distribution (see Figure 4.10).

Similar to the Markov decision tree model, the sender and the receiver are assumed to be initialized with state \mathbf{h}_0 . From then on, a successful transmission of packet \mathbf{h}_{n+1} updates the receiver state ($\hat{\mathbf{h}}_{n+1} = \mathbf{h}_{n+1}$) with probability p . Otherwise, the receiver holds its most recently successfully received update at time $i \leq n$, hence $\hat{\mathbf{h}}_{n+1} = \hat{\mathbf{h}}_i$ with probability $(1 - p)$.

$$\Pr\{\hat{\mathbf{h}}_{n+1} = \mathbf{h}_i\} = \begin{cases} \Pr\{\hat{\mathbf{h}}_n = \mathbf{h}_i\} \cdot (1 - p) & : 0 \leq i \leq n \\ p & : i = n + 1 \end{cases} \quad (4.12)$$

By using (4.12), we can iteratively calculate the sample mean $\overline{\hat{\mathbf{h}}_{n+1}}$ of all possible receiver states after $n + 1$ transmissions which can serve as an estimate of the expected mean of the

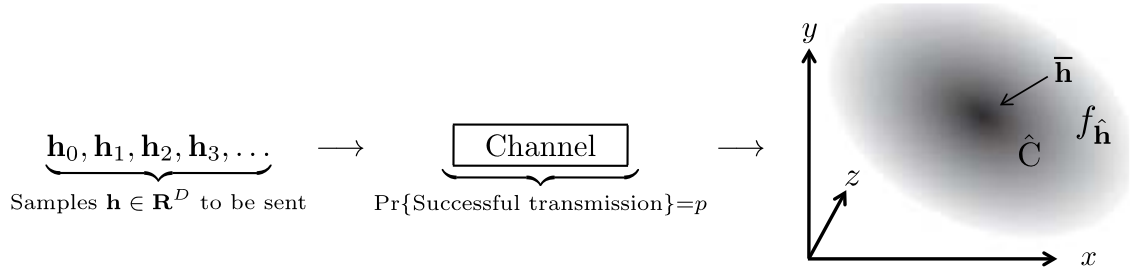


Figure 4.10: Illustration of a multivariate Gaussian distribution for statistically describing the receiver state.

receiver state.

$$\overline{\mathbf{h}_{n+1}} = \sum_{i=0}^{n+1} \Pr\{\hat{\mathbf{h}}_{n+1} = \mathbf{h}_i\} \cdot \mathbf{h}_i \quad (4.13)$$

$$= \sum_{i=0}^n \underbrace{\Pr\{\hat{\mathbf{h}}_{n+1} = \mathbf{h}_i\}}_{\Pr\{\hat{\mathbf{h}}_n = \mathbf{h}_i\} \cdot (1-p)} \cdot \mathbf{h}_i + \underbrace{\Pr\{\hat{\mathbf{h}}_{n+1} = \mathbf{h}_{n+1}\}}_p \cdot \mathbf{h}_{n+1} \quad (4.14)$$

$$= (1-p) \cdot \overline{\mathbf{h}_n} + p \cdot \mathbf{h}_{n+1} \quad (4.15)$$

Similarly, the sample mean of all vector products $\mathbf{h}_i \mathbf{h}_i^\top$ can be iteratively updated with every triggered network transmission:

$$\overline{\mathbf{h}_{n+1} \mathbf{h}_{n+1}^\top} = \sum_{i=0}^{n+1} \Pr\{\hat{\mathbf{h}}_{n+1} = \mathbf{h}_i\} \cdot \mathbf{h}_i \mathbf{h}_i^\top \quad (4.16)$$

$$= \sum_{i=0}^n \Pr\{\hat{\mathbf{h}}_{n+1} = \mathbf{h}_i\} \cdot \mathbf{h}_i \mathbf{h}_i^\top + \Pr\{\hat{\mathbf{h}}_{n+1} = \mathbf{h}_{n+1}\} \cdot \mathbf{h}_{n+1} \mathbf{h}_{n+1}^\top \quad (4.17)$$

$$= (1-p) \cdot \overline{\mathbf{h}_n \mathbf{h}_n^\top} + p \cdot \mathbf{h}_{n+1} \mathbf{h}_{n+1}^\top \quad (4.18)$$

With the help of the continuously updated sample mean values $\overline{\mathbf{h}_{n+1}}$ and $\overline{\mathbf{h}_{n+1} \mathbf{h}_{n+1}^\top}$, an estimate of the covariance matrix $\hat{\mathbf{C}}_{n+1}$ can be determined which expresses the uncertainty of the current receiver state estimation. It is defined by:

$$\hat{\mathbf{C}}(\hat{\mathbf{h}}_{n+1}) = \overline{\mathbf{h}_{n+1} \mathbf{h}_{n+1}^\top} - \overline{\mathbf{h}_{n+1}} \cdot \overline{\mathbf{h}_{n+1}}^\top \quad (4.19)$$

$$= \left[(1-p) \cdot \overline{\mathbf{h}_n \mathbf{h}_n^\top} + p \cdot \mathbf{h}_{n+1} \mathbf{h}_{n+1}^\top \right] - \left[(1-p) \cdot \overline{\mathbf{h}_n} + p \cdot \mathbf{h}_{n+1} \right] \cdot \left[(1-p) \cdot \overline{\mathbf{h}_n}^\top + p \cdot \mathbf{h}_{n+1}^\top \right] \quad (4.20)$$

Hence, the receiver state can be statistically modeled with every network transmission by successively updating the mean and covariance estimates of $\hat{\mathbf{h}}_{n+1}$. This iterative estimation procedure can be performed with low computational effort and at high update/transmission rates at the sender.

Note that the estimated covariance matrix \hat{C} incorporates correlations within the transmitted signal \mathbf{h} . The principal axes of the recently transmitted haptic samples \mathbf{h}_i are reflected by the eigenvectors of the covariance matrix $\hat{C}(\hat{\mathbf{h}})$. Hence, the uncertainty described by the covariance matrix increases towards the direction of current signal change and, consequently, stays within smaller bounds along an orthogonal direction to the current signal trajectory. If \hat{C} is nonsingular and positive definite (which is usually the case after a few iterations), its determinate $\det(\hat{C})$ can be used to obtain a measure of uncertainty of the current receiver state estimation process. If $\det(\hat{C})$ falls below a small threshold ϵ , the sample mean $\overline{\hat{\mathbf{h}}_{n+1}}$ can be considered to be a precise estimate of the current receiver state $\hat{\mathbf{h}}_{n+1}$. Consequently, a perceptual evaluation of the sample mean $\overline{\hat{\mathbf{h}}_{n+1}}$ at the sender allows a reliable decision over the transmission of possibly lost packets to be obtained. However, if $\det(\hat{C})$ exceeds the uncertainty threshold ϵ , additional steps are required to decide over possibly required redundancy on the haptic channel which are discussed in the following.

As the receiver output $\hat{\mathbf{h}}_i$ is unknown at the sender at time i , the region in the receiver state space is of interest, within which haptic output samples $\hat{\mathbf{h}}$ are in PD compliance with the current input sample \mathbf{h}_i at the sender. If \mathbf{h}_i falls into this region, the difference in signal between sender input \mathbf{h}_i and receiver output $\hat{\mathbf{h}}_i$ can be considered to be imperceptible and no additional network transmissions are required.

Interestingly, the region assuring a PD compliance is of circular/spherical shape with center \mathbf{s} and radius r , as shown in the following equations:

$$|\hat{\mathbf{h}} - \mathbf{h}| \leq k|\hat{\mathbf{h}}| \quad (4.21)$$

$$(\hat{h}_x - h_x)^2 + (\hat{h}_y - h_y)^2 + (\hat{h}_z - h_z)^2 \leq k^2\hat{h}_x^2 + k^2\hat{h}_y^2 + k^2\hat{h}_z^2 \quad (4.22)$$

$$(k^2 - 1)\hat{h}_x^2 + 2\hat{h}_x h_x - h_x^2 \quad (4.23)$$

$$+(k^2 - 1)\hat{h}_y^2 + 2\hat{h}_y h_y - h_y^2$$

$$+(k^2 - 1)\hat{h}_z^2 + 2\hat{h}_z h_z - h_z^2 \leq 0$$

$$\left(\hat{h}_x \sqrt{k^2 - 1} + \frac{h_x}{\sqrt{k^2 - 1}}\right)^2 - \left(1 + \frac{1}{k^2 - 1}\right) h_x^2 \quad (4.24)$$

$$+ \left(\hat{h}_y \sqrt{k^2 - 1} + \frac{h_y}{\sqrt{k^2 - 1}}\right)^2 - \left(1 + \frac{1}{k^2 - 1}\right) h_y^2$$

$$+ \left(\hat{h}_z \sqrt{k^2 - 1} + \frac{h_z}{\sqrt{k^2 - 1}}\right)^2 - \left(1 + \frac{1}{k^2 - 1}\right) h_z^2 \leq 0$$

$$(k^2 - 1) \left(\hat{h}_x + \frac{h_x}{k^2 - 1}\right) \quad (4.25)$$

$$+(k^2 - 1) \left(\hat{h}_y + \frac{h_y}{k^2 - 1}\right)$$

$$+(k^2 - 1) \left(\hat{h}_z + \frac{h_z}{k^2 - 1}\right) \leq \frac{k^2}{k^2 - 1} (h_x^2 + h_y^2 + h_z^2)$$

$$\underbrace{\left(\hat{h}_x - \frac{h_x}{1 - k^2}\right)^2}_{=:s_x} + \underbrace{\left(\hat{h}_y - \frac{h_y}{1 - k^2}\right)^2}_{=:s_y} + \underbrace{\left(\hat{h}_z - \frac{h_z}{1 - k^2}\right)^2}_{=:s_z} \leq \underbrace{\frac{k^2}{(k^2 - 1)^2} (h_x^2 + h_y^2 + h_z^2)}_{\leq:r^2}$$

$$|\hat{\mathbf{h}} - \mathbf{s}| \leq r \quad (4.26)$$

Hence, if $|\hat{\mathbf{h}} - \mathbf{s}| \leq r$, the current haptic input \mathbf{h} at the sender is PD compliant with the receiver output $\hat{\mathbf{h}}$. Consequently, the probability of being in PD compliance can be calculated by integrating over the PD assuring spherical region within the probability density function $f_{\hat{\mathbf{h}}}$ of the modeled receiver state distribution

$$\Pr[\text{PD Compliance}] = \int_{\{\mathbf{x} | r \geq |\mathbf{x} - \mathbf{s}|\}} f_{\hat{\mathbf{h}}}(\mathbf{x}) d\mathbf{x} \quad (4.27)$$

using the probability density function $f_{\hat{\mathbf{h}}}$ of a D -dimensional multivariate Gaussian distribution:

$$f_{\hat{\mathbf{h}}}(\mathbf{x}) = (2\pi)^{-\frac{D}{2}} \det(\hat{\mathbf{C}})^{-\frac{1}{2}} \exp\left(-\frac{1}{2}(\mathbf{x} - \bar{\mathbf{x}})^T \hat{\mathbf{C}}^{-1}(\mathbf{x} - \bar{\mathbf{x}})\right) \quad (4.28)$$

As long as the probability of the signal error being in PD compliance with the input signal \mathbf{h} stays below a target probability ψ , transmissions of possibly lost packets need to be executed until the desired PD compliance probability ψ is retained.

This sender-driven packet transmission approach using multivariate Gaussian distribution models can be further extended to first-order PD compression scenarios (see Section 2.3.4.2). Here, the prediction coefficient/gradient \mathbf{g} is typically jointly transmitted together with the current absolute haptic sample value \mathbf{h} . This allows the separate modeling of not only the statistical distribution of the absolute signal \mathbf{h} , but also of the prediction gradient \mathbf{g} . However, transmission errors in predictive coding schemes propagate over time which requires updating of the mean and covariance estimates of $\hat{\mathbf{h}}$ and $\hat{\mathbf{g}}$ at every sampling instance (and not only when network transmissions are triggered). According to linear regression theory in statistics, the absolute sample amplitude and the corresponding gradient can be understood as independent random variables. As the sum of normally distributed independent random variables is again normally distributed, the signal prediction step can be easily applied to the probabilistic models during periods of network inactivity:

$$\overline{\mathbf{h}_{n+1}} = \overline{\mathbf{h}_n} + \overline{\mathbf{g}_n} \quad (4.29)$$

$$\hat{\mathbf{C}}(\hat{\mathbf{h}}_{n+1}) = \hat{\mathbf{C}}(\hat{\mathbf{h}}_n) + \hat{\mathbf{C}}(\hat{\mathbf{g}}_n) \quad (4.30)$$

Hence, the modeled uncertainty of the receiver state described by the covariance estimate $\hat{\mathbf{C}}(\hat{\mathbf{h}}_n)$ grows linearly over time. However, each triggered update reduces again the uncertainty in the haptic communication system. Consequently, the presented approach does not require acknowledgments and feedback information from the receiver. However, feedback of the remote receiver state can be optionally used to support the receiver state estimation process.

4.2.3.1 Experimental Study

A psychophysical study has been conducted to investigate the performance of perceptually robust haptic communication using the novel multivariate Gaussian receiver state model. In the experiment, 16 students from the Institute for Media Technology, TUM, participated. The experimental setup consists of a Phantom Omni HSI device from SensAble [163] and

a simulated virtual TPTA environment. It contains a touchable virtual sphere with smooth surface which can be approached and haptically touched from any direction. During contact with the TPTA environment, contact forces are rendered by the *CHAI3D* library [57] at a rate of 1000 Hz. In the experiment, a uniform packet loss during the transmission of the haptic feedback signal is simulated. The uncertainty threshold ϵ applied to the determinant of \hat{C} is set to 10^{-15} . The integral in (4.27) is numerically evaluated with a resolution of $0.01N$ in every dimension.

The experiment consists of two runs which investigate the performance of the proposed packet loss concealment scheme applied to zeroth-order and first-order PD compression, respectively (see Section 2.3.2) with PD parameter $k = 10\%$. In each run, ten different system configurations with varying packet loss and deadband compliance probability ψ are evaluated which are blindly presented to the subjects. Specifically, the impact of network packet loss of 0%, 20%, 40%, 60% on PD compressed force feedback signals is investigated. In addition, for each of the test configurations with a packet loss probability $> 0\%$, the influence of the proposed packet loss compensation scheme using the multivariate Gaussian receiver model on subjective quality and packet rates are observed. Here, three PD compliance probabilities $\psi = 0\%, 70\%, 95\%$ are used to configure the sender-driven transmission scheme. The subject can freely choose between the ten test configurations by pressing the number 0-9 on a keyboard. As soon as a test configuration is selected, the corresponding feedback is immediately displayed to the subject which allows for a pairwise comparison between the test items. In addition, a reference configuration is provided to the subject which deactivates the simulated packet loss on the haptic channel. This enables the direct comparison and subjective rating the different test configurations against the presented reference configuration. The subjects are asked to perceptually evaluate any perceived difference in the haptic feedback compared to the reference setting in accordance with the subjective evaluation scheme illustrated in Table 2.1 in Section 2.1.4.

The experimental results are shown in Figure 4.11. The upper figures show the mean packet rates and mean subjective ratings for the zeroth-order PD compression scheme. It can be observed that with increasing packet loss probability, the subjective quality of the haptic feedback becomes clearly impaired. The light and the dark gray bars illustrate the results with applied packet loss compensation using the multivariate Gaussian receiver model. In order to conceal the packet loss on the haptic channel, additional packet transmissions are triggered as soon as disturbing signal distortion at the receiver becomes likely, which can be seen in Figure 4.11(b). The subjective ratings in Figure 4.11(a) show that by adding redundancy to the haptic channel, the disturbing packet loss effects in the TPTA system can be successfully compensated. Even at a PD compliance probability of 70%, the transparency of the TPTA system is almost completely restored. The lower figures illustrate the mean packet rates and the mean subjective rating of the first-order PD compression scheme. The results clearly show that first-order PD compression is significantly more sensitive to data loss on the communication channel. Here, already a low packet loss probability significantly impairs the subjective quality of haptic feedback. This is mainly due to incorrect signal predictions which occur as soon as haptic predictor updates are lost during transmission. However, the results in Figure 4.11(c) demonstrate that also for the first-order PD compression scheme, the sender-driven transmission scheme successfully compensates the network data loss. Interestingly, the additional packet rates required for packet loss compensation seem to be similar for the zeroth-order and first-order PD compression scheme.

In summary, the experimental results reveal that the multivariate receiver model is able to compensate even high packet loss up to a loss probability of 60% at the cost of increased packet rates on the haptic channel. This can be achieved with low computational complexity and without the need for acknowledgement feedback. Furthermore, the presented error-resilient communication scheme does not introduce any additional processing latency to the haptic signals.

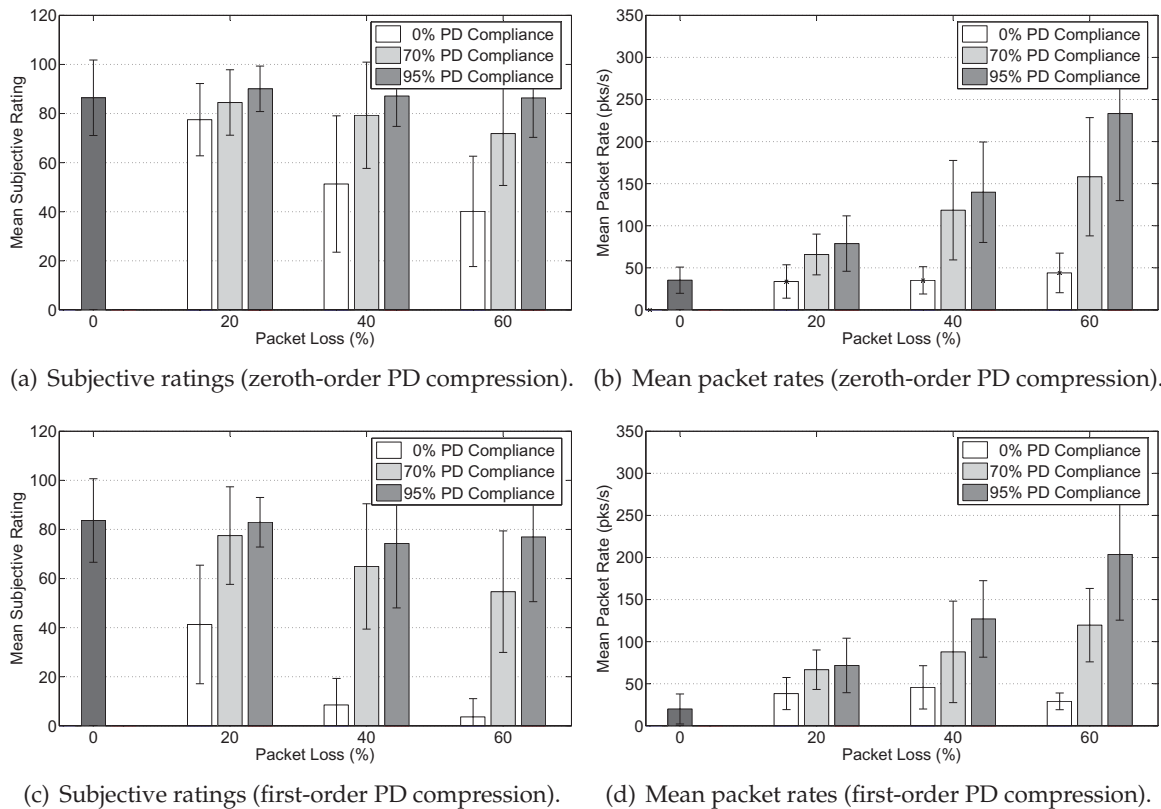


Figure 4.11: Experimental results of error-resilient haptic communication based on multivariate Gaussian models. In all test configurations, PD compression with a PD parameter of $k = 10\%$ is applied to the force feedback signals. The results show that packet loss on the haptic channel can be successfully compensated at the cost of increased packet rates.

4.3 Multimodal Telepresence Sessions using the Session Initiation Protocol (SIP)

In TPTA systems, not only haptic sensory data needs to be exchanged between the HSI device and the TOP. In addition to the communication of multimodal audio and video data streams, the exchange of session control commands is also required during a TPTA session.

Although research in telerobotics is quickly advancing, the communication architectures typically used in TPTA systems are still that of pre-Internet point-to-point networks. It is common for each TPTA system to be programmed with a fixed configuration of its remote partners and to communicate via an individual proprietary network protocol [30, 125, 150], a practice with limited flexibility. Furthermore, there are no established protocols for locating remote TOPs or established standard formats for exchanging TOP control data. Many available software platforms in robotics include networked communication [80, 152, 184]. However, these are not typically designed for TPTA systems, and are unsuited for the low-latency requirements and high packet rates of haptic communication. A common framework is therefore needed to allow a variety of haptic and teleoperation systems to work together flexibly.

In this section, a flexible framework for initiating, handling and terminating TPTA sessions using the widely deployed *Session Initiation Protocol* (SIP) is discussed. This research work has been conducted in cooperation with Hawkeye King [19].

4.3.1 Internet-based Transport Streams and Session Control

Haptic data communication is characterized by strict delay constraints required to maintain control loop stability. Lost or out-of-order packets need to be discarded as triggered retransmissions significantly increase the communication latency. In Internet-based communication, this suggests using the *User Datagram Protocol* (UDP), as it works without handshaking dialogues and does not provide reliability, ordering, or data integrity functionality. An additional requirement for the transport of haptic signals is the availability of timestamps for each transmission. This enables the detection of delayed packets and supports dejittering and stream synchronization. Furthermore, in TPTA systems with many DoFs, the haptic transport system needs to be capable of addressing/updating only a subset of DoFs by grouping and assigning data identifiers. All these requirements match the widely applied *Real-Time Transport Protocol* (RTP). It is an application layer protocol for real-time streaming of media data and deploys the lightweight, yet unreliable UDP protocol as the underlying transport mechanism. It also provides build-in mechanisms for jitter compensation enabling the TPTA system to trade-off additional latency for more consistent timing. RTP has a companion protocol, the *RTP Control Protocol* (RTCP), that operates in parallel collecting out of band statistics such as round-trip delay and packet loss. Based on this information, RTP can perform stream synchronization between multiple data streams. This would allow haptic and video data to be presented in a time-coordinated manner if desired. Multicast is also supported by RTP, which is beneficial in cooperative TPTA scenarios.

In addition, session control commands need to be exchanged between the OP and the TOP in order to initiate, control and finish a TPTA session. TPTA system related operation commands for changing/switching tools, sensors, system states, etc. also need to be

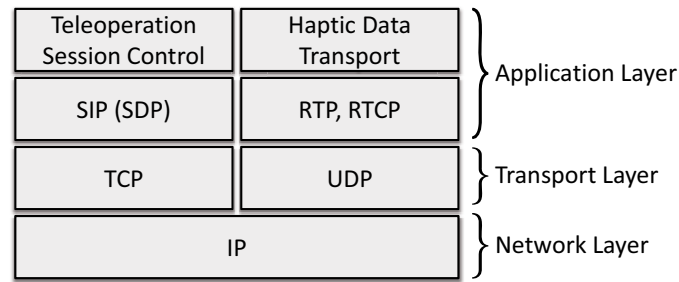


Figure 4.12: Illustration of the SIP-based protocol stack for TPTA session control. The protocol suite uses SIP for session management, SDP for codec and parameter negotiation, and RTP for transport of encoded media.

signaled. Furthermore, to enable flexible interconnection between different TPTA systems, the exchange of system relevant characteristics describing the properties of the HSI and the TOP system must be communicated during the session initialization procedure. In contrast to the transmission of the haptic data streams, the communication of session commands and system meta information is not affected by strict latency constraints. Here, the reliability of a successfully signaled command and/or system state update is of the highest importance. In an Internet-based network scenario, the communication of session commands and system description information should therefore use the reliable *Transmission Control Protocol* (TCP) protocol.

4.3.2 System Parameter Negotiation

In order to allow for flexible dynamic connections between multiple haptically enabled interfaces and devices, detailed knowledge of the system parameters and functional capabilities is essential. In the context of TPTA systems, the exchange of system descriptions and hardware characteristics of the HSI device and the TOP is of great relevance. It enables the negotiation and optimization of the functional capabilities of the HSI and the TOP during the initialization of a TPTA session. In contrast to audio, video and text communication where only a small set of system parameters such as resolution, color depth, frame and sampling rate, audio channels, etc. are required to configure the application, a TPTA system can vary in several aspects. Interoperability among unique TPTA systems with widely varying designs and capabilities can only be achieved by negotiating and determining what data is to be transmitted in which format and how that data should be applied to the HSI and TOP.

In this context, important system characteristics of a TPTA system are:

- *System parameters:* amount of DoFs, kinematics, coordinate systems, controller type/rates, sensory dynamics, transforms (rotation/translation matrices), workspace and joint limits, initialization parameters (initial position)
- *Compression system:* applied compression method (codec), compression parameterization, data encoding, error correction scheme, error concealment techniques
- *Control architecture:* deployed control architecture, control gains, haptic signals to be transmitted (position, velocity, orientation, forces, torques, wave variables, total energy)

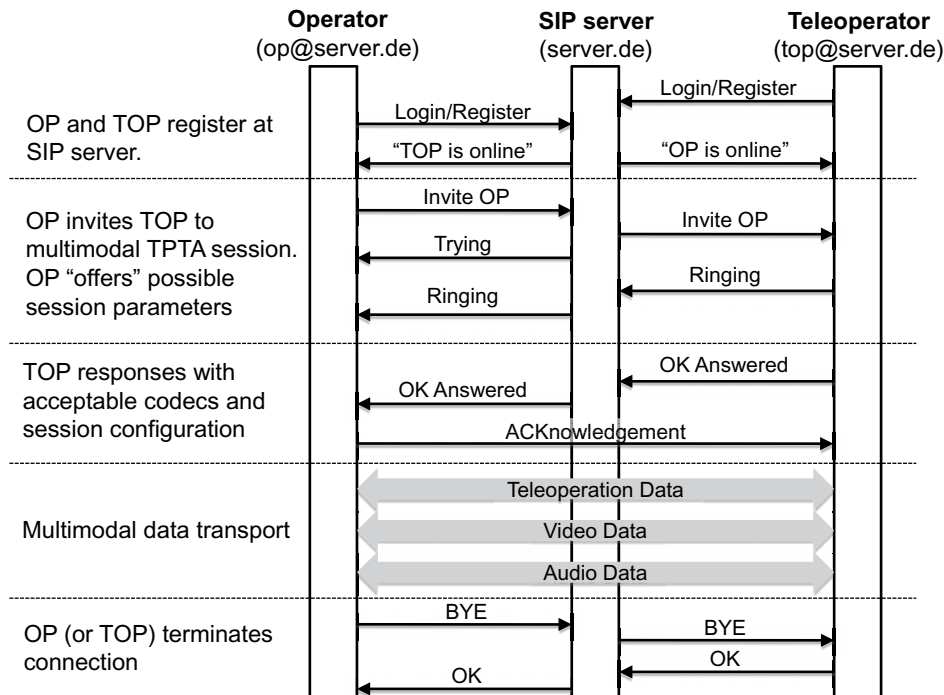


Figure 4.13: Illustration of a SIP-based OP to TOP call (reproduced from [19]).

- *Communication system*: error detection scheme, network conditions/statistics (time delay, jitter, packet loss)

Solving the challenges of establishing communication sessions among different types of computer systems is fundamental to computer networking and has been extensively addressed in literature. For instance, in multimedia teleconferencing, a wide range of network protocols exist for real-time audio and visual media exchange, which are used by NetMeeting, AIM, Google Talk and others. These protocols solve complex engineering tasks such as resource location, media and codec negotiation, data transport, and security. Particularly, the widely adopted Session Initiation Protocol (SIP) is well suited for the initialization and controlling of multimodal transport streams [155]. By taking advantage of synergies between teleconferencing technology and the telerobotics domain, the teleconferencing protocols and the teleconferencing infrastructure can be used to also improve flexibility and interoperability among different types of TPTA systems.

An overview of the proposed protocol stack for SIP-based TPTA session management is illustrated in Figure 4.12.

4.3.3 SIP-based Communication Framework

The proposed TPTA session management framework uses the SIP protocol for multimodal TPTA sessions including streaming audio, video and haptic modalities [155]. SIP uses the Session Description Protocol (SDP) during initial call handshake to negotiate network parameters and select optimal codecs for streaming media [87]. These features are not unique to SIP, but are also common to other Internet session protocols like IAX2 and H.323.

Figure 4.13 gives an overview of session initiation, parameter negotiation, transport, and session termination processes. To start a SIP session the HSI sends a SIP invitation to the TOP. It includes a SDP description of media types, codecs, and codec parameters supported by the inviting client. The remote user subsequently acknowledges the invitation and answers the call, sending a SIP answer message. The SIP answer contains a SDP message which describes the media codecs and parameters supported by both parties, selected by comparing local capabilities to those indicated in the offer. For the haptic modality, codec and parameter negotiation may select the applied control architecture and parameters, workspace and device degrees of freedom, endeffector capabilities, and any other haptics-specific requirements. The master and slave capabilities and the codec in use will determine the parameters to be negotiated. At this point, all communication parameters have been decided on and the multimodal data streaming begins.

Figure 4.15 shows an example of a *SIP INVITE* message containing a SDP descriptor. In this SIP invitation, three media types are specified: video, audio and the new type *haptic* which is added for bilateral TPTA session control. For each media type, one or more codecs may be provided. In this packet the GSM codec for voice is offered to support the audio media type, and for video streaming, the h.264 codec is offered. In addition, the codec *Haptic_Coder* is offered for the media type *haptic*.

A codec is essentially a method for transcoding data to and from a raw format to another format that is of better rate-distortion ratio and/or has better error resiliency properties. In the context of TPTA systems, a haptic codec can be used to provide an interface to different compression algorithm, control architecture and error concealment schemes. Accordingly, the integration of a codec abstraction layer for the haptic transport enables the negotiation of all global communication and control parameters of a TPTA system. Furthermore, it frees the control engineer from the details of networking and session management.

For complete control of a telemanipulation system, additional commands and information may need to accompany the haptic data stream. Specifically, important control data like tool-change commands, emergency stops, or user information should be transmitted with a reliable transport mechanism. The SIP architecture provides the *SUBSCRIBE* and *NOTIFY* interface which allows SIP clients to request notification from and exchange data with remote nodes [154].

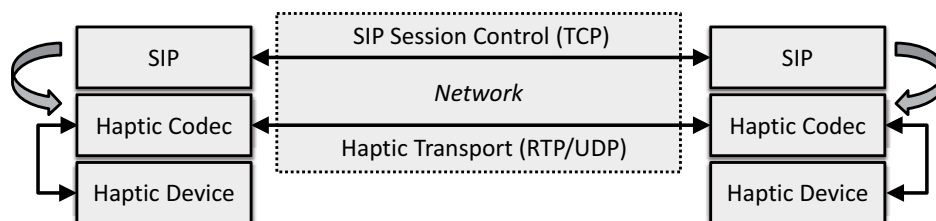


Figure 4.14: Haptic codec transcodes raw haptic device data into formats for haptic communication according to the selected haptic compression and control scheme (adapted from [19]). The codec is controlled by the session management application, which also manages the transport streams.

```
INVITE sip:m1@server.de SIP/2.0
CSeq: 1 INVITE
v: SIP/2.0/TCP 10.152.4.89:5060
Allow: INVITE,ACK,OPTIONS,BYE,
CANCEL,SUBSCRIBE,NOTIFY...
c: application/sdp
l: 1675
m=audio 5000 RTP/AVP 106 112 3...
c=IN IP4 10.152.4.89
a=sendrecv
a=rtpmap:3 gsm/8000/1
...
m=video 5002 RTP/AVP 102 103 ...
c=IN IP4 10.152.4.89
a=rtpmap:102 h264/90000
...
m=haptic 5004 RTP/AVP 0
c=IN IP4 10.152.4.89
a=sendrecv
a=rtpmap:0 Haptic_Coder/1000
a=fmtp:0 DoF=3;Control="PosControl";..
Coordinate="Cartesian";World="Global"
```

Figure 4.15: SIP INVITE along with SDP media-type and codec offer.

4.3.4 Demonstrator System

In order to demonstrate the SIP-based session framework, a proof-of-concept system has been implemented. The demonstrator hardware comprises two Linux PCs equipped with PHANToM Omni haptic devices [163]. The HSI system tracks the OP's hand movements and displays force feedback. The OP host computer also displays audio and video feedback captured by the TOP robot. The TOP, as shown in Figure 4.16(a), consists of a PHANToM Omni which is equipped with a Logitech Webcam with integrated microphone attached. It also has a writing pen attached as an endeffector.

The software developed for the demonstrator prototype is based on the Open Phone Abstraction Library (OPAL). It is cross-platform compatible with the Linux, Mac OS X and Windows operating systems and provides a full featured SIP protocol stack including the SDP codec negotiation functionality and low-latency RTP protocol implementation.

The OPAL's media handling routines are extended to support haptic media types, alongside audio and video media types. A haptic device interface wrapper is developed using the OpenHaptics API from SensAble [163]. OPAL has built in support for loading binary codec plugins for every available media format. This enables the SDP to provide auto-negotiation of optimal codecs during the initial SIP handshake.

For the demonstrator system, OpenPhone, a GUI-frontend for OPAL, is compiled against the modified OPAL libraries. Once the SIP-based TPTA session is established, the media streams for each modality are set up automatically with no human intervention. The haptic codec used in the system implements a bilateral position-position control of the haptic

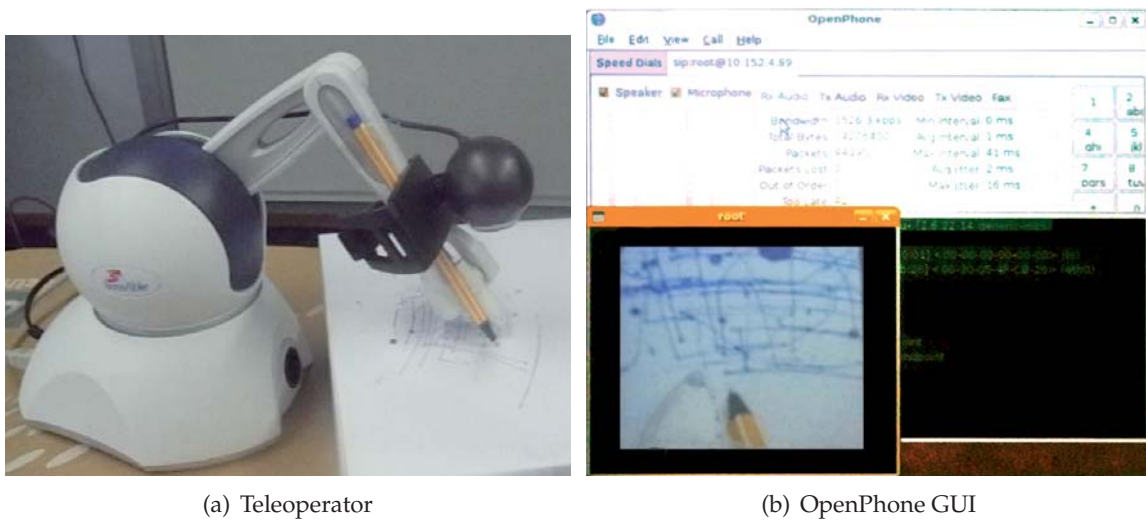


Figure 4.16: Overview of the demonstrator and prototyping system for SIP-based teleoperation (reproduced from [19]). Figure 4.16(a) shows an image of the teleoperator. The system employs a SensAble PHANTOM Omni haptic device equipped with a Logitech audio/video Webcam and an endeffector writing instrument. Figure 4.16(b) shows a screenshot of the operator display with GUI and visual feedback.

devices with local PD control. A screenshot of the application is shown in Figure 4.16(b).

In the demonstration scenario, the OP-side host computer calls the TOP to initiate a SIP call. As soon as the call is accepted, the SDP stack selects codecs for the audio, video and haptic media communication. After the codec negotiation, three RTP transport streams are created, one for each modality. During the TPTA session, the SIP-based session control framework handles the haptic data flow between the device, codec and network (see Figure 4.14). The demonstrator successfully establishes haptics, audio, and video media streams, transmitting haptic data at close to 1 kHz.

4.4 Chapter Summary

The performance of perceptual haptic data compression in TPTA systems significantly depends on the properties of the haptic signals. They are influenced by many factors such as the deployed control architecture, the network performance, the hardware characteristics of the TPTA system, etc. In order to address these important influencing factors, the development of methods for perceptual haptic communication needs to be approached from a combined signal processing, control engineering and networking point of view. In this context, several contributions have been presented in this chapter which are briefly summarized in the following.

In bilateral TPTA systems, the wave variable control scheme has become a popular control approach to address the stability issues of time-delayed communication. By transmitting wave variables over the communication channel, the passivity of the haptic communication system can be guaranteed under the assumption of arbitrarily long, but constant time delay. The wave variables represent linear transformations of combined local and remote haptic sensory information which makes it difficult to apply perceptual arguments for data compression in the wave variable domain. To address this limitation, a modified wave variable control approach has been presented which allows for a local decoupling of the wave variable loop. Consequently, the direct transmission and application of perceptual compression in time-delayed TPTA communication is enabled while preserving the stabilization ability of the wave variable control approach. Furthermore, a passivity-preserving PD compression scheme has been presented. It considers the TPTA system to be a cascade of interconnected one-port and two-port subsystems and investigates the energy balance within the HSI and the TOP subsystem. The performance of the local wave variable rendering approach combined with the passivity-preserving PD compression approach has been experimentally investigated in a simulated TPTA environment. The results demonstrate improved transparency at lower packet rates compared to the standard wave variable architecture.

Not only network latency but also data loss on the communication channel impairs the performance of perceptual haptic data communication techniques. As the PD compression scheme only transmits haptic samples which are considered to be perceivable to the human OP, packet loss in the network immediately leads to perceivable distortion. To address this issue, a sender-driven retransmission scheme for low-latency packet loss compensation has been proposed. By deploying a probabilistic model of the receiver, a probabilistic decision about possibly required retransmissions can be obtained. If a likely receiver state is assumed to deviate from the undistorted signal by more than the applied perception thresholds, additional redundancy can be adaptively added to the haptic channel in order to compensate for the data loss. In addition to the Markov decision tree based receiver model, a novel multivariate Gaussian model for receiver state estimation has been proposed and experimentally evaluated. Its computational complexity is significantly lower and does not require the transmission of acknowledgement feedback. Conducted experiments validate that the packet loss compensation scheme using the multivariate Gaussian receiver model can successfully restore the transparency of the TPTA system when operating on a highly erroneous network channel.

Furthermore, a novel communication framework leveraging Internet session and presence protocols for TPTA systems has been discussed. It is based on the widely adopted Session Initiation Protocol (SIP), which is designed for Internet telephony and teleconferencing. En-

tirely within the SIP architecture, a method for TPTA session control has been presented which allows for flexible and dynamic connections between multiple haptic enabled interfaces and devices. In addition, it provides a standard interface for integrating the discussed perceptual communication and control approaches. To this end, interoperability among heterogeneous TPTA systems can be achieved. For prototyping and evaluating the SIP-based communication and control codecs, a proof-of-concept system has been developed.

5 Conclusion and Outlook

5.1 Concluding Remarks

The broad range of TPTA systems and their application scenarios promise great scientific and economical interest for the future. Their goal is to locally provide a realistic immersion of a distant, scaled, inaccessible and/or hazardous environment.

In this context, the exchange of haptic signals plays a central role in TPTA systems. In contrast to the transmission of audio and video signals, haptic signals are bidirectionally exchanged and thereby close a global control loop between the HSI device and the TOP. In order to assure system stability and transparency, introduced communication delay on the haptic channel needs to be kept at an absolute minimum. These strict delay constraints require haptic samples to be transmitted immediately upon generation which leads to transmission rates up to the applied haptic sampling rate of 1000 Hz. In packet-switched networks, e.g., the Internet, the increased amount of transmitted packet header information leads to significant network overhead. In addition, modern TPTA systems deploy a large number of DoFs to provide intuitive and flexible remote manipulation. As every DoF is individually sampled and controlled, the bidirectional exchange of haptic signals leads to high data rates which are particularly challenging in large-distance or wireless TPTA scenarios.

This dissertation addresses the challenges of perceptual haptic data communication in TPTA systems. To this end, the consideration of human haptic perception is of fundamental interest and intensively discussed. Limitations in haptic perception can be exploited for the detection and removal of imperceptible signal content. As long as changes in haptic signals cannot be perceived by the human operator, they can be considered to be irrelevant for transmission and processing.

Several contributions presented in this thesis focus on improving perceptual haptic data compression.

By incorporating additional findings of human haptic perception into the psychophysical model, the performance of perceptual haptic data compression can be increased. Particularly, the integration of psychophysical findings on directional dependencies of force feedback perception has shown to significantly improve compression performance. Similarly, the adaption to psychophysical findings on velocity-dependent discrimination thresholds during human operator's hand movements can be exploited in the context of perceptual haptic data communication.

Furthermore, an architecture for combined model-mediated control and compression has been proposed. Instead of haptic feedback, it transmits the parameters of estimated environment models over the haptic channel. Conducted experiments on a real TPTA system indicate that the integration of environment models into haptic compression algorithms allows for improved compression performance and system transparency. The model-mediated compression scheme is further extended to enable the design of a model-mediated haptic

signal prediction scheme. Experimental results reveal improved compression performance when PD compression is combined with model-mediated haptic prediction algorithms. In addition, a model-based coding scheme for haptic contact events is proposed which addresses the increased haptic update rates during the initial contact phase. By transmitting a single event-of-contact message from the TOP to the HSI device, haptic feedback can be locally generated and used for substituting the transmission of remote haptic feedback. The experimental results show that by integrating the concept of *Event-based Haptics*, the quality of contact feedback can also be improved.

In addition to the delay critical real-time communication of haptic signals, the development of perceptual offline compression algorithms is also of great interest. To this end, a haptic recording and playback scheme has been presented which allows the OP to immerse into the previously recorded TPTA session. Once haptic data needs to be stored on a storage device, methods for haptic offline compression become relevant. In contrast to haptic online compression algorithms which mainly address the high update rate on the communication channel, methods for haptic offline compression strictly focus on reducing the amount of data to be stored. To this end, a first perceptual haptic offline compression scheme has been presented and experimentally evaluated. It exploits knowledge about applied perception thresholds resulting in reduced entropy of the encoded data.

In order to investigate perceptual haptic communication from a theoretical point of view, the concept of a *Perceptual Deadband Sampler* has been proposed. It provides a framework for analytically evaluating the compression performance based on a statistical model of haptic signals. In particular, a first-order Gaussian random walk model has been used to model the signal trajectories of haptic signals which allows for the mathematic determination of the expected packet rates on the communication channel.

Perceptual haptic data communication has been further investigated from a combined signal processing, control engineering and networking point of view. Several contributions based on this integrated approach have been made.

In real-world telepresence scenarios, transmission delays on the haptic channel quickly destabilize the global control loop closed by the communication system. In order to enable stable TPTA operation in the presence of network delay, the passivity-based wave variable control scheme can be applied. Instead of haptic sensory signals, combined velocity and force signals are exchanged over the communication channel which excludes a perceptual evaluation of the transmitted signals. To address this issue, a novel control architecture has been proposed which enables the combination of the wave variable control scheme with perceptual haptic data compression.

In addition to communication latency, data loss on the haptic channel also affects the performance of perceptual haptic communication in TPTA systems. Particularly, the transmission of compressed haptic signals is sensitive to data loss on the haptic channel. To this end, an error-resilient perceptual communication scheme has been proposed which is based on a probabilistic model of the PD decoder. Whenever the actual sender state and the estimated receiver state are expected to deviate by more than the applied perception thresholds, additional data transmissions are adaptively triggered in order to compensate for the packet loss.

Furthermore, a flexible communication framework for initiating, handling and terminating TPTA sessions has been presented which takes advantage of synergies between the Internet-

based teleconferencing technology and the TPTA system domain. Based on the widely deployed SIP teleconferencing protocol, it enables flexible and dynamic connections between multiple haptic enabled interfaces and devices. In addition, the framework provides a standard interface to haptic codecs which enable the seamless integration of the developed perceptual communication and control approaches into the communication system of a TPTA system. For prototyping and evaluating the SIP-based communication and control codecs, a proof-of-concept system has been developed.

5.2 Outlook

With recent advances in man-machine interaction, sensor and actuator hardware, network capacities, signal processing, control schemes, etc., TPTA systems are increasingly gaining in relevance. Their development will always be accompanied by the need for efficient algorithms for haptic data communication.

In the following, some exciting directions for future research emerging from this dissertation are briefly discussed:

- *Extending the psychophysical model of human haptic perception:* Research in psychophysics investigates the limitations and characteristics of the human haptic perception system. The integration of additional psychophysical findings into the perceptual model for perceptual haptic data compression may further improve the performance of perceptual haptic communication algorithms. In this context, the integration of human haptic discrimination thresholds for the perception of stiffness, acceleration, inertia, etc. seems promising.
- *Multimodal data multiplexing:* Human haptic discrimination thresholds are influenced by cross-modal dependencies. Particularly, the temporal integration of multimodal feedback is of great interest in the context of TPTA systems. It allows for the development of a multiplexer which incorporates upper and lower latency bounds for each modality. In this way, a high degree of immersiveness and transparency can be achieved even in scenarios with capacity limited communication channels.
- *Improving perceptual communication of velocity/position signals:* The perceptual deadband approach can be applied on force feedback as well as on velocity and position signals, as shown by Hinterseer *et al.* [98]. However, changes in the velocity/position signals are only indirectly reflected in the visual and haptic feedback over the remote environment. In this context, a comprehensive study of human cross-modal velocity and limb position perception is required in order to further improve perceptual haptic communication systems.
- *Extending environment models for model-mediated control, compression, and prediction:* In order to quickly adapt to environment changes, the environment models used for model-mediated control, compression, and prediction are characterized by a small number of parameters. However, there is a trade-off between model complexity and environment adaption performance which should be studied in more detail. In particular, the integration of surface friction effects into environment models seems promising.
- *Combining human behavior models with model-mediated compression:* Similar to the model-mediation concepts using environment models, the development of a mathematical

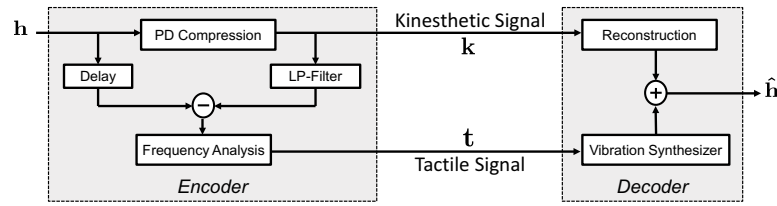


Figure 5.1: Suggested architecture for separating kinesthetic and tactile feedback from force sensory data.

model describing human haptic behavior would allow for estimating changes in velocity as a function of displayed force feedback [151]. Consequently, this would enable model-mediated prediction and compression of haptic velocity signals which should be addressed in future research.

- *Investigating block-based algorithms for haptic offline compression:* In contrast to haptic low-latency signal processing in TPTA systems, haptic offline compression algorithms do not have to take the strict delay constraints into account. Correspondingly, block based coding techniques from the field of audio and video compression, such as vector quantization, subband coding, predictive coding, etc. can be applied. In this context, the development and integration of perceptual models in the frequency domain could also further improve the performance of haptic offline compression.
- *Haptic communication in shared collaborative haptic virtual environments:* Shared cooperative virtual haptic environments enable multiple users to haptically collaborate towards a common objective. As soon as users are haptically coupled during events of joint manipulation, communication latency becomes a critical factor. To address this issue, methods for detecting joint haptic interaction and decentralizing the rendering and control system are of great interest. In particular, the development of an adaptive grouping scheme of active users should be addressed. Furthermore, delayed network transmissions leads to inconsistencies within the global virtual world representation. In this context, an energy-constrained update strategy could be used where interconnected clients always agree to the state that reflects the least physical energy.
- *Separate processing of kinesthetic and tactile feedback:* The haptic perception system involves the kinesthetic and the tactile sense. In order to address their individual properties with respect to haptic discrimination thresholds, methods for separating kinesthetic and tactile components from the haptic sensory data need to be designed. Figure 5.1 proposes an architecture for perceptual haptic communication which processes tactile and kinesthetic signal components separately. Here, the perceptual deadband scheme is used to compress the low-frequent kinesthetic signal component. Experimental studies have shown that the signal content typically lost during PD compression often contains high-frequent tactile components [18]. The signal characteristics of tactile signals suggest a frequency-based compression scheme, such as LPC coding.
- *Processing of haptic multi-point contact signals:* Modern TPTA systems integrate more and more DoFs. During multi-point contacts with the environment, the control and sensory signals typically correlate with each other which should be exploited in the context of perceptual haptic data communication. In addition, a joint analysis of the multi-point contact sensory data would support the estimation of environment models used in model-mediated control, compression and prediction.

List of Figures

1.1	Overview of addressed research areas.	3
1.2	Overview of the dissertation.	4
2.1	Overview of the main components of a TPTA system.	8
2.2	Overview of haptic signals in a TPTA system.	9
2.3	TPTA system as a cascade of one-port and two-port subsystems.	11
2.4	Absolute and relative perception thresholds of tactile stimuli.	19
2.5	Illustration of perceptual predictive coding.	21
2.6	Illustration of multi-DoF isotropic perceptual deadzones.	23
2.7	Perceptual deadband compression using a zeroth-order prediction algorithm.	24
2.8	Perceptual deadband compression using a first-order prediction algorithm.	25
3.1	Illustration of the construction of a direction-adaptive deadzone.	29
3.2	Overview of sampled orientations and investigated contact paths.	30
3.3	Experimental results investigating preferred PD parameters k as a function of force direction.	31
3.4	Means and standard deviations of angular thresholds quantifying the just perceptible change in the direction of force feedback for different reference force directions.	32
3.5	Experimental evaluation of the compression performance in terms of subjective quality and packet rate.	33
3.6	Adaptive PD parameter ϕ as a function of velocity.	35
3.7	Architecture of the velocity-adaptive PD data reduction principle.	36
3.8	Illustration of the experimental testbed for velocity-dependent PD compression.	37
3.9	Mean values and standard deviations of packet rates and subjective quality with respect to velocity level and deadband type.	40
3.10	Illustration of the haptic sample selection and plane fitting process.	42
3.11	Proposed architecture for model-mediated compression.	44
3.12	Overview of the experimental setup for model-mediated haptic data compression.	45
3.13	Experimental results for model-mediated compression.	48
3.14	Estimation of the surface contact point \hat{x}_s using a planar and a spherical surface model.	50
3.15	Simulation of model-mediated prediction of haptic force-feedback based on simple geometric surface models.	51
3.16	Virtual TPTA simulation used in the experimental study.	52
3.17	Experimental results for PD compression using signal-based and model-mediated prediction.	54
3.18	Illustration of the PD violations during contact events.	56

3.19	Illustration of improving contact realism by superimposing acceleration forces during contact events.	57
3.20	Proposed architecture for event-based coding using contact models.	58
3.21	Illustration of local proportional force feedback approximation with friction compensation.	59
3.22	Superimposition of contact transients onto proportional forces.	59
3.23	Local generation and display of proportional forces during the contact phase.	60
3.24	Experimental results for event-based coding using contact models.	64
3.25	Schematic overview of recording and playback of a visual-haptic TPTA session.	67
3.26	Illustration of PD-based differential encoding.	69
3.27	Schematic diagram of the PD-based offline data reduction scheme including the proposed signal prediction and deadband-based differential coding approach.	70
3.28	Principle of interpolative signal reconstruction.	71
3.29	Differences between online and offline signal reconstruction of PD-encoded haptic signals.	72
3.30	Mean subjective ratings of the haptic offline compression experiments.	73
3.31	Schematic diagram of the binary tree structure for the theoretical analysis.	77
3.32	Illustration of finding an acceptable value range λ_1 for the random summand η to assure that the AR process output continuously stays in compliance with the currently defined PD bound.	79
3.33	Illustration of possible signal trajectories and value ranges λ for the random summand η leading to a PD compliance during a period of j samples with autoregression factor $\theta = 0.5$	80
3.34	Illustration of possible signal trajectories and value ranges λ for the random value η ensuring a PD compliance during a period of $j - 1$ samples, followed by a PD violation event at time $i + j$ ($\theta = 0.5$).	81
3.35	Examples of conditional density functions $f(\hat{\mathbf{h}} s)$ for different configurations of the PD parameter k , the autoregression factor θ , and the PD event sequence s	83
3.36	Simulation and analytical derivation of the probability of a perception threshold violation for different configurations of autoregression factors θ and PD parameters k	84
4.1	Signal diagram of the wave variable approach.	88
4.2	Illustration of the passivity-preserving perceptual deadband compression scheme.	91
4.3	Schematic overview of the architecture for combined PD compression and wave variable control	92
4.4	Performance of local wave variables: Displayed impedance for stiff environments.	93
4.5	Performance of local wave variables: Displayed impedance for free space motion.	94
4.6	Architecture for error-resilient haptic communication.	95
4.7	Markov decision tree considering cases of successful and unsuccessful transmissions of haptic packets.	96
4.8	Size limitation techniques of the Markov decision tree.	97

4.9	Distribution of haptic signal errors originating from packet loss.	98
4.10	Illustration of a multivariate Gaussian distribution for statistically describing the receiver state.	99
4.11	Experimental results of error-resilient haptic communication based on multivariate Gaussian models.	103
4.12	Illustration of the SIP-based protocol stack for TPTA session control.	105
4.13	Illustration of a SIP-based OP to TOP call.	106
4.14	Illustration of haptic codecs in the SIP-based session management framework.	107
4.15	SIP INVITE along with SDP media-type and codec offer.	108
4.16	Overview of the demonstrator and prototyping system for SIP-based teleoperation.	109
5.1	Suggested architecture for separating kinesthetic and tactile feedback from force sensory data.	116

List of Figures

List of Tables

2.1	Rating scheme used for subjective evaluation.	15
2.2	Perception thresholds of the kinesthetic sense.	18
3.1	Preferred configuration for the parameters k and ν of the adaptive deadband coding scheme.	38
3.2	Experimental results of the perceptual haptic offline compression scheme. . .	74

Bibliography

Publications by the Author

Journal Publications

- [1] Jongeun Cha, Ahmad Barghout, Julius Kammerl, Eckehard Steinbach, and Abdulmoteleb El Saddik. Improving spatial perception in telepresence and teleaction systems by displaying distance information through visual and vibrotactile feedback. *PRESENCE - Teleoperators and Virtual Environments*, 19(5), 2010.
- [2] Julius Kammerl, Rahul Gopal Chaudhari, and Eckehard Steinbach. Combining contact models with perceptual data reduction for efficient haptic data communication in networked VEs. *IEEE Transactions on Instrumentation & Measurement*, 60(1):57–68, 2011.
- [3] Julius Kammerl, Iason Vittorias, Verena Nitsch, Berthold Faerber, Eckehard Steinbach, and Sandra Hirche. Perception-based data reduction for haptic force-feedback signals using velocity-adaptive deadbands. *PRESENCE - Teleoperators and Virtual Environments*, 19(5), 2010.
- [4] Eckehard Steinbach, Sandra Hirche, Marc Ernst, Fernanda Brandi, Rahul Gopal Chaudhari, Julius Kammerl, and Iason Vittorias. Haptic communications. *Proceedings of the IEEE, Special Issue on Frontiers of Audiovisual Communications: Convergence of Broadband, Computing and Rich Media*, 2011. (accepted for publication).
- [5] Eckehard Steinbach, Sandra Hirche, Julius Kammerl, Iason Vittorias, and Rahul Gopal Chaudhari. Haptic data compression and communication for telepresence and teleaction. *IEEE Signal Processing Magazine*, 28(1):87–96, 2011.

E-Letter Publications

- [6] Fernanda Brandi, Rahul Gopal Chaudhari, Sandra Hirche, Julius Kammerl, Eckehard Steinbach, and Iason Vittorias. Perceptual haptic data reduction in telepresence and teleaction systems. *Multimedia Communication Technical Committee (MMTC) E-Letter*, 6(1):7–10, 2011.

Conference Publications

- [7] Ahmad Barghout, Julius Kammerl, Jongeun Cha, Eckehard Steinbach, and Abdulmoteleb El Saddik. Spatial resolution of vibrotactile perception on the human forearm when exploiting funneling illusion. In *Proceedings of the IEEE International Workshop on Haptic Audio Visual Environments and Games*, Lecco, Italy, November 2009.
- [8] Robert Bauernschmitt, Eva U. Braun, Martin Buss, Florian Fröhlich, Sandra Hirche, Gerhard Hirzinger, Julius Kammerl, Alois Knoll, Rainer Konietschke, Bernhard Kübler, Rüdiger Lange, Hermann Mayer, Markus Rank, Gerhard Schillhuber,

- Christoph Staub, Eckehard Steinbach, Andreas Tobergte, Heinz Ulbrich, Iason Vittorias, and Chen Zhao. On the role of multimodal communication in telesurgery systems. In *Proceedings of the International Workshop on Multimedia Signal Processing 2009*, Rio de Janeiro, Brazil, October 2009.
- [9] Fernanda Brandi, Julius Kammerl, and Eckehard Steinbach. Error-resilient perceptual coding for networked haptic interaction. In *Proceedings of the ACM Multimedia (Full Paper)*, Firenze, Italy, October 2010.
- [10] Rahul Gopal Chaudhari, Julius Kammerl, and Eckehard Steinbach. On the compression and rendering of event-triggered force transients in networked virtual environments. In *Proceedings of the IEEE International Workshop on Haptic Audio Visual Environments and Games*, Lecco, Italy, November 2009.
- [11] Peter Hinterseer, Julius Kammerl, Eckehard Steinbach, and Subhasis Chaudhuri. The weber quantizer: Perceptual coding for networked telepresence and teleaction. In *Proceedings of the First International Conference on Robot Communication and Coordination*, Athens, Greece, October 2007.
- [12] Julius Kammerl, Nico Blodow, Radu Bogdan Rusu, Suat Gedikli, Michael Beetz, and Eckehard Steinbach. Real-time compression of point cloud streams. In *Proceedings of the IEEE International Conference on Robotics and Automation (ICRA)*, Minnesota, USA, May 2012.
- [13] Julius Kammerl, Fernanda Brandi, Florian Schweiger, and Eckehard Steinbach. Error-resilient perceptual haptic data communication based on probabilistic receiver state estimation. In *Proceedings of the EuroHaptics Conference*, Tampere, Finland, June 2012.
- [14] Julius Kammerl, Rahul Gopal Chaudhari, and Eckehard Steinbach. Exploiting directional dependencies of force perception for lossy haptic data reduction. In *Proceedings of the IEEE International Symposium on Haptic Audio Visual Environments and Games (HAVE)*, Phoenix, Arizona, USA, October 2010.
- [15] Julius Kammerl, Peter Hinterseer, and Eckehard Steinbach. A novel signal reconstruction algorithm for perception based data reduction in haptic signal communication. In *Proceedings of the First International Workshop on Networking Technology for Robotics and Applications, NeTRA 2007, in conjunction with the 16th International Conference on Computer Communications and Networks ICCCN*, Honolulu, Hawaii, August 2007.
- [16] Julius Kammerl, Peter Hinterseer, Eckehard Steinbach, and Subhasis Chaudhuri. A theoretical analysis of data reduction using the weber quantizer. In *Proceedings of the Data Compression Conference DCC*, Snowbird, Utah, USA, March 2008.
- [17] Julius Kammerl and Eckehard Steinbach. Deadband-based offline-coding of haptic media. In *Proceedings of the ACM Multimedia 2008 (Full Paper)*, Vancouver, Kanada, October 2008.
- [18] Julius Kammerl and Eckehard Steinbach. High-fidelity recording, compression, and replay of visual-haptic telepresence sessions. In *Proceedings of the International Conference on Image Processing (ICIP)*, Hong Kong, China, September 2010.

-
- [19] Hawkeye King, Julius Kammerl, Blake Hannaford, and Eckehard Steinbach. Establishing multimodal telepresence sessions using the session initiation protocol (SIP) and advanced haptic codecs. In *Proceedings of the Haptics Symposium 2010*, Massachusetts, USA, March 2010.
- [20] Verena Nitsch, Julius Kammerl, Berthold Faerber, and Eckehard Steinbach. On the impact of haptic data reduction and feedback modality on quality and task performance in a telepresence and teleaction system. In *Proceedings of the EuroHaptics Conference 2010*, Amsterdam, Netherlands, July 2010.
- [21] Helena Pongrac, Berthold Färber, Peter Hinterseer, Julius Kammerl, and Eckehard Steinbach. Limitations of human 3d force discrimination. In *Proceedings of the Human-Centered Robotics Systems 2006*, Munich, Germany, October 2006.
- [22] Lara Rahal, Julius Kammerl, Jongeun Cha, Eckehard Steinbach, and Abdulmotaleb El Saddik. Investigating the influence of temporal intensity changes on the apparent movement phenomenon. In *Proceedings of the Conference on Virtual Environments, Human-Computer Interfaces and Measurement Systems*, Hong Kong, China, May 2009.
- [23] T. Schauss, C. Passenberg, N. Stefanov, D. Feth, I. Vittorias, A. Peer, S. Hirche, M. Buss, M. Rothbucher, K. Diepold, J. Kammerl, and E. Steinbach. Beyond classical teleoperation: Assistance, cooperation, data reduction, and spatial audio. In *Proceedings of the IEEE International Conference on Robotics and Automation (ICRA)*, Minnesota, USA, May 2012.
- [24] Iason Vittorias, Julius Kammerl, Sandra Hirche, and Eckehard Steinbach. Perceptual coding of haptic data in time-delayed teleoperation. In *Proceedings of the Third Joint Eurohaptics Conference and Symposium on Haptic Interfaces for Virtual Environment and Teleoperator Systems (Best Paper: Haptic Technology)*, Salt Lake City, UT, USA, March 2009.
- [25] Xiao Xu, Julius Kammerl, Rahul Chaudhari, and Eckehard Steinbach. Hybrid signal-based and geometry-based prediction for haptic data reduction. In *Proceedings of the IEEE International Symposium on Haptic Audio Visual Environments and Games*, Nanchang, Jiangxi, China, October 2011.

Other Publications and Sources

- [26] A. Achhammer, C. Weber, A. Peer, and M. Buss. Improvement of model-mediated teleoperation using a new hybrid environment estimation technique. In *Proceedings of the IEEE International Conference on Robotics and Automation*, pages 5358–5363, Anchorage, Alaska, May 2010.
- [27] P. K. Allen and K. S. Roberts. Haptic object recognition using a multi-fingered dextrous hand. In *Proceedings of the IEEE International Conference on Robotics and Automation*, pages 342–347, Leuven, Belgium, 1989.
- [28] S. Allin, Y. Matsuoka, and R. Klatzky. Measuring just noticeable differences for haptic force feedback: Implications for rehabilitation. In *Proceedings of the 10th Symposium*

REFERENCES

- on Haptic Interfaces for Virtual Environment and Teleoperator Systems*, pages 299–302, Orlando, FL, USA, 2002.
- [29] R. J. Anderson and M. W. Spong. Bilateral control of teleoperators with time delay. *IEEE Transactions on Automatic Control*, 34(5):494–501, May 1989.
- [30] J. Arata, H. Takahashi, P. Pitakwatchara, S. Warisawa, K. Tanoue, K. Konishi, S. Ieiri, S. Shimizu, N. Nakashima, K. Okamura, Y. Fujino, Y. Ueda, P. Chotiwan, M. Mitsuishi, and M. Hashizume. A remote surgery experiment between japan and thailand over internet using a low latency codec system. In *Proceedings of the IEEE International Conference on Robotics and Automation*, pages 953–959, Roma, Italy, April 2007.
- [31] F. Barbagli, K. Salisbury, C. Ho, C. Spence, and H.Z. Tan. Haptic discrimination of force direction and the influence of visual information. *ACM Transactions on Applied Perception*, 3(2):135, 2006.
- [32] C. Basdogan, C. Ho, M. Slater, and M. A. Srinivasan. The role of haptic communication in shared virtual environments. In *Proceedings of the Third PHANToM Users Group Workshop*, Massachusetts, USA, 1998.
- [33] C. Basdogan, C. Ho, M. Srinivasan, and M. Slater. An experimental study on the role of touch in shared virtual environments. *ACM Transactions on Computer-Human Interaction*, 7(4):443–460, 2000.
- [34] M. Benali-Khoudja, M. Hafez, J. M. Alexandre, and A. Kheddar. Tactile interfaces: A state-of-the-art survey. In *Proceedings of International Symposium of Robotics*, pages 23–26, Paris, France, 2004.
- [35] P. Berestesky, N. Chopra, and M. W. Spong. Discrete time passivity in bilateral teleoperation over the internet. In *Proceedings of the IEEE International Conference on Robotics and Automation, ICRA*, volume 5, pages 4557 – 4564, New Orleans, LA, USA, April 2004.
- [36] P. Berestesky, N. Chopra, and M. W. Spong. Theory and experiments in bilateral teleoperation over the internet. In *Proceedings of the IEEE International Conference on Control Applications*, pages 456–463, Taipei, Japan, 2004.
- [37] E. G. Boring. The two-point limen and the error of localization. *The American Journal of Psychology*, 42(3):446–449, 1930.
- [38] C. W. Borst. Predictive coding for efficient host-device communication in a pneumatic force-feedback display. In *Proceedings of the First Joint Eurohaptics Conference and Symposium on Haptic Interfaces for Virtual Environment and Teleoperator Systems, World Haptics*, pages 596–599, Pisa, Italy, March 2005.
- [39] C. W. Borst and C. D. Cavanaugh. Haptic controller design and palm-sized vibrotactile array. Technical report, University of Louisiana at Lafayette, 2004.
- [40] F. Brandi and E. Steinbach. Perceptual coding of recorded telemanipulation sessions. In *Proceedings of the ACM Multimedia*, Scottsdale, Arizona, USA, November 2011.

-
- [41] C. Braun, M. Haug, K. Wiech, N. Birbaumer, T. Elbert, and L. E. Roberts. Functional organization of primary somatosensory cortex depends on the focus of attention. *Neuroimage*, 17:1451–1458, 2002.
- [42] S. Brewster, F. Chohan, and L. Brown. Tactile feedback for mobile interactions. In *Proceedings of the SIGCHI conference on Human factors in computing systems*, pages 159–162, Gaithersburg, Maryland, USA, 2007.
- [43] G. Burdea, G. Patounakis, V. Popescu, and R. E. Weiss. Virtual reality-based training for the diagnosis of prostate cancer. *IEEE Transactions on Biomedical Engineering*, 46(10):1253–1260, 1999.
- [44] G.C. Burdea. *Force and touch feedback for virtual reality*. Wiley, 1996.
- [45] F. Carpi, D. De Rossi, R. Kornbluh, R. Pelrine, and P. Sommer-Larsen. *Dielectric elastomers as electromechanical transducers*. Elsevier, 2008.
- [46] J. Chakareski and B. Girod. Computing rate-distortion optimized policies for streaming media with rich acknowledgments. In *Proceedings of the Data Compression Conference*, pages 202–211, Snowbird, Utah, USA, 2004.
- [47] C. Chapman, M. Bushnell, D. Miron, G. H. Duncan, and J. P. Lund. Sensory perception during movement in man. *Experimental Brain Research*, 68(3):516–524, 1987.
- [48] R. G. Chaudhari. Exploiting the concept of event-based haptics in perceptual coding of haptic data for networked virtual environments. Master’s thesis, Technische Universität München, Institute for Media Technology, September 2009.
- [49] Z. Chen. Geometry-based prediction of haptic force-feedback signals. Master’s thesis, Technische Universität München, Institute for Media Technology, August 2009.
- [50] N. Chopra, M. W. Spong, S. Hirche, and M. Buss. Bilateral teleoperation over internet: The time varying delay problem. In *Proceedings of the American Control Conference*, pages 155–160, Denver, USA, 2003.
- [51] P. Chou and Z. Miao. Rate-distortion optimized streaming of packetized media. *IEEE Transactions on Multimedia*, 8(2):390–404, April 2006.
- [52] V. G. Chouvardas, A. N. Miliou, and M. K. Hatalis. Tactile display applications: A state-of-the-art survey. In *Proceedings of the 2nd Balkan Conference in Informatics*, pages 290–303, Ohrid, Macedonia, November 2005.
- [53] F. J. Clark, K. J. Larwood, M. E. Davis, and K. A. Deffenbacher. A metric for assessing acuity in positioning joints and limbs. *Experimental Brain Research*, 107(1):73–79, 1995.
- [54] S. Clarke, G. Schillhuber, M. Zaeh, and H. Ulbrich. Prediction-based methods for teleoperation across delayed networks. *Multimedia Systems*, 13(4):253–261, Januar 2008.
- [55] A. Cockburn and S. Brewster. Multimodal feedback for the acquisition of small targets. *Ergonomics*, 48(9):1129–1150, 2005.
- [56] E. Colgate and G. Schenkel. Passivity of a class of sampled-data systems: Application to haptic interfaces. *Journal of Robotic Systems*, 14:37–47, 1997.

- [57] F. Conti, F. Barbagli, D. Morris, and C. Sewell. CHAI 3D: An open-source library for the rapid development of haptic scenes. In *Proceedings of the IEEE World Haptics Conference*, Pisa, Italy, March 2005.
- [58] M. Corno and M. Zefran. Haptic playback: Modeling, controller design, and stability analysis. In *Proceedings of Robotics: Science and Systems*, Philadelphia, USA, August 2006.
- [59] J. C. Craig. Difference threshold for intensity of tactile stimuli. *Attention, Perception, & Psychophysics*, 11(2):150–152, 1972.
- [60] J. C. Craig. Vibrotactile difference thresholds for intensity and the effect of a masking stimulus. *Attention, Perception, & Psychophysics*, 15(1):123–127, 1974.
- [61] J. C. Craig. Vibrotactile masking: A comparison of energy and pattern maskers. *Attention, Perception, & Psychophysics*, 31(6):523–529, 1982.
- [62] A. Crossan and S. Brewster. Multimodal trajectory playback for teaching shape information and trajectories to visually impaired computer users. *ACM Transactions on Accessible Computing*, 1(2):1–34, 2008.
- [63] A. Crossan, J. Williamson, and S. Brewster. A general purpose control-based playback for force feedback systems. In *Proceedings of Eurohaptics*, Paris, France, 2006.
- [64] G. De Gerssem, H. Van Brussel, and F. Tendick. Reliable and enhanced stiffness perception in soft-tissue telemanipulation. *The International Journal of Robotics Research*, 24(10):805, 2005.
- [65] T. Debus, T. Becker, P. Dupont, T. Jang, and R. Howe. Multichannel vibrotactile display for sensory substitution during teleoperation. *Proceedings of the SPIE - The International Society for Optical Engineering*, 4570:42–49, 2001.
- [66] S. Dehaene. Subtracting pigeons: Logarithmic or linear? *Psychological Science*, 12(3):244–246, 2001.
- [67] S. Dehaene. The neural basis of the weber-fechner law: A logarithmic mental number line. *Trends in Cognitive Sciences*, 7(4):145–147, 2003.
- [68] J. T. Dennerlein, D. B. Martin, and C. J. Hasser. Force-feedback improves performance for steering and combined steering-targeting tasks. In *Proceedings of the SIGCHI conference on Human factors in computing systems*, pages 423–429, The Hague, Netherlands, 2000.
- [69] K. Drewing, M. Fritschi, R. Zopf, M. O. Ernst, and M. Buss. First evaluation of a novel tactile display exerting shear force via lateral displacement. *ACM Transactions on Applied Perception*, 2:118–131, 2005.
- [70] K. Drewing, T. Wiecki, and M. Ernst. Material properties determine how force and position signals combine in haptic shape perception. *Acta Psychologica*, 128(2):264–273, June 2008.

-
- [71] M. A. Eid, M. Mansour, A. H. El Saddik, and R. Iglesias. A haptic multimedia handwriting learning system. In *Proceedings of the International Workshop on Educational Multimedia and Multimedia Education*, page 108, Augsburg, Germany, 2007.
- [72] M. W. Eysenck and M. T. Keane. *Cognitive Psychology. A student's handbook*. Psychology Press, 2000.
- [73] W. R. Ferrell. Delayed force feedback. *Human Factors: The Journal of the Human Factors and Ergonomics Society*, 8(5):449–455, 1966.
- [74] W. R. Ferrell and T. B. Sheridan. Supervisory control of remote manipulation. *IEEE Spectrum*, 4(10):81–88, 1967.
- [75] D. Feygin, M. Keehner, and F. Tendick. Haptic guidance: Experimental evaluation of a haptic training method for a perceptual motor skill. In *Proceedings of the 10th Symposium on Haptic Interfaces for Virtual Environment and Teleoperator Systems*, volume 1, page 40, Washington, USA, 2002.
- [76] A. Field. *Discovering statistics using SPSS*. Second Edition. Sage Publications, London, GB, 2005.
- [77] M. Fujimoto and Y. Ishibashi. Packetization interval of haptic media in networked virtual environments. In *Proceedings of 4th ACM SIGCOMM Workshop on Network and System Support for Games*, page 6, Portland, Oregon, USA, 2005.
- [78] J. Funda and R. P. Paul. Efficient control of a robotic system for time-delayed environments. In *Proceedings of the 5th International Conference on Advanced Robotics - Robots in Unstructured Environments*, pages 219–224, Pisa, Italy, June 1991.
- [79] F. A. Geldard, c. e. Sherrick, and R. W. Cholewiak. Princeton cutaneous research project report. In N.J. Princeton, editor, *Princeton University*, number 36, pages 30–36. Princeton University, 1980.
- [80] B. Gerkey, R. T. Vaughan, and A. Howard. The player/stage project: Tools for multi-robot and distributed sensor systems. In *Proceedings of the 11th International Conference on Advanced Robotics*, pages 317–323, Coimbra, Portugal, June 2003.
- [81] G.A. Gescheider. *Psychophysics*. Lawrence Erlbaum, 1985.
- [82] J. J. Gibson. *The senses considered as perceptual systems*. Houghton Mifflin, 1966.
- [83] R. B. Gillespie, M. Modhrain, P. Tang, D. Zaretzky, and C. Pham. The virtual teacher. In *Proceedings of the ASME Dynamic Systems and Control Division*, volume 64, pages 171–178, Anaheim, California, USA, November 1998.
- [84] J. Greenspan and S. Bolanowski. The psychophysics of tactile perception and its peripheral physiological basis. In L. Kruger, editor, *Pain and touch*. Academic Press Inc., New York, 1996.
- [85] J. D. Greenspan and S. J. Bolanowski. *The psychophysics of tactile perception and its peripheral physiological basis*. Academic Press Inc., 1996.

REFERENCES

- [86] B. Gu. Offline compression of haptic data streams. Master's thesis, Technische Universität München, Institute for Media Technology, 2008.
- [87] M. Handley and V. Jacobson. SDP: Session Description Protocol. RFC 2327 (Proposed Standard), April 1998. Obsoleted by RFC 4566, updated by RFC 3266.
- [88] M. Handlykken and T. Turner. Control system analysis and synthesis for a six degree-of-freedom universal force-reflecting hand controller. In *Proceedings of the IEEE Conference on Decision and Control including the Symposium on Adaptive Processes*, volume 19, pages 1197–1205, 1980.
- [89] B. Hannaford. A design framework for teleoperators with kinesthetic feedback. *IEEE Transactions on Robotics and Automation*, 5(4):426–434, 1989.
- [90] B. Hannaford. Stability and performance tradeoffs in bi-lateral telemanipulation. In *Proceedings of the IEEE International Conference on Robotics and Automation*, volume 3, pages 1764–1767, Scottsdale, USA, May 1989.
- [91] B. Hannaford and J. H. Ryu. Time-domain passivity control of haptic interfaces. *IEEE Transactions on Robotics and Automation*, 18(1):1–10, 2002.
- [92] K. Hashtrudi-Zaad and S. E. Salcudean. Adaptive transparent impedance reflecting teleoperation. In *Proceedings of the IEEE International Conference on Robotics and Automation*, volume 2, pages 1369–1374, Minneapolis, Minnesota, USA, 1996.
- [93] K. Hashtrudi-Zaad and S. E. Salcudean. Analysis of control architectures for teleoperation systems with impedance/admittance master and slave manipulators. *International Journal of Robotics Research*, 20(6):419–445, 2001.
- [94] V. Hayward, O. R. Astley, M. Cruz-Hernandez, D. Grant, and G. Robles-De-La-Torre. Haptic interfaces and devices. *Sensor Review*, 24(1):16–29, 2004.
- [95] V. Hayward and K. E. MacLean. Do it yourself haptics, Part I. *IEEE Robotics and Automation Magazine*, 3(2):88–104, 2008.
- [96] K. Henmi and T. Yoshikawa. Virtual lesson and its application to virtual calligraphy system. In *Proceedings of the International Conference on Robotics and Automation*, volume 2, pages 1275–1280, Leuven, Belgium, May 1998.
- [97] P. Hinterseer. *Compression and transmission of haptic data in telepresence and teleaction Systems*. Dissertation, Technische Universität München, Munich, Germany, 2009.
- [98] P. Hinterseer, S. Hirche, S. Chaudhuri, E. Steinbach, and M. Buss. Perception-based data reduction and transmission of haptic data in telepresence and teleaction systems. *IEEE Transactions on Signal Processing*, 56(2):588–597, February 2008.
- [99] P. Hinterseer and E. Steinbach. Model-based data compression for 3d virtual haptic teleinteraction. In *Proceedings of the IEEE International Conference on Consumer Electronics*, Las Vegas, USA, January 2006.
- [100] P. Hinterseer and E. Steinbach. A psychophysically motivated compression approach for 3d haptic data. In *Proceedings of the 14th Symposium on Haptic Interfaces for Virtual Environment and Teleoperator Systems*, pages 35–41, Washington D.C., USA, March 2006.

-
- [101] P. Hinterseer, E. Steinbach, and S. Chaudhuri. Model-based data compression for 3d virtual haptic teleinteraction. In *International Conference on Consumer Electronics*, pages 23–24, Las Vegas, USA, January 2006.
- [102] P. Hinterseer, E. Steinbach, and S. Chaudhuri. Perception-based compression of haptic data streams using kalman filters. In *Proceedings of the International Conference on Acoustics, Speech, and Signal Processing*, Toulouse, France, May 2006.
- [103] P. Hinterseer, E. Steinbach, S. Hirche, and M. Buss. A novel, psychophysically motivated transmission approach for haptic data streams in telepresence and teleaction systems. In *Proceedings of the International Conference on Acoustics, Speech, and Signal Processing*, volume 2, Philadelphia, PA, USA, March 2005.
- [104] S. Hirche. *Haptic telepresence in packet-switched communication networks*. PhD thesis, Technische Universität München, Düsseldorf, 2005.
- [105] S. Hirche, A. Bauer, and M. Buss. Transparency of haptic telepresence systems with constant time delay. In *Proceedings of the IEEE International Conference on Control Applications*, pages 328–333, Toronto, Canada, 2005.
- [106] S. Hirche and M. Buss. Packet loss effects in passive telepresence systems. In *Proceedings of the 43rd IEEE Conference on Decision and Control*, volume 4, pages 4010–4015, Nassau, Bahamas, December 2004.
- [107] S. Hirche, M. Ferre, J. Barrio, C. Melchiorri, and M. Buss. Bilateral control architectures for telerobotics. In M. Ferre, M. Buss, R. Aracil, C. Melchiorri, and C. Balaguer, editors, *Advances in telerobotics*, STAR, pages 163–176. Springer-Verlag, Berlin, 2007.
- [108] S. Hirche, P. Hinterseer, E. Steinbach, and M. Buss. Network traffic reduction in haptic telepresence systems by deadband control. In *Proceedings of the IFAC World Congress, International Federation of Automatic Control*, Prague, Czech Republic, 2005.
- [109] S. Hirche, P. Hinterseer, E. Steinbach, and M. Buss. Towards deadband control in networked teleoperation systems. In *Proceedings of the IFAC World Congress, International Federation of Automatic Control*, Prague, Czech Republic, 2005.
- [110] S. Hirche, P. Hinterseer, E. Steinbach, and M. Buss. Transparent data reduction in networked telepresence and teleaction systems. part i: Communication without time delay. *Presence: Teleoperators & Virtual Environments*, 16(5):523–531, 2007.
- [111] N. Hogan. Controlling impedance at the man/machine interface. In *Proceedings of the IEEE International Conference on Robotics and Automation*, pages 1626–1631, Scottsdale, USA, 1989.
- [112] P. F. Hokayem and M. W. Spong. Bilateral teleoperation: An historical survey. *Automatica*, 49(12):2035–2057, December 2006.
- [113] R. Höver, M. Luca, and M. Harders. User-based evaluation of data-driven haptic rendering. *ACM Transactions on Applied Perception*, 8:7:1–7:23, November 2010.

REFERENCES

- [114] L. Huijun and S. Aiguo. Virtual-environment modeling and correction for force-reflecting teleoperation with time delay. *IEEE Transactions on Industrial Electronics*, 54(2):1227–1233, 2007.
- [115] J. Hwang, M. Williams, and G. Niemeyer. Toward event-based haptics: Rendering contact using open-loop force pulses. In *Proceedings of the International Symposium on Haptic Interfaces for Virtual Environment and Teleoperator Systems*, pages 24–31, Chicago, IL, USA, March 2004.
- [116] Y. Iguchi, Y. Hoshi, and I. Hashimoto. Selective spatial attention induces short-term plasticity in human somatosensory cortex. *Neuroreport*, 12:3133–3136, 2001.
- [117] W. Ijsselsteijn, H. de Ridder, J. Freeman, and S. E. Avons. Presence: Concept, determinants and measurement. *Proceedings of the International Society for Optics and Photonics (SPIE)*, 3959:520–529, 2000.
- [118] Immersion Corp. CyberGlove II Wireless Data Glove, 2011.
- [119] A. Israr, H. Z. Tan, and C. M. Reed. Frequency and amplitude discrimination along the kinesthetic-cutaneous continuum in the presence of masking stimuli. *The Journal of the Acoustical Society of America*, 120:2789, 2006.
- [120] R. S. Johansson and A. B. Vallbo. Tactile sensibility in the human hand: relative and absolute densities of four types of mechanoreceptive units in glabrous skin. *The Journal of Physiology*, 286(1):283, 1979.
- [121] L. A. Jones. Kinesthetic sensing. In *Proceedings of the Conference on Human and Machine Haptics*, Cambridge, USA, 2000.
- [122] L. A. Jones and I. W. Hunter. A perceptual analysis of stiffness. *Experimental Brain Research*, 79(1):150–156, 1990.
- [123] L. A. Jones, I. W. Hunter, and R. J. Irwin. Differential thresholds for limb movement measured using adaptive techniques. *Perception and Psychophysics*, 52:529–535, 1992.
- [124] Y. S. Kim and B. Hannaford. Some practical issues in time domain passivity control of haptic interfaces. In *Proceedings of the IEEE International Conference on Intelligent Robots and Systems*, volume 3, pages 1744–1750, Maui, USA, 2001.
- [125] H. Hawkeye King, K. Tadano, R. Donlin, D. Friedman, M. Lum, V. Asch, C. Wang, K. Kawashima, and B. Hannaford. A preliminary protocol for interoperable telesurgery. In *Proceedings of the 17th International Conference on Advanced Robotics*, Munich, Germany, 2009.
- [126] A. Kron and G. Schmidt. A bimanual haptic telepresence system - design issues and experimental results. In *Proceedings of the International Workshop on High-Fidelity Telepresence and Teleaction jointly with IEEE Humanoids*, Munich, Germany, 2003.
- [127] D. Kubus, I. Weidauer, and F. M. Wahl. 1khz is not enough - how to achieve higher update rates with a bilateral teleoperation system based on commercial hardware. In *Proceedings of the International Conference on Intelligent Robots and Systems*, pages 5107–5114, St. Louis, MO, USA, October 2009.

-
- [128] K. Kuchenbecker, J. Fiene, and G. Niemeyer. Event-based haptics and acceleration matching: Portraying and assessing the realism of contact. In *Proceedings of the First Joint Eurohaptics Conference and Symposium on Haptic Interfaces for Virtual Environment and Teleoperator Systems*, pages 381–387, Washington, DC, USA, 2005.
- [129] K. J. Kuchenbecker, J. Fiene, and G. Niemeyer. Improving Contact Realism through Event-Based Haptic Feedback. *IEEE Transactions on Visualization and Computer Graphics*, 12(2):219–230, 2006.
- [130] M. Kuschel, P. Kremer, S. Hirche, and M. Buss. Lossy data reduction methods for haptic telepresence systems. In *Proceedings of the International Conference on Robotics and Automation*, pages 2933–2938, Orlando, Florida, USA, May 2006.
- [131] D. A. Lawrence. Stability and transparency in bilateral teleoperation. *IEEE Transactions on Robotics and Automation*, 9(5):624–637, October 1993.
- [132] K. M. Loeb. Membrane keyboards and human performance. *The Bell System Technical Journal*, 26:1733–1749, 1983.
- [133] C. Mahlo, C. Hoene, A. Rosami, and A. Wolisz. Adaptive coding and packet rates for tcp-friendly voip flows. In *Proceedings of the 3rd International Symposium on Telecommunications*, Shiraz, Iran, September 2005.
- [134] J. Marescaux, J. Leroy, F. Rubino, M. Smith, M. Vix, M. Simone, and D. Mutter. Transcontinental robot-assisted remote telesurgery: Feasibility and potential applications. *Annals of surgery*, 235(4):487, 2002.
- [135] M. Matysek, P. Lotz, T. Winterstein, and H. Schlaak. Dielectric elastomer actuators for tactile displays. In *Proceedings of the Third Joint Eurohaptics Conference and the International Symposium on Haptic Interfaces for Virtual Environment and Teleoperator Systems (World Haptics)*, pages 290–295, March 2009.
- [136] M. L. McLaughlin, G. Sukhatme, C. Shahabi, J. Hespanha, A. Ortega, and G. Medioni. The haptic museum. In *Proceedings of the EVA 2000 Conference on Electronic Imaging and the Visual Arts*, Florence, Italy, 2000.
- [137] M. Minsky. Telepresence. *Omni Magazine*, June 1980.
- [138] P. Mitra, D. Gentry, and G. Niemeyer. User perception and preference in model mediated telemanipulation. In *Proceedings of the Second Joint EuroHaptics Conference and Symposium on Haptic Interfaces for Virtual Environment and Teleoperator Systems*, pages 268–273, Tsukuba, Japan, March 2007.
- [139] Probal Mitra and Günter Niemeyer. Model-mediated telemanipulation. *International Journal of Robotics Research*, 27:253–262, February 2008.
- [140] F. Mobasser and K. Hashtrudi-Zaad. Predictive teleoperation using laser rangefinder. In *Proceedings of the Canadian Conference on Electrical and Computer Engineering*, pages 1279–1282, Ottawa, Canada, May 2006.

REFERENCES

- [141] A. M. Murray, R. L. Klatzky, and P. K. Khosla. Psychophysical characterization and testbed validation of a wearable vibrotactile glove for telemanipulation. *Presence: Teleoperators & Virtual Environments*, 12(2):156–182, 2003.
- [142] G. Niemeyer and J. E. Slotine. Stable adaptive teleoperation. *IEEE Journal of Oceanic Engineering*, 16(1):152–162, 1991.
- [143] V. Nitsch, B. Farber, L. Geiger, P. Hinterseer, and E. Steinbach. An experimental study of lossy compression in a real telepresence and teleaction system. In *Proceedings of the International Workshop on Haptic Audio visual Environments and Games*, pages 75–80, Ottawa, Canada, 2008.
- [144] M. V. Noyes and T. B. Skridan. A novel predictor for telemanipulation through a time delay. In *Proceedings of 20th Annual Conference on Manual Control*, NASA Ames Research Center, Moffett Field CA, USA, 1984.
- [145] A. M. Okamura, J. T. Dennerlein, and R. D. Howe. Vibration feedback models for virtual environments. In *Proceedings of the IEEE International Conference on Robotics and Automation*, volume 1, pages 674 – 679, Lueven, Belgium, 1998.
- [146] A. Ortega and Y. Liu. Lossy compression of haptic data. In *Touch in Virtual Environments: Haptics and the Design of Interactive Systems*, chapter 6, pages 119–136. Prentice Hall, 2002.
- [147] P. G. Otanez, J. R. Moyne, and D. M. Tilbury. Using deadbands to reduce communication in networked control systems. In *Proceedings of the American Control Conference*, Anchorage, Alaska, 2002.
- [148] J. Paillard and M. Brouchon. Active and passive movements in the calibration of position sense. In *The Neuropsychology of Spatially Oriented Behavior*, pages 37–55. Irwin Homewood, 1968.
- [149] C. Passenberg, A. Peer, and M. Buss. Model-mediated teleoperation for multi-operator multi-robot systems. In *Proceedings of the International Conference on Intelligent Robots and Systems*, pages 4263–4268, Taipei, Taiwan, 2010.
- [150] A. Peer, S. Hirche, C. Weber, I. Krause, M. Buss, S. Miossec, P. Evrard, O. Stasse, E. S. Neo, A. Kheddar, et al. Intercontinental cooperative telemanipulation between Germany and Japan. In *Proceedings of the IEEE/RSJ International Conference on Intelligent Robots and Systems*, Nice, France, 2008.
- [151] L. F. Penin, A. Caballero, R. Aracil, and A. Barrientos. Human behavior modeling in master-slave teleoperation with kinesthetic feedback. In *Proceedings of the IEEE International Conference on Robotics and Automation*, pages 2244–2249, Leuven, Belgium, May 1998.
- [152] M. Quigley, B. Gerkey, K. Conley, J. Faust, T. Foote, J. Leibs, E. Berger, R. Wheeler, and A. Ng. Ros: an open-source robot operating system. In *Proceedings of the ICRA Workshop on Open Source Software*, Kobe, Japan, 2009.

-
- [153] G. J. Raju, G. C. Verghese, and T. B. Sheridan. Design issues in 2-port network models of bilateral remote manipulation. In *Proceedings of the IEEE International Conference on Robotics and Automation*, pages 1316–1321, Scottsdale, USA, 1989.
- [154] A. B. Roach. Session Initiation Protocol (SIP)-Specific Event Notification. RFC 3265 (Proposed Standard), June 2002. Updated by RFC 5367.
- [155] J. Rosenberg, H. Schulzrinne, G. Camarillo, A. Johnston, J. Peterson, R. Sparks, M. Handley, and E. Schooler. SIP: Session Initiation Protocol. RFC 3261 (Proposed Standard), June 2002. Updated by RFCs 3265, 3853, 4320, 4916, 5393, 5621.
- [156] L. B. Rosenberg. The use of virtual fixtures as perceptual overlays to enhance operator performance in remote environments. Technical Report AL-TR-0089, USAF Armstrong Laboratory, 1992.
- [157] S. Saga, K. Vlack, H. Kajimoto, and S. Tachi. Haptic video. In *Proceedings of the ACM SIGGRAPH Conference on Emerging Technologies*, Los Angeles, USA, 2005.
- [158] N. Sakr, N. D. Georganas, J. Zhao, and X. Shen. Motion and force prediction in haptic media. In *Proceedings of the IEEE International Conference on Multimedia and Expo*, pages 2242–2245, Beijing, Japan, 2007.
- [159] N. Sakr, J. Zhou, N. D. Georganas, J. Zhao, and X. Shen. Prediction-based haptic data reduction and compression in tele-mentoring systems. *IEEE Transactions on Instrumentation and Measurement*, 58(5):1727–1736, May 2008.
- [160] K. Salisbury, F. Conti, and F. Barbagli. Haptic rendering: Introductory concepts. *IEEE Computer Graphics and Applications*, 24(2):24–32, March-April 2004.
- [161] W. Schiff and E. Foulke. *Tactual perception: A sourcebook*. Cambridge Univ Press, 1982.
- [162] D. W. Schloerb. A quantitative measure of telepresence. *Presence: Teleoperators and Virtual Environments*, 4(1):64–80, 1995.
- [163] SensAble. PHANTOM haptic devices, 2011. <http://www.sensable.com/products-haptic-devices.htm>.
- [164] R. Sepulchre, M. Jankovic, and P. Kokotovic. *Constructive nonlinear control*. Springer-Verlag, 1997.
- [165] C. Shahabi, M. R. Kollahdouzan, G. Barish, R. Zimmermann, D. Yao, K. Fu, and L. Zhang. Alternative techniques for the efficient acquisition of haptic data. *ACM SIGMETRICS Performance Evaluation Review*, 29(1):334–335, 2001.
- [166] C. Shahabi, A. Ortega, and M. R. Kollahdouzan. A comparison of different haptic compression techniques. In *Proceedings of the International Conference on Multimedia & Expo*, pages 657–660, Lausanne, Switzerland, August 2002.
- [167] J. Sheng and M. W. Spong. Model predictive control for bilateral teleoperation systems with time delays. In *Proceedings of the Canadian Conference on Electrical and Computer Engineering*, volume 4, pages 1877–1880, Niagara Falls, Ontario, Canada, 2004.

REFERENCES

- [168] T. B. Sheridan. Musings on telepresence and virtual presence. *Presence: Teleoperators and Virtual Environments*, 1(1):120–126, 1992.
- [169] T. B. Sheridan. *Telerobotics, automation, and human supervisory control*. MIT Press, Cambridge, MA, USA, 1992.
- [170] C. E. Sherrick and J. C. Craig. The psychophysics of touch. In W. Schiff & E. Foulke, editor, *Tactual Perception: A Sourcebook*, pages 55 – 81. Cambridge University Press, 1982.
- [171] Z. Shi, S. Hirche, W. X. Schneider, and H. Muller. Influence of visuomotor action on visual-haptic simultaneous perception: A psychophysical study. In *Proceedings of the Symposium on Haptic interfaces for Virtual Environment and Teleoperator Systems*, pages 65–70, Reno, Nevada, USA, March 2008.
- [172] Z. Shi, H. Zou, M. Rank, L. Chen, S. Hirche, and H. Mueller. Effects of packet loss and latency on temporal discrimination of visual-haptic events. *IEEE Transactions on Haptics*, 3(1):28–36, 2009.
- [173] M. Sitti, B. Aruk, H. Shintani, and H. Hashimoto. Scaled teleoperation system for nano-scale interaction and manipulation. *Advanced Robotics*, 17(3):275–291, 2003.
- [174] S. S. Stevens. *Psychophysics: Introduction to its perceptual, neural, and social prospects*. Transaction Publishers, 1975.
- [175] W. H. Talbot, I. Darian-Smith, H. H. Kornhuber, and V. B. Mountcastle. The sense of flutter-vibration: Comparison of the human capacity with response patterns of mechanoreceptive afferents from the monkey hand. *Journal of Neurophysiology*, 31(2):301, 1968.
- [176] H. Z. Tan, F. Barbagli, K. Salisbury, C. Ho, and C. Spence. Force-direction discrimination is not influenced by reference force direction. *Haptics-e*, 4(1):1–6, 2006.
- [177] H. Z. Tan and A. Pentland. Tactual displays for wearable computing. In *Proceedings of the First International Symposium on Wearable Computers*, pages 84–89, Cambridge, MA, USA, October 1997.
- [178] H. Z. Tan, M. A. Srinivasan, B. Eberman, and B. Cheng. Human factors for the design of force-reflecting haptic interfaces. *Dynamic Systems and Control*, 55(1):353–359, 1994.
- [179] J. L. Taylor and D. I. McCloskey. Detection of slow movements imposed at the elbow during active flexion in man. *The Journal of Physiology*, 457(1):503, 1992.
- [180] G. Tholey, J. P. Desai, and A. E. Castellanos. Force feedback plays a significant role in minimally invasive surgery. *Annals of Surgery*, 241(1):102–109, 2005.
- [181] C. Tzafestas, S. Velanas, and G. Fakiridis. Adaptive impedance control in haptic teleoperation to improve transparency under time-delay. In *Proceedings of the IEEE International Conference on Robotics and Automation*, pages 212–219, Sao Paulo, Brazil, 2008.

-
- [182] M. Ueberle, N. Mock, and M. Buss. ViSHaRD10, a novel hyper-redundant haptic interface. In *Proceedings of the International Symposium on Haptic Interfaces for Virtual Environment and Teleoperator Systems, in conjunction with the IEEE Virtual Reality Conference*, pages 58–65, Chicago, IL, USA, March 2004.
- [183] M. W. Ueberle. *Design, control, and evaluation of a family of kinesthetic haptic interfaces*. PhD thesis, Technische Universität München, Munich, Germany, 2006.
- [184] H. Utz, S. Sablatnög, S. Enderle, and G. Kraetzschmar. Miro-middleware for mobile robot applications. *IEEE Transactions on Robotics and Automation*, 18(4):493–497, August 2002.
- [185] Å. B. Vallbo and RS Johansson. Properties of cutaneous mechanoreceptors in the human hand related to touch sensation. *Human Neurobiology*, 3(1):3–14, 1984.
- [186] R. T. Verrillo. Effect of contractor area on the vibrotactile threshold. *Journal of the Acoustical Society of America*, 1963.
- [187] J. Vertut, A. Micaelli, P. Marchal, and J. Guittet. Short transmission delay on a force reflective bilateral manipulator. In *Prococeedings of the 4th Roman-Symposium*, Warsaw, Poland, 1981.
- [188] D. Wang, K. Tuer, M. Rossi, L. Ni, and J. Shu. The effect of time delays on tele-haptics. In *Proceedings of the 2nd IEEE International Workshop on Haptic, Audio and Visual Environments and Their Applications*, pages 7–12, Ottawa, Ontario, Canada, September 2003.
- [189] C. Weber, V. Nitsch, U. Unterhinninghofen, B. Farber, and M. Buss. Position and force augmentation in a telepresence system and their effects on perceived realism. In *Proceedings of the EuroHaptics Conference and Symposium on Haptic Interfaces for Virtual Environment and Teleoperator Systems. World Haptics*, pages 226–231, Salt Lake City, Utah, USA, March 2009.
- [190] E. Weber. *Die Lehre vom Tastsinn und Gemeingefühl, auf Versuche gegründet*. Vieweg: Braunschweig, Germany, 1851.
- [191] P. Wellman and R. D. Howe. Towards realistic vibrotactile display in virtual environments. In *Proceedings of the International Symposium on Haptic Interfaces for Virtual Environment and Teleoperator Systems, ASME International Mechanical Engineering Congress and Exposition*, volume 57, pages 713–718, San Francisco, CA, USA, November 1995.
- [192] B. Willaert, P. Goethals, D. Reynaerts, H. Van Brussel, and E. Vander Poorten. Transparent and shaped stiffness reflection for telesurgery. *Advances in Haptics*, pages 259–282, April 2010.
- [193] B. Willaert, E. Vander Poorten, D. Reynaerts, and H. Van Brussel. A pragmatic method for stable stiffness reflection in telesurgery. In *Proceedings of the 6th International Conference on Haptics*, pages 73–82, Madrid, Spain, 2008. Springer.
- [194] R. L. Williams, M. Srivastava, R. Conaster, and J. N. Howell. Implementation and evaluation of a haptic playback system. *Haptics-e*, 3(3):160–176, 2004.

REFERENCES

- [195] B. G. Witmer and M. J. Singer. Measuring presence in virtual environments: A presence questionnaire. *Presence*, 7(3):225–240, 1998.
- [196] M. Wright, A. Green, and S. Baker. Limitations for change detection in multiple garbor targets. *Visual Cognition*, 7:237–252, 2000.
- [197] M. Wu, J. J. Abbott, and A. M. Okamura. In *Proceedings of the First Joint Eurohaptics Conference and Symposium on Haptic Interfaces for Virtual Environment and Teleoperator Systems, World Haptics*, Pisa, Italy.
- [198] Y. Xing-Dong, W. F. Bischof, and P. Boulanger. Perception of haptic force magnitude during hand movements. In *Proceedings of the International Conference on Robotics and Automation*, pages 2061–2066, Pasadena, CA, USA, May 2008.
- [199] Y. Yokokohji, T. Tsujioka, and T. Yoshikawa. Bilateral control with time-varying delay including communication blackout. In *Proceedings of the International Symposium on Haptic Interfaces for Virtual Environment and Teleoperator Systems*, pages 285–292, Los Alamitos, CA, USA, April 2002.
- [200] Y. Yokokohji and T. Yoshikawa. Bilateral control of master-slave manipulators for ideal kinesthetic coupling-formulation and experiment. *IEEE Transactions on Robotics and Automation*, 10(5):605–620, October 1994.
- [201] W. K. Yoon, T. Goshozono, H. Kawabe, M. Kinami, Y. Tsumaki, M. Uchiyama, and M. Oda. Model-based space robot teleoperation of ets-vii manipulator. *IEEE Transactions on Robotics and Automation*, 20(3):602–612, 2004.
- [202] M. Zadeh, D. Wang, and E. Kubica. Factors affecting the perception-based compression of haptic data. In *Advances in Haptics*. InTech, April 2010.
- [203] M. F. Zaeh, S. Clarke, P. Hinterseer, and E. Steinbach. Telepresence across networks: A combined deadband and prediction approach. In *Proceedings of the International Conference on Information Visualization*, pages 597–604, London, UK, July 2006.